Republic of Iraq
Ministry of Higher Education and Scientific Research
University of Diyala
College of Science
Department of Physics

Surface Plasmon Resonance of Gold and Silver Nanoparticles for Biomedical Physics Applications

A thesis
Submitted to the Council of the College of Science University of Diyala in Partial Fulfillment of Requirements for the Degree of Doctor of Philosophy in Physics

By

Rusul Kareem Ismail AL-Ageedie
B.Sc. Physics Science 2012
M.Sc. Solid State Physics Science 2015

Supervised by

Prof. Dr.
Tahseen H. Mubarak

Prof. Dr.
Raad M. S. Al-Haddad

2019 A.D.

1441 A.H.

بِسْمِ اللَّهِ الرَّحْمَٰنِ الرَّحِيمِ

وَفِي أَنفُسِكُمْ ۚ أَفَلَا تُبْصِرُونَ

صدق الله العظيم

سورة الذاريات

أية (٢١)

Dedication

To.....

Father and Mother

Brother and Sisters

Acknowledgement

First of all, I thank the high Almighty Allah (SWT), whose Grace enabled me to continue this work and overcome all difficulties and our prophet Mohammed (peace and blessings of Allah be upon him) who invites us to science and knowledge.

I would like to express my sincere gratitude to my supervisor **Prof. Dr. Tahseen H. Mubarak** and **Prof. Dr. Raad M. S. Al-Haddad** who granted me the opportunity to do this research. I am indebted to them for their guidance, suggestions, valuable remarks and unfailing patience throughout my research work.

I would like to express my profound gratitude to **Prof. Dr. Nabeel A. Bakr** for his kind cooperation and constant supporting and I am indebted to him for his guidance, suggestions and valuable remarks.

My highly indebted is to **Prof. Dr. Sabah A. Salman** for his constant encouragement throughout my study in the Department of Physics, College of Science, University of Diyala.

Express my thanks to head of Physics Department **Asst. Prof. Dr. Ziad T. Khuthair** and **Asst. Prof. Dr. Ammar A. Habeeb,** for their endless support**.**

Special thanks are extended to the University of Diyala, College of Science and all the Staff of the Department of Physics for their assistance. I would also like to thank the staff of the Library of College of Science **Adnan J. Abd, Rafat A. Abbas and Anwar Kh. Raieed**, who continued to provide excellent service, tireless support and scientific resources to all students.

I would like to express my profound gratitude to **Dr. Zakariya Y. Sulaiman**/ University of Baghdad/ College of Science/ Department of Physics, **Dr. Maeda H. Mohammad, Dr. Zaynab S. Abdulghany & Dr. Ayman A. Hassan**/ Iraqi Center for Cancer and Medical Genetic

Researches/ Al-Mustansiriyah Universit**, Prof. Dr. Karim Al-Jashamy**/ Bilad ALrafidain University College**/** Department of Radiology Techniques**, Prof. Dr. Karim H. Hassan, Assist. Prof Dr. Fadhil L. Faraj & Zaid H. Mahmoud**/ University of Diyala/ College of Science/ Department of Chemistry and **Dr. Habeeb S. Jasim**/ University of Diyala/ College of Engineering**,** for their generous cooperation and continued support. Special thanks are extended to all the Staff of the Central Printing,University of Diyala.

My greatest indebtedness goes to my **Father, Mother, Brothers and Sisters** for their valuable advice, and to my Friends **Intesar K. Abd and Maher N. Abdulla** for their endless support.

I express my deep gratitude to my best friend **Chia H. Kareem** for her encouragement and cooperative.

Rusul K. Ismail

2019

Supervisors Certification

We certify that this thesis entitled "**Surface Plasmon Resonance of Gold and Silver Nanoparticles for Biomedical Physics Applications**" for the student (**Rusul Kareem Ismail**), was prepared under our supervisions at the Department of Physics, College of Science, University of Diyala in partial fulfillment of requirements needed to award the degree of **Doctor of Philosophy (Ph.D.) in Physics**.

Signature:
Name: **Dr. Tahseen H. Mubarak**
Title: Professor
Address: College of Science
University of Diyala
Date: 16 / 9/ 2019

Signature:
Name: **Dr. Raad M. S. Al-Haddad**
Title: Professor
Address: College of Science
University of Baghdad
Date: 16 /9/ 2019

Head of the Physics Department

In view of available recommendation, I forward this thesis for debate by the examining committee.

Signature:
Name: **Dr. Ziad T. Khodair**
Title: Assist. Professor
Head of the department of physics
Address: College of Science/ University of Diyala
Date: 17/9/ 2019

Linguistic Amendment

I certify that the thesis entitled **"Surface Plasmon Resonance of Gold and Silver Nanoparticles for Biomedical Physics Applications"** presented by student **(Rusul Kareem Ismail)** has been corrected linguistically, therefore, it is suitable for debate by examining committee.

Signature: K. Hass

Name: **Dr. Karim H. Hassan**

Title: Professor

Address: University of Diyala/ College of Science/ Department of Chemistry

Date: 24/11/ 2019

Scientific Amendment

I certify that the thesis entitled **"Surface Plasmon Resonance of Gold and Silver Nanoparticles for Biomedical Physics Applications"** presented by student **(Rusul Kareem Ismail)** has been evaluated scientifically, therefore, it is suitable for debate by examining committee.

Signature:

Name: Dr. **Estabraq T. Abdullah**

Title: Assistant Professor

Address: University of Baghdad/ College of Science/ Department of Physics

Date: 20/ 11 / 2019

Committee Certification

We certify that we have read this thesis, entitled "**Surface Plasmon Resonance of Gold and Silver Nanoparticles for Biomedical Physics Applications**", and as examining committee, examined the student "**Rusul Kareem Ismail**" on its content, and that in our opinion, it is adequate for the partial fulfillment of the requirements for the degree of **Doctor of Philosophy in (Physics)**.

Signature:
Name: **Dr. Nabeel A. Bakr**
Title: Professor
Date: 3 / 2 / 2020
(Chairman)

Signature:
Name: **Dr. Ziad T. Khodair**
Title: Assistant Professor
Date: 3 / 2 / 2020
(Member)

Signature:
Name: **Dr. Amer D. Majeed**
Title: Professor
Date: 3 / 2 / 2020
(Member)

Signature:
Name: **Dr. Adnan R. Ahmed**
Title: Assistant Professor
Date: 5 / 2 / 2020
(Member)

Signature:
Name: **Dr. Raheem G. Kadhim**
Title: Professor
Date: 6 / 2 / 2020
(Member)

Signature:
Name: **Tahseen H. Mubarak**
Title: Professor
Date: 9 / 2 / 2020
(Member/Supervisor)

Signature:
Name: **Dr. Raad M. S. Al-Haddad**
Title: Professor
Date: 4 / 2 / 2020
(Member/Supervisor)

Approval by the Dean of collage of science, University of Diyala

Signature
Name: **Dr. Tahseen H. Mubarak**
Title: Professor
Behave/ The Dean of the College of Science/ University of Diyala
Date: 9 / 2 / 2020

Published and Accepted Research Articles

- Rusul k. Ismail, Raad M. S. Al-Haddad and Tahseen H. Mubarak, "Time Effect on the Red Shift of Surface Plasmonic Resonance Core-Shell SiO_2: Gold Nanoparticles (AuNPs)", IP Conference Proceedings 2190, pp. 1-6, (2019).
- Rusul k. Ismail, Tahseen H. Mubarak and Raad M. S. Al-Haddad Surface Plasmon Resonance of Silver Nanoparticles: Synthesis, Ch3aracterization and Applications, J Biochem Tech, 10 (2), pp. 62-64, (2019).

Abstract

In this study, an identical surface plasmon resonance (SPR) within high surface energy of gold and silver nanoparticles spherical was chemically synthesized without and with coating by nano thin film layer of silica for treating the cell lines (MCF-7 and HBL-100).

Gold nanoparticles were chemically synthesized by Turkevich method from chloroauric acid and trisodium citrate dihydrate. The determination of the parameters effect such as temperature, trisodium citrate dihydrate content, deionized water volume, mixing speed, SiO_2 content, deionized water volume, gold nanoparticles solution volume and ethanol volume on the position of surface plasmon resonance (SPR), particle size, size distribution and shape gold nanoparticles in the blue and red shift regions were confirmed. While silver nanoparticles were chemically synthesized by reduction with gallic acid from silver nitrate and gallic acid, also the parameters effect such as time, gallic acid weight, temperature, SiO_2 content, silver nanoparticles solution volume and ethanol volume on position of surface plasmon resonance (SPR) of silver nanoparticles in blue and red shift regions were confirmed.

Optical measurements results showed peak band surface plasmon resonance (SPR) of gold nanoparticles (AuNPs) at 515nm and this peak shifted to 518nm after coating. In same time, the optical measurements of silver nanoparticles (AgNPs) adjusted by NaOH and NH_4OH showed that the peak band surface plasmon resonance (SPR) was shifted from 396nm to 398nm and from 405nm to 414nm respectively.

FTIR spectrum measurements results showed strong absorption peaks of the gold nanoparticles at 3431, 2341, 1627, 1506, 1388, 975, 962,632, 524 and 499 cm^{-1}, also strong absorption peaks showed at 3431, 2866, 2802, 2343, 2320 ,1622, 1616, 1494 1489 ,1384, 1379, 1072, 1062,

966, 655,636 543, 484 and 426 cm^{-1} of silver nanoparticles adjusted by NaOH and NH_4OH, also it is observed that the gold and silver nanoparticles after coating almost have the same absorption peaks with a little shift for some absorption peaks this means that the coating method led to a little increase in the size with maintaining on nanoparticles shape and prevents it from deforming, the absorption bands 524 and 499 cm^{-1} of gold nanoparticles refer to harmony happening between inorganic elements (gold) and organic compounds (Trisodium Citrate Dihydrate), while refer the absorption bands 543, 484 and 426 cm^{-1} of silver nanoparticles to harmony happening between inorganic elements (silver) and organic compounds (Gallic acid).

Structure measurements results showed that the gold nanoparticles have a narrow size distribution and spherical shape with an average size 3-6nm. On another hand, there was a narrow size distribution and a little increase in the particles size 9-18nm that retaining its spherical shape with stability increase from (−25.02mV) to (−25.92mV) after coating by nano thin film layer of silica. In same time, the structure measurements of silver nanoparticles (AgNPs) adjusted by NaOH and NH_4OH showed have a narrow size distribution and spherical shape with an average 6-8nm and 3-6nm respectively. On another hand, there was a narrow size distribution and a little increase in the particles size10-19nm and 12.9-16.7nm of coated AgNPs adjusted by NaOH and NH_4OH respectively that retaining its spherical shape with stability increase from (−58.17mV) and (−15.68mV) to (−62.86mV) and (−43.60mV) respectively after coating by nano thin film layer of silica.

Toxicity examination results showed of the surface plasmon resonance (SPR) of gold and silver nanoparticles without and with coating by nano thin film layer of silica have ability to destroy for MCF-7

cells at all concentrations. While, surface plasmon resonance (SPR) of gold and silver nanoparticles showed different effects on the normal HBL -100 cell line.

Therefore, the best optimization concentration of surface plasmon resonance (SPR) of gold nanoparticles (AuNPs) before and after coating by nano thin film layer of silica on MCF-7 and HBL-100 cell lines was 50μg/ml and 25μg/ml respectively showed the best rate of destroy MCF-7 cell line and on same time 50μg/ml and 25μg/ml was less the destroy rate of HBL-100 cell. While, the best optimization concentration of surface plasmon resonance (SPR) of silver nanoparticles (AgNPs) adjusted by NaOH and NH_4OH before and after coating by nano thin film layer of silica on MCF-7 and HBL-100 cell lines was 50μg/ml showed the best rate of destroy MCF-7 cell line and on same time 50μg/ml was increased the growth rate of HBL-100 cell.

Therefore, this study also provides the conclusive evidence of surface plasmon resonance (SPR) of gold and silver nanoparticles has toxic effect against breast cancer MCF-7 cell line at all concentrations compared with HBL-100 normal breast cell line. Further studies are required to elucidate the precise molecular mechanism involved in cell growth inhibition thereby permitting the synthesized chemically surface plasmon resonance (SPR) of gold and silver nanoparticles of cancer chemopreventive and/or therapeutic agents.

List of Contains

List of Figures

List of Tables

List of Abbreviations

Symbol	Definition
SPR	Surface Plasmon Resonance
SPE	Surface Plasmon Extinction
SERS	Surface Enhanced Raman Scattering
LSPR	Localized Surface Plasmon Resonance
SP	Surface Plasmon
SPB	Surface Plasmon Band
CNT	Carbon Nanotubes
QDs	Quantum Dots
QD	Quantum Dot
QC	Quantum Confinement
NPs	Nanoparticles
AuNPs	Gold Nanoparticles
GNPs	Gold Nanoparticles
AgNPs	Silver Nanoparticles
SNPs	Silver Nanoparticles
TCD	Trisodium Citrate Dihydrate
GA	Gallic Acid
NTFL	Nano Thin Film Layer
SA:V	Surface Area per Unit Volume Ratio
AR	Aspect Ratio
NIR	Near-Infra Red
ROS	Reactive Oxygen Species
PDT	Photodynamic Therapy
PVs	Photovoltics
BNCs	Bio-nanocomposites
UV-Vis	Ultraviolet-Visible
FTIR	Fourier Transform Infrared
AFM	Atomic Force Microscope
TEM	Transmission Electron Microscopy
FESEM	Field Emission Scanning Electron Microscope

AAS	Atomic Absorption Spectroscopy
SEM	Scanning Electron Microscope
SPM	Scanning Probe Microscope
STEM	Scanning Transmission Electron Microscopy
SAXS	Small Angle X-ray Scattering
DLS	Dynamic Light Scattering
MCF-7	Michigan Cancer Foundation-7
HBL-100	Human Breast Lactating, donor 100
SAR	Specific Absorption Rate
ROS	Reactive Oxygen Species
IC	Inhibitory Concentration
RPMI	Rosswell Park Memorial Institute
PBS	Phosphate Buffer Saline
MEM	Minimal Essential Medium
SFM	Serum Free Medium
FBS	Fetal Bovine Serum
DDW	Double Distilled Water
DDDW	Double Distilled Deionized Water
HEPES	(-hydroxyethyl)-1-piperazineethanesulfonic acid)-2)4
ICCMGR	Iraqi Center for Cancer and Medical Genetic Researches

List of Symbols

Symbol	Definition	Unit
A	Absorbance	-
λ	Wavelength	nm
I(z)	Intensity of the Incoming Beam After a Distance	eV/m^2. S
I_0	Incidient Intensity	eV/m^2. S
I	Transmit Intensity	eV/m^2. S
n_o , N	Number of Particles Per Unit Volume	cm^{-3}
σ_{ext}	Extinction Cross-Section of a Single Particle	cm^{-2}
σ_{sca}	Scattering Cross Sections of a Single Particle	cm^{-2}
σ_{abs}	Absorption Cross Sections of a Single Particle	cm^{-2}
ω_d	Scattering Frequency	Hz
v_F	Electron Velocity at Fermi Level	m/s
r_∞	Mean Free Path of the Electron in the Bulk Metal	nm
G	Free Energy or Gibbs Free Energy	J
ΔG	Gibbs Free Energy Change	$J\ m^{-3}$
ΔG*	Critical Free Energy Change	J
ΔH_f	Latent Heat of Fusion	$J\ m^{-3}$
H	Enthalpy	$J\ mol^{-1}$
S	Entropy	$J\ mol^{-1}\ K^{-1}$
γ	Surface Free Energy	$J\ m^{-2}$
T	Temperature	Kelvin
T_m	Melting Point	Kelvin
R"	Mean Free Path	nm
r , R	Particle Radius	nm
r*	Critical Radius	nm
C	Concentration	µg/ml
Mo	Molar Concentration	mol/l
M.Wt	Molecular Weight	g/mol
V	Volume of Solution	ml
Wt	Weight	g

Chapter One

Concept of Nanoscience and Literature Review

1.1 Introduction

This chapter includes general introduction about the history of nanophysics, nanoparticles and their distinctive characteristics that made them enter in many different applications physical and biological. In addition to the literature review and aim of the work.

1.2 History of Nanophysics

The nanophysics is halfway between the size scales of quantum mechanics and macroscopic physics governed by the laws of Newton and Einstein. The correct definition of nanophysics is the physics of structures and artefacts with dimensions in the nanometer range or of phenomena occurring in nanoseconds. Modern physical methods whose fundamentals are developed in physics laboratories have become critically important in nanoscience. Nanophysics brings together multiple disciplines, using theoretical and experimental methods to determine the physical properties of materials in the nanoscale size range. Interesting properties include the structural, electronic, optical, and thermal behavior of nanomaterials; electrical and thermal conductivity; the forces between nanoscale objects; and the transition between classical and quantum behavior. Nanophysics has now become an independent branch of physics, simultaneously expanding into many new areas and playing a vital role in fields that were once the domain of engineering, chemical, or life sciences [1].

Nanoscience and nanotechnology are all about relating and exploiting phenomena for materials having one, two or three dimensions reduced to the nanoscale. Breakthroughs in nanotechnology require a firm grounding in the principles of nanophysics. It is intended to fulfill a crucial purpose. Nanophysics aims to connect scientists with disparate interests to begin interdisciplinary projects and incorporate the theory and

methodology of other fields into their work. Their evolution may be related to three exciting happenings that took place in a short span from the early to mid-1980s with the award of Nobel prizes to each of them. These were: (i) the discovery of quantum Hall effect in a two-dimensional electron gas; (ii) the invention of scanning tunnelling microscopy (STM); and (iii) the discovery of fullerene as the new form of carbon. The latter two, within a few years, further led to the remarkable invention of the atomic force microscope (AFM) and, in the early 1990s the extraordinary discovery of carbon nanotubes (CNT), which soon provided the launch pad for the present-day nanotechnology [2].

The STM and AFM have emerged as the most powerful tools to examine, control and manipulate matter at the atomic, molecular and macromolecular scales and these functionalities constitute the mainstay of nanotechnology. Interestingly, this exciting possibility of nanolevel tailoring of materials was envisioned way back in 1959 by Richard Feynman in his lecture, "There's plenty of room at the bottom" [3].

1.3 Classification of Nanomaterials

Nanoscale materials are defined as a set of substances where at least one dimension is less than approximately 100 nanometers. Nanomaterials are of interest because at this scale unique optical, magnetic, electrical, and other properties emerge. These emergent properties have the potential for great impacts in electronics, medicine, and other fields.

According to the order of dimensionality, Nano materials can be classified as zero, one, two and three dimensional nanostructures [4].

1. Zero-dimensional (0-D) nanostructures

Zero-dimensional Nano materials are materials where all the dimensions are measured within the Nano scale. Also named as NPs with all possible morphologies, such as spheres, cubes and platelets these NPs include single crystal, polycrystalline and amorphous particles. If the NPs are single crystalline, they are often referred to as Nano crystals. When the NPs have dimension sufficiently small and quantum confinement effects are observed, the common term used to describe such NPs is quantum dots [4].

2. One-dimensional (1-D) nanostructures

The one-dimension Nano materials have one dimension that is outside the Nano scale. This type has been called by a change of names such as: whiskers, fibers or fibrils, nanowires and Nano rods. In many cases one-dimensional systems take into account carbon-based, metal-based or even oxide-based systems. Nanotubes and Nano cables are also considered one dimensional structures if the extension over one dimension is predominant over the other types [4-6].

3. Two-dimensional (2-D) nanostructures

Two-dimensional Nano materials are materials in which two of the dimensions are not confined to the Nano scale. They are one more important nanostructure, they include many shapes such as Nano films, Nano layers, Nano coatings and Nano discs, and thus they have been a subject of intensive study for almost a century [4-6].

4. Three dimensions (3-D) system

Three-dimensional Nano materials, as well known as bulk Nano materials, are relatively difficult to classify. However, it is true to say that bulk Nano materials are materials that are not confined to the Nano scale

in any dimension. These materials are thus characterized by having 3 randomly dimension above 100 nm [4].

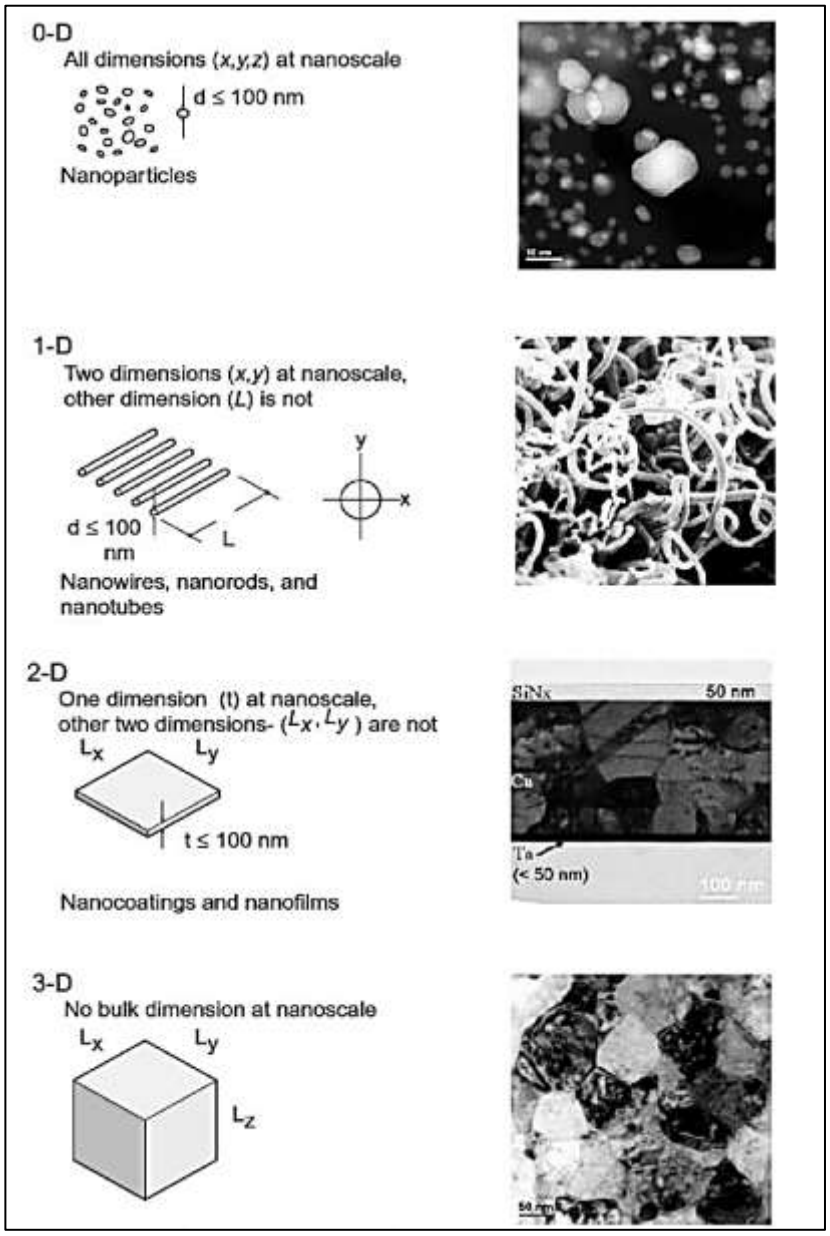

Fig 1.1: Classification of nanomaterial according to 0-D, 1-D, 2-D and 3-D [4].

1.4 Nanoparticles

The term "nanoparticles" is used to describe a particle with size in the range of 1-100nm, at least in one of the three possible dimensions. In this size range, the physical, chemical and biological properties of the nanoparticles changes in fundamental ways from the properties of both

individual atoms/molecules and of the corresponding bulk materials. Nanoparticles can be made of materials of diverse chemical nature, the most common being metals, metal oxides, silicates, non-oxide ceramics, polymers, organics, carbon and biomolecules. Nanoparticles exist in several different morphologies such as spheres, cylinders, platelets, tubes etc. Generally the nanoparticles are designed with surface modifications tailored to meet the needs of specific applications they are going to be used for [7].

1.5 Types of Nanoparticles

Nanoparticles can be broadly grouped into two, namely, organic nanoparticles which include carbon nanoparticles (fullerenes) while, some of the inorganic nanoparticles include magnetic nanoparticles, noble metal nanoparticles such as (gold and silver) and semi-conductor nanoparticles such as (titanium oxide and zinc oxide). There is a growing interest in inorganic nanoparticles i.e. of noble metal nanoparticles (gold and silver) as they provide superior material properties with functional versatility. Due to their size features and advantages over available chemical imaging drug agents and drugs, inorganic particles have been examined as potential tools for medical imaging as well as for treating diseases. Inorganic nonmaterial have been widely used for cellular delivery due to their versatile features like wide availability, rich functionality, good compatibility, and capability of targeted drug delivery and controlled release of drugs [7].

1.6 Noble Metal Nanoparticles

Noble metal nanoparticles such as Ag and Au NPs have been a source of great interest due to their novel electrical, optical, physical,

chemical and magnetic properties [8,9]. They were very attractive for biophysical, biochemical, and biotechnological applications due to their unusual physical properties, especially due to their sharp plasmon absorption peak at the visible region. Gold and silver nanoparticles are chemically stable and typically exhibit surface enhanced Raman scattering (SERS) in the visible wavelength range, where they may cause a tremendous increase in various optical cross-sections. The resonance frequencies strongly depend on particle shape and size as well as on the optical properties of the material within the near-field of the particle [10]. Silver, for example, has been for thousands of years, used as a disinfectant; from the other side nobody can neglect its value as a catalyst [11]. On the other hand, gold nanoparticles have gained considerable attention in recent years for potential applications in nanomedicine due to their interesting size dependent chemical, electronic and optical properties. Also, gold nanoparticles show promise in four enhancing the effectiveness of various targeted cancer treatments such as radiotherapy and photothermal therapy [12].

Metals nanoparticles exhibit improved properties such as plasmon resonance characteristics depending upon their size and morphologies [13]. An interesting thing about some metallic nanoparticles and especially silver and gold nanoparticles, is that these particles show strong plasmonic properties. When light photons interact with the surface of metal nanoparticles, the outer free electrons of the particles form localized plasmons [14]. Plasmons are density waves of the free outer electrons. Specific wavelengths of light cause the outer electrons to oscillate. This phenomenon is called the surface plasmon resonance (SPR). When these resonances occur, the intensities of absorption and scattering are much higher than those of the same particles without plasmonic properties. SPR are highly dependent on particle

characteristics [15]. A wide range of metal nanoparticles applications has emerged in consumer products ranging from disinfecting medical devices and home appliances to water treatments. Here we mainly discuss the applications of metal nanoparticles in biomedical.

1.6.1 Advantages of Metallic Nanoparticle

- Enhance Rayleigh scattering
- Surface enhanced Raman scattering
- Strong plasma absorption
- Biological system imaging
- Determine chemical information on metallic nanoscale substrate [16].

1.6.2 Disadvantages of Metallic Nanoparticles

- **Particles instability:** Nanomaterials can undergo transformation, as they are thermodynamically unstable and lie in the region of high energy local minima. This leads to deterioration of quality, poor corrosion resistance, and main concerned is retaining the structure becomes difficult.
- **Impurity:** While synthesising nanoparticles, nitrides, oxides, formation can aggravated from the impure environment. As nanoparticles are highly reactive, there can also be high chances of impurity as well. In solution form, nanoparticles should be synthesized in form of encapsulation. So, it becomes a challenge to overcome impurity in nanoparticles.
- **Biologically harmful:** nanomaterials has been reported toxic, carcinogenic and cause irritation as they become transparent to the cell dermis.

- **Explosion:** exothermic combustion can lead to explosion, as fine metal particles act as strong explosives.
- **Difficulty in synthesis:** while synthesizing nanoparticles, it should be encapsulated, because it is extremely challenging to retain the nanoparticles size in solution form [17].

1.6.3 Characteristics of Metallic Nanoparticles

- Large surface energies
- As compared to bulk they have large surface area to volume ratio
- Quantum confinement
- Plasmon excitation
- Increased number of kinks [18].

1.7 Literature Review

Castanon *et al*. (2008) prepared silver nanoparticles chemically from gallic acid, and studied antibacterial activity of silver nanoparticles with different sizes. UV–Vis spectrum show that the absorption spectrum of spherical silver nanoparticles present a maximum 420-450nm. TEM show that AgNPs are spherical and pseudospherical shape with the size ranges 7-89nm. It was found that the antibacterial activity of the nanoparticles varies when their size diminishes [19].

Tabrizi *et al*. (2009) prepared gold nanoparticle chemically by Turkevich method from chloroauric acid and trisodium citrate dehydrate, and also determined the effect of initial gold concentration, trisodium citrate concentration and mixing rate on particle size and size distribution were investigated the advantages for self-assembled monolayer formation and enhanced surface area [20].

Bahadur *et al*. (2011) prepared gold nanoparticles chemically from chloroauric acid and trisodium citrate dehydrate with a mean particle size 16nm. Au@SiO_2 nanoparticles prepared by microwave method the size uniformity and monodispersity were found to be better compared to the particles prepared by conventional methods. UV–Vis spectrum showed that the absorbance of SPR of AuNPs without coating at 522nm and this peak was shifted to longer wavelength after coating. Zeta potential of AuNPs before coating -52 mV and increase zeta potential of AuNPs after coating [21].

Amarnath *et al*. (2011) studied facile synthesis of biocompatible gold nanoparticles from vites vinefera and its cellular internalization against HBL-100 cells. Absorption measurements indicated that the Plasmon resonance wavelength of GAuNPs was 535 nm. TEM shows that AuNPs have spherical shape with the size ranges 20-45nm. Higher concentration of AuNPs conjugate, there was an asymmetric accumulation of AuNPs in the periphery of the cell nucleus of the HBL-100 cells which was confirmed by fluorescence microscopy [22].

Vivek *et al*. (2012) studied green biosynthesis of silver nanoparticles from Annona squamosa leaf extract and its in vitro cytotoxic effect on MCF-7and normal HBL-100 cells. UV–Vis spectrum showed an absorption peak SPR of AgNPs at 444nm. TEM photography showed that AgNPs have spherical shape with the size ranges 20-100nm. The zeta potential value was -37mV. The cytotoxicity effect of AgNPs against MCF-7 increases with increasing concentration of AgNPs and did not affect the normal cells (HBL-100). However, increased concentration of AgNPs produced significant toxicity against the normal HBL 100 cells [23].

Jeyaraj *et al*. (2013) prepared biogenic silver nanoparticles from sesbania grandiflora leaf extract, and studied cytotoxicity effect of (AgNPs) against

MCF-7 cells. UV–Vis spectrum showed an absorption peak SPR 420nm. FT-IR spectrum shows the strong band at 1646cm^{-1} corresponds to the C=C stretches and broad peaks at 3394cm^{-1} clearly indicates the N-H stretches. The prominent bands at 1070cm^{-1} can be assigned as absorption bands of C-O-C. The band at 1397cm^{-1} in AgNPs may attribute to C-O stretching mode. FESEM micrograph, shows spherical shaped particles with the average size range 22 nm. AgNPs induce cytotoxicity on MCF-7 cell lines was found to be higher with increased concentration of AgNPs [24].

Britto and Química (2013) prepared silver nanoparticles using polyvinylpyrrolidone (PVP) as stabilizing agent, and capping AgNPs with mesoporous silica was obtained by sol-gel reaction using tetraethylorthosilicate (TEOS) in the presence of hexadecyltrimethyl ammonium bromide (CTAB). UV–Vis spectrum showed a single narrow band of AgNPs and AgNPs-SiO_2 at 419nm and 425nm respectively. Zeta potential analysis revealed stable AgNPs and AgNPs-SiO_2 -1.10mV and -28.9mV respectively. STEM shows silver-mesoporous silica nanoparticles, where nanoparticles with core-shell architecture and spherical shape are observed. SAXS shows AgNPs have 19 nm size whereas AgNPs- SiO_2 have 21 nm size [25].

Rejeeth *et al*. (2014) studied biosynthesis of silver nanoscale particles using spirulina platensis induce growth-inhibitory effect on MCF-7. UV–Vis spectrum showed an absorption peak SPR of AgNPs at 420nm. The zeta potential value of -36mV revealed the stability of AgNPs. SEM analysis, shows less aggregation with particles are spherical in shape and the size ranges 10-200nm. The in vitro screening of the AgNPs showed potential cytotoxic activity against MCF-7 and HBL-100 cells the inhibitory concentration (IC_{50}) were found to be 20, 40, 60 and 80 µg/ml

for AgNPs against MCF-7 and HBL-100 cells at 24 and 48h incubation respectively [26].

Sulthana *et al*. (2014) prepared silver nanoparticle chemically from gallic acid and studied antiphytopathogenic activity. The reduction of pure Ag^{+} ions was monitored by measuring in the UV-Vis Spectroscopy at 426nm. The plasma resonance of the gallic acid reduced silver particle is brownish yellow. TEM photography showed that AgNPs are spherical shape with the size range 14-60nm. Broth dilution method revealed antiphytopathogenic activity of the gallic acid reduced Terminalia chebula Retz. Silver nanoparticles against Xanthomonos axonopodis pv. malvacearum at a concentration of 70μg/ml [27].

Lakshmipathy and Nanda (2015) prepared silver nanoparticle chemically from gallic acid, and studied its biomedical application. UV–Vis spectrum showed narrow peak with λ_{max} at 424nm. FESEM micrograph show the narrow size distribution of AgNPs with size <30nm and spherical to nearly spherical in shape. AgNPs showed potent antiproliferative activity on HEp-2 cells with IC_{50}<1mg/mL concentration accompanied by morphological disturbances and membrane damage. The strong affinity toward intracellular proteins and thiol formation accounts for its toxicity which may further be extended for varied biomedical applications as a broad spectrum therapeuticagent [28].

Loutfy *et al*. (2015) prepared gold nanoparticles and silver nanoparticle chemically from (chloroauric acid and trisodium citrate dehydrate) and (Silver nitrate, sodium citrate and polyvinyl pyrrolidone (PVP)) respectively, and studied the cytotoxic effects of metallic nanoparticles on MCF-7 cells. UV-Vis spectrum revealed a peak at 522nm and 405nm of AuNPs and AgNPs respectively. TEM photography showed that AuNPs and AgNPs are spherical shape. Zeta potential of AuNPs and AgNPs -33.6mV and -9.45mV respectively. Treatment of MCF-7 different with

different concentrations, with IC_{50} value at 14.48μM of AuNPs and IC_{50} value at 6.28μM of AgNPs [29].

Rahman (2016) prepared gold nanoparticles chemically by Turkevich method from chloroauric acid and trisodium citrate dehydrate. UV–Vis spectrum showed SPR Peaks occurs 517nm. SEM images showed that GNPs are spherical shape and different size GNPs exist in the solution which would cause some discrepancy between the actual and theoretical calculation [30].

Yahia and Al-Haddad. (2017) prepared gold nanoparticles chemically by Turkevich method from chloroauric acid and trisodium citrate dehydrate, then they were coated with sodium silicate stock solution and studied the effect of silica concentrations on the absorbance of AuNPs. UV-Vis spectrophotometer showed that the absorbance of SPR of AuNPs without coating at 521nm and 522nm with coating [31].

Acharya *et al*. (2017) studied comparative antibacterial properties of Ag and Ag@SiO_2 core-shell nanoparticles. UV–Vis spectrum showed the SPR peak of AgNPs at 425nm while for silica coated silver nanoparticles, the SPR peak shifts to 426nm. TEM photography showed that average size of AgNP ~14nm and average size of silica coated silver nanoparticles ~17nm [32].

Afrapoli *et al*. (2018) [35] prepared gold nanoparticles chemically by Inversed Turkevich from chloroauric acid and trisodium citrate dehydrate, and studied the effect of concentration and temperature on size. UV- Vis spectra show that absorbance curve of each samples had a single visible peak that was positioned in range of 519-531nm and it was related to spherical monodisperse gold nanoparticles. TEM photography showed that gold nanoparticles are spherical shape with the average size of 11.82±1.77nm [33].

Yadav (2018) Prepared gold nanoparticles chemically by Turkevich method from chloroauric acid and trisodium citrate dehydrate. UV–Vis spectrum showed peak band at 520nm. FTIR spectrum shows peaks at 3129.94 and 3003cm^{-1} are assigned to C-H ring stretching vibrations. The peaks at 1637 and 1474.79 cm^{-1} correspond to N-H bending (or C=C-bond) and the symmetric component of the C-C (or C-H) stretching modes. The bands at 1231 and 1059.30 cm^{-1} can be attributed to C-N bonding. Zeta potential of AuNPs -19 mV [34].

Thapliyal and Chandra (2018) Prepared silver nanoparticle chemically from gallic acid, and studied its antibacterial and anticancer potential of silver nanoparticles synthesized. UV–Vis spectrum showed narrow peak with λ_{max} at 412nm. SEM and DLS measurements showed spherical nanoparticles with a mean size of 68.06±0.2 nm. The negative surface zeta potential with -32±0.25 mV has indicated colloidal stability of nanoparticles. The synthesized AgNPs in bio-nanocomposites (BNCs) is a potential candidate for inhibiting the growth of pathogenic bacteria and showed significant cytotoxicity against MCF-7 cancer cell line with IC_{50} of 160±0.014μg [35].

Dong *et al.* (2019) prepared gold nanoparticles chemically by Turkevich method from chloroauric acid and trisodium citrate dehydrate. The effect of the molar ratio of the reagent mixture (trisodium citrate to gold chloride), the scaled-up batch size, the initial gold chloride concentration, and the reaction temperature were studied. The AuNPs size was tuned from 15nm to 50nm by decreasing the molar ratio of NaCt to $HAuCl_4$ from 2.8 to 1.5. However, the AuNPs became more polydispersed and less spherical as the molar ratio de-creased. The batch synthesis was scaled up to 1.5L and the as-synthesized AuNPs exhibited identical optical property and morphology as the AuNPs synthesized in 50ml batches. At a constant molar ratio, the initial con-centration of $HAuCl_4$

had minimal effect on the final particle size and size distribution within the range tested. The particle size increased with decreasing reaction temperature at the molar ratio of 2.5. However, there was no significant effect of temperature on the particle size at the molar ratio of 7.6 [36].

1.8 Aim of the Work

- To synthesis the surface plasmon resonance (SPR) of gold and silver spherical nanoparticles.
- To determine the identical surface plasmon resonance (SPR) within high surface energy of gold and silver spherical nanoparticles in the blue and red shifts.
- To maintain and control on the shape and size of the nanoparticles and increasing its stability by coating nano thin film layer of silica.
- To evaluate the biological effect of gold and silver spherical nanoparticles without and with coating by nano thin film layer of silica on the treatment of the human breast cancer cell line (MCF-7) and normal cell (HBL-100).

Chapter Two

Theoretical Considerations

2.1 Introduction

This chapter includes nanoparticles a general description of the theoretical aspect of the subject of the present study, in terms of ideas, theoretical physical concepts, scientific explanations, relationships and mathematical laws through which the results obtained can be interpreted scientifically.

2.2 Interaction of Light with Noble Metal Nanoparticles

The intensity of light which propagates through a medium containing small particles is reduced by scattering and absorption. The extinction of the light beam is given by [37]:

$$I(z) = I_0 \exp(-n_0 \sigma_{ext} z) \qquad \text{……..(2.1)}$$

where I(z) are the intensity of the incoming beam after a distance z, n_0 the number of particles per unit volume and σ_{ext} the extinction cross section of a single particle. It holds [37]

$$\sigma_{ext} = \sigma_{abs} + \sigma_{sca} \qquad \text{…….. (2.2)}$$

where σ_{abs} and σ_{sca}: is the absorption and scattering cross sections of a single particle, respectively.

The optical properties of such particles, as a consequence of their reduced dimensions, are dominated by a coherent collective oscillation of their conduction band electrons. As a result, the absorption cross section, which scales with their volume, can reach values several orders of magnitude larger compared to common organic dye molecules. Such collective oscillation is known as surface plasmon resonance [37].

2.2.1 Surface Plasmon Resonance (SPR) in Metal Nanoparticles

The free electrons in conduction band in some of the noble metals like Au and Ag are able to move through the materials bulk. However,

the mean free path of electrons in the material's molecules is actually smaller than their bulk (for example for Au~50nm). Therefore, when free electrons of these metals with smaller dimensions (nanometer scale), couple with electromagnetic waves of incident light, they start to oscillate collectively on the surface of metal NPs. This phenomenon, which occurs in the metal-dielectric medium interface is called Surface Plasmon Resonance (SPR). One of the typical behaviors that can be observed by plasmonic materials is called Localized Surface Plasmon Resonance (LSPR). As it is shown in Figure (2.1), LSPR takes place when metal NPs have smaller dimensions than the wavelength of incident light and it causes coherent oscillation of the electrons in conduction band. The plasmonic resonance can be simply detected by absorption or scattering spectroscopy and it is found to be altered by several parameters like shape, size and surrounding materials dielectric constant [38,39].

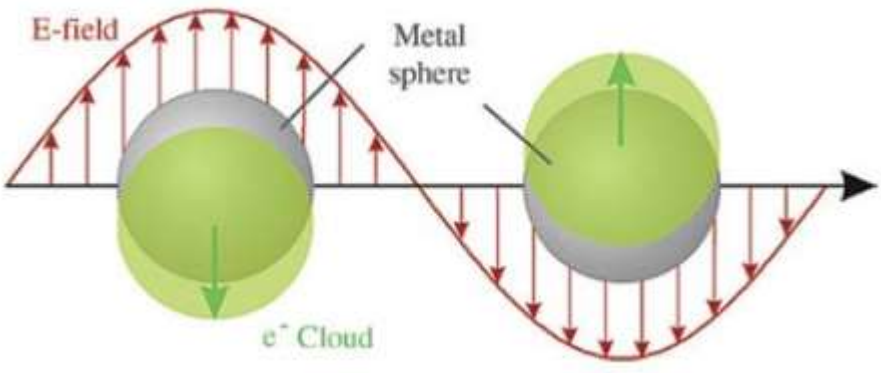

Fig 2.1: Oscillation of the electrons in the conduction band of the metal NP by incident light with certain wavelength [40].

Nowadays the interests in unique properties of plasmonic particles (mainly Au and Ag), have raised several investigations in different fields such as surface enhanced Raman spectroscopy, sensing technologies and photovoltics (PVs) [41].

2.2.2 Mie Theory

The general solution of the interaction problem of a single homogeneous sphere, of the radius R, and of arbitrary material with an incident electromagnetic field was first given by Mie in 1908[44]. Mie presented a solution to Maxwell's equations that describes the extinction spectra of spherical particles of arbitrary size embedded in a homogeneous medium. One of the reasons why Mie's theory has remained important for so long is that it is the only simple, exact solution to Maxwell's equations that is relevant to particles. It is also worth mentioning that in his calculation, he introduces the dielectric function $\varepsilon(\omega,R)$ at the angular frequency ω to treat the material problem, which can incorporate all the size effects. The spherical symmetry suggests the use of a multipole extension of the fields, giving Mie's calculations a series of multipole oscillations (dipole, quadrupole, etc.) for the absorption and the scattering cross section of the particles as a function of the particle radius. The extinction spectrum is then composed of the sum of absorption and scattering modes, each of which has a contribution that depends on the particle size. Higher-order modes become more dominant with increasing particle size. Physically, this can be explained by the fact that for larger particles, the light cannot polarize the nanoparticles homogeneously and retardation effects lead to the excitation of higher-order modes. Mie's theory and experimental spectra agree well until for bulk metals, the normal incidence absorption no longer shows a plasmon resonance. Although his theory describes accurately the optical extinction spectra of metal nanoparticles, it does not explain the physical process, i.e. the collective oscillation of the conduction band electrons. The term plasmon for the Mie resonances was proposed first by Schopper in 1931[42-44].

Mie theory plays a crucial role in describing the optical properties of metal nanoparticles, especially gold particles. One of the important uses of this theory in describing the size dependence of position SPR. Mie theory easily describes red shifts and broadening of the dipole Plasmon resonance as particle size is increased, as well as the appearance of quadrupole and higher resonance contributions [45].

First we define that when a spherical metal nanoparticle with radius r embedded in homogeneous medium resonates at certain wavelengths, the orders (dipole or multiples) of different resonant modes are expressed with m = 1 (first order, dipole), 2 (second order,), 3 (third order), ..., as shown in figure (2.2,a and b). Then we assume that for each order, when the surface plasmon resonance happens, it is a standing wave formed by two SPR waves propagating clockwise and counterclockwise along the surface. So the wavelength of the wave will be

$$\lambda_m = \frac{2\pi r}{\mathrm{m}} \qquad \text{..... (2. 3)}$$

When m=1 (dipole resonance), the wavelength of the surface plasmons equals to the perimeter of the sphere, i.e. 2πr [46].

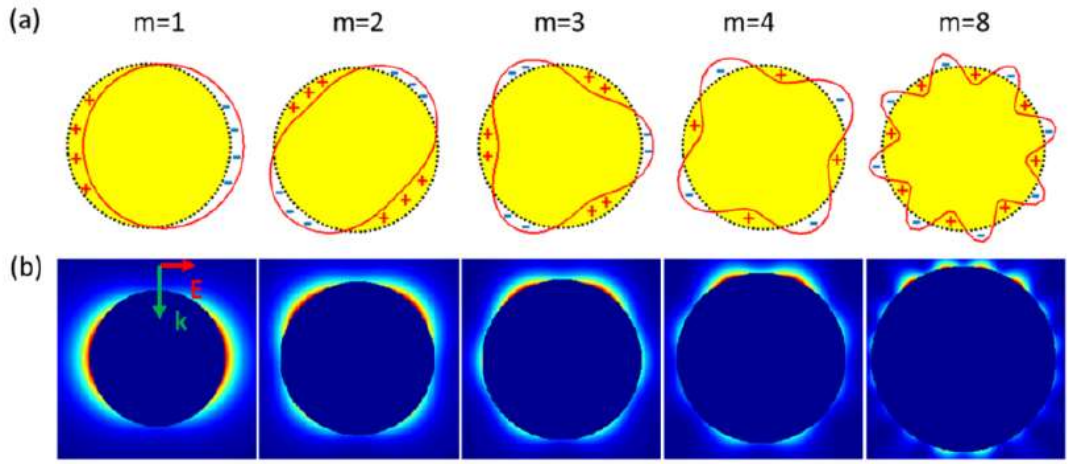

Fig 2.2: (a) Illustration of charge distributions of different orders of surface plasmon resonant modes. (b) Corresponding electric field patterns of a silver nanosphere in air calculated by Mie theory [46].

2.3 Surface Area per Unit Volume Ratio

The surface area divided by the volume is known as the surface to the volume ratio - and variously denoted sa/vol or SA:V (L^{-1} inverse length) is the amount of the surface area per unit volume of an object or a collection of objects. Despite their small dimensions, nanomaterials have an extremely large surface area compared to the volume or large surface area to the volume ratio, which makes a large fraction of atoms to be on the surface or interfacial atoms of the material, resulting in more "surface" dependent material properties [47].

The surface properties of the nanomaterials in turn will be effected in the entire material. This may modify or enhance the properties of the bulk materials. The gold is an inert element at the macro scale, and it does not react with many chemicals reactivity, whereas the quantum dot of the gold nanoparticles at the nanoscale are become extremely reactive and can be used as a catalyst in order to speed up the chemical reactions [48]. The surface area to volume ratio is an important factor for the reactivity in the chemical reactions involving a solid material at which the rate of reactivity will proceed [49], see Figure (2.3).

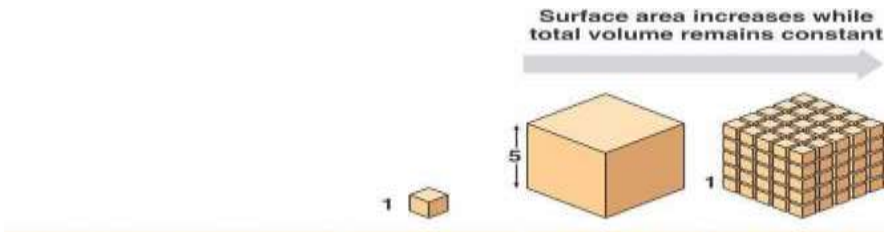

Total surface area (height × width × number of sides × number of boxes)	6	150	750
Total volume (height × width × length × number of boxes)	1	125	125
Surface-to-volume ratio (surface area / volume)	6	1.2	6

Fig 2.3: SA:V for cubic shape [49].

The sphere for a given volume is the object with the smallest surface area and therefore with the smallest SA:V, a consequence of the isoperimetric inequality in 3 dimensions. By contrast, the objects which have tiny spikes will have a very large surface area for a given volume, For example, let us consider r is the radius of a sphere then the surface area will be $4\pi r^2$, and the volume is $4/3\pi r^3$, therefore the surface area to the volume ratio will be $4\pi r^2/\{4/3(\pi r^3)\} = 3/r$. It means that the surface area to volume ratio increases with the decrease in radius of the sphere and vice versa [50]. See Figure (2.4) and Table (2.1).

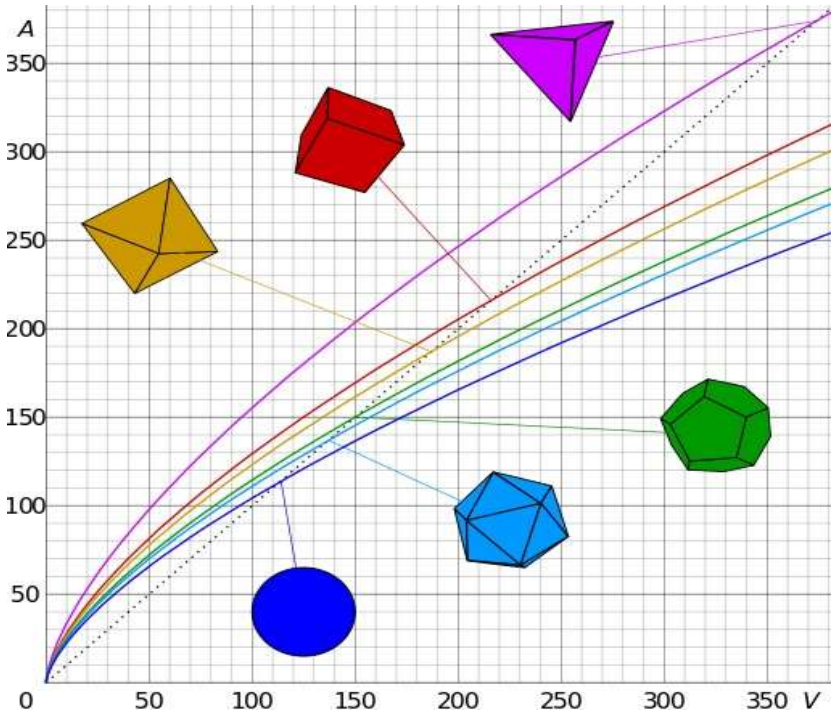

Fig 2.4: Graphs of surface area, A against volume, V of the Platonic solids and a sphere, showing that the surface area decreases for rounder shapes, and the surface-area-to-volume ratio decreases with increasing volume [50].

When the great amount of atoms are found on the surface material, the size of these particles have been decreased compared to those inside the same material. For instance, a particle size 30 nm has 5% of atoms on surface. At size 10 nm, 20% of atoms on surface, and at size 3 nm has 50% of atoms on surface (Fig 2.5a, b) [51].

Table 2.1: The sphere has the lowest sa/v ratio [50].

Name	shape	SA/V ratio for unit volume (L^{-1})
Tetrahedron		7.21
Cube		6
Octahedron		5.72
Dodecahedron		5.31
Icosahedron		5.148
Sphere		4.836

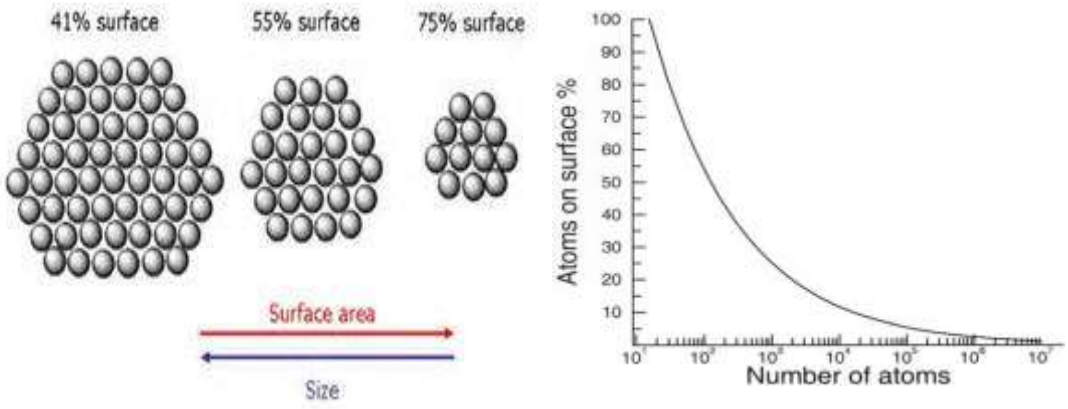

(a) **(b)**

Fig 2.5: (a) Size, area and atoms at the surface relation. (b) Atoms number on the surface and size relation [51].

2.4 Quantum Confinement and Quantum Dot

A transition from the behavior of classical physics to the behavior of quantum mechanics occurs when the size of the particles is decreased and started to modify the properties of the material. As a result, the continuous optical transitions of electrons between the electronic energy

bands become discrete or the energy of electronic levels are quantized [52]. In the nano scales the electronic energy levels are confinement of the wave function of the electron to the physical dimensions of the particles, this phenomenon is called or known as quantum confinement (QC), and crystals are referred as quantum dots (QD). This phenomenon is called the exciton Bohr radius which is a resultant from electron holes and electrons are being aqueezed and approached into a dimension to a critical quantum measrments, where the motion of a particle is restricted by potential well in one or more dimensions and the energy is increased. In the bulk materials where the particle behaved as it free when the confining dimension is large as compared to the wavelength of the particle [53]. When the nanomaterials approach to nanometer scale and feature their sizes, it also have a spatial confinement effect on the materials, which the quantum effects is appeared. Nanoparticles can be viewed as quantum dot of zero dimension while nanotubes and nanowires are quantum wires of one dimension. The quantum confinement of nano materials has profound effects on their properties [54, 55].

2-5 High Surface Energy

In materials, the energy band structure and the density of the charge carrier can be modified quite differently form their bulk and in turn will modify the optical and electronic properties. Nanoparticles can be stabilized in solutions, electrostatically. The diffused layers around nanoparticles is a repulsive interactions called Van der Waals interactions [56]. The summation of two energies determines the stability of the particle. Low electrolyte concentrations and high diffuse layer potentials will increase the repulsion range which are necessary for the stability of nanoparticles. The ligands which form a chemical bonds with surface of the particle surface are an effective method for stabilization of

nanoparticles which also enable to use them for a variety of purposes. The stabilized nanoparticles can be repeatedly isolated from and dissolved in the dispersing solvent without irreversible aggregation or decomposition [57].

2.6 The Kinetics of Phase Transformations

With phase transformations, normally at least one new phase is formed that has different physical / chemical characteristics and/or a different structure than the parent phase. Furthermore, most phase transformations do not occur instantaneously. Rather, they begin by the formation of numerous small particles of the new phase (s), which increase in size until the transformation reached completion. The progress of a phase transformation may be broken down into two distinct stages: nucleation and growth. Nucleation involves the appearance of very small particles, or nuclei of the new phase (often consisting of only a few hundred atoms), which are capable of growth. During the growth stage these nuclei in size, which results in the disappearance of some (or all) of the parent phase. The transformation reaches completion if the growth of these new phase particles is allowed to proceed until the equilibrium fraction is attained. We now discuss the mechanics of these two processes, and how they relate to solid-state transformation [58].

2.6.1 Nucleation

There are two types of nucleation: homogeneous and heterogeneous. The distinction between them is made according to the site at which nucleating events occur. For the homogeneous type, nuclei of the new phase is formed uniformly throughout the parent phase, whereas for the heterogeneous type, nuclei is formed preferentially at structural in

homogeneities, such as container surface, insoluble impurities, grain boundaries, dislocations and so on. We begin by discussing homogeneous nucleation because its description and theory are simpler to treat. Principles are then extended to a discussion of the heterogeneous type [58].

2.6.1.1 Homogeneous Nucleation

A discussion of the theory of nucleation involves a thermodynamic parameter called free energy (or Gibbs free energy), G. In brief, free energy is a function of other thermodynamic parameters, of which one is the internal energy of the system (i.e., the enthalpy, H), and another is a measurement of the randomness or disorder of the atoms or molecules (i.e., the entropy, S). It is not our purpose here to provide a detailed discussion of the principles of thermodynamics as they apply to materials systems. However, relative to phase transformations, an important thermodynamic parameter is the change in free energy ΔG; a transformation will occur spontaneously only when ΔG has a negative value. For the sake of simplicity, let us first consider the solidification of a pure material, assuming that nuclei of the solid phase form in the interior of the liquid as atoms cluster together so as to form a packing arrangement similar to that found in the solid phase. Furthermore, it will be assumed that each nucleus is spherical in geometry and has a radius r. This situation is represented schematically in Figure (2.6). There are two contributions to the total free energy change that accompany a solidification transformation. The first is the free energy difference between the solid and liquid phases, or the volume free energy, ΔGv. Its value will be negative if the temperature is below the equilibrium solidification temperature, and the magnitude of its contribution is the

product of ΔGv, and the volume of the spherical nucleus (i.e., $\frac{4}{3}\pi r^3$). The second energy contribution results from the formation of the Solid-liquid phase boundary during the solidification transformation [58].

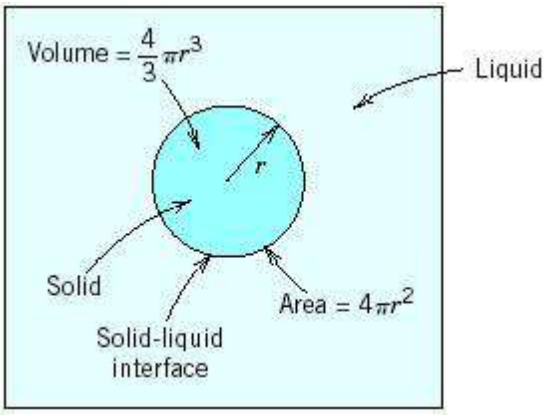

Fig 2.6: Schematic diagram showing the nucleation of a spherical solid particle in a liquid [58].

Associated with this boundary is a surface free energy, γ, which is positive; furthermore, the magnitude of this contribution is the product of γ and the surface area of the nucleus (i.e,. $4\pi r^2$). Finally, the total free energy change is equal to the sum of these two contribution- that is,

$$\Delta G = \frac{4}{3}\pi r^3 \Delta G_v + 4\pi r^2 \gamma \quad \ldots\ldots\ldots\ldots (2.4)$$

These volume, surface, and total free energy contributions are plotted schematically as a function of nucleus radius in figures (2.7,a and 2.7,b). It will be noted from figure (2.7a) that for the curve corresponding to the first term on the right-hand side of Equation (2.4), the free energy (which is negative) decreases with the third power of r. Furthermore, for the curve resulting from the second term in Equation (2.4), energy values are positive and increase with the square of the radius. Consequently, the curve associated with the sum of both terms (Figure 2.7b) first increases, passes through a maximum, and finally decreases. In a physical sense, this means that as a solid particle begins to

form as atoms in the liquid cluster together, its free energy first increases. If this cluster reaches a size corresponding to the critical radius r*, then growth will continue with the accompaniment of a decrease in free energy [58].

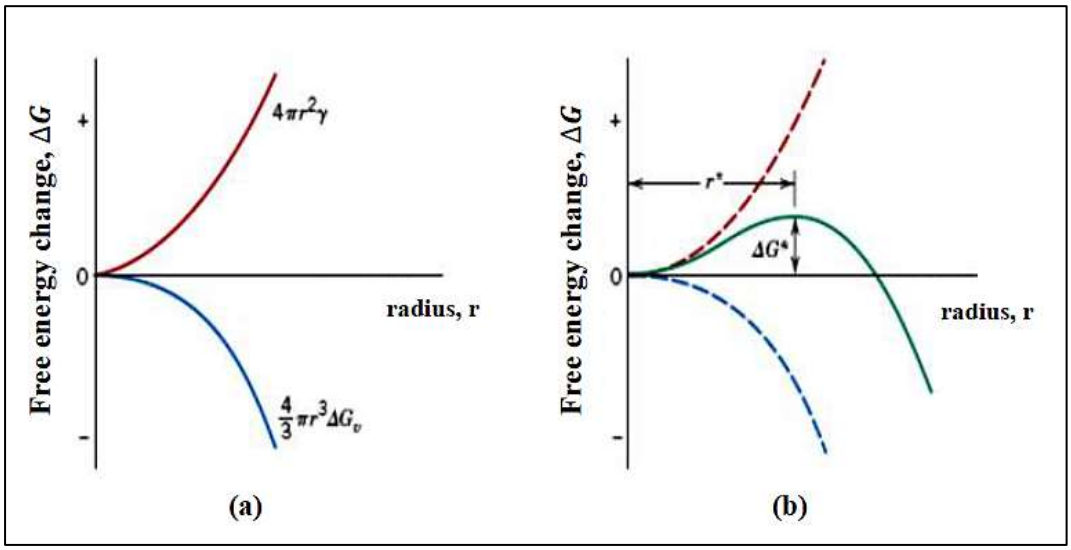

Fig 2.7: (a) Schematic curves for volume free energy and surface free energy contributions to the total free energy change attending of a spherical embryo/nucleus during solidification. (b) Schematic plot of free energy versus embryo/nucleus radius, on which is shown the critical free energy change (ΔG*) and the critical nucleus radius (r*) [58].

On the other hand, a cluster of radius less than the critical will shrink and redissolve. This subcritical particle is an embryo, whereas the particle of radius and, consequently, at the maximum of the curve in Figure (2.7b). This ΔG* corresponds to an activation free energy, which is the free energy required for the formation of a stable nucleus. Equivalently, it may be considered an energy barrier to the nucleation process. Since r* and ΔG* appear at the maximum on the free energy-versus-radius curve of Figure (2.7b), derivation of expressions for these two parameters is a simple matter. For r*, we differentiate Equation (2.4) with respect to r, set the resulting expression equal to zero, and then solve for r (= r*). That is,

$$\frac{d(\Delta G)}{dr} = \frac{4}{3}\pi\Delta G_v(3r^2) + 4\pi\gamma(2r) = 0 \quad \ldots\ldots\ldots\ldots\ldots (2.5)$$

Which leads to the result

$$r^* = \frac{-2\gamma}{\Delta G_v} \quad \ldots\ldots\ldots\ldots\ldots\ldots\ldots\ldots (2.6)$$

Now, substitution of this expression for r* into Equation (2. 4) yields the following expression for ΔG*:

$$\Delta G^* = \frac{16\pi\gamma^3}{3(\Delta G_v)} \quad \ldots\ldots\ldots\ldots\ldots\ldots\ldots\ldots (2.7)$$

This volume free energy change ΔG_v is the driving force for the solidification transformation, and its magnitude is a function of temperature. At the equilibrium solidification temperature T_m the value of ΔG_v is zero, and with diminishing temperature its value becomes increasingly more negative. It can be shown that ΔG_v is a function of temperature as

$$\Delta G_v = \frac{\Delta H_f\,(T_m - T)}{T_m} \quad \ldots\ldots\ldots\ldots\ldots\ldots\ldots (2.8)$$

Where ΔH_f is the latent heat of fusion (i.e., the heat given up during solidification), and T_m and the temperature T are in Kelvin. Substitution of this expression for ΔG_v into Equations (2.6) and (2.7) yields

$$r^* = \left(\frac{-2\gamma T_m}{\Delta H_f}\right)\left(\frac{1}{T_m - T}\right) \quad \ldots\ldots\ldots\ldots\ldots\ldots\ldots (2.9)$$

and $\Delta G^* = \left(\frac{16\pi\gamma^3 T_m^2}{3\Delta H_f^2}\right)\frac{1}{(T_m - T)^2}$ $\ldots\ldots\ldots\ldots\ldots\ldots\ldots (2.10)$

Thus, from these two equations, both the critical radius r* and the activation free energy ΔG^* decrease as temperature T decreases. The γ and ΔH_f parameters in these expressions are relatively insensitive to temperature changes Figure (2.8), a schematic ΔG-versus-r plot that shows curves for two different temperatures, illustrates these relationships. Physically, this means that with a lowering of temperature at temperatures below the equilibrium solidification temperature (T_m), nucleation occurs more readily [58].

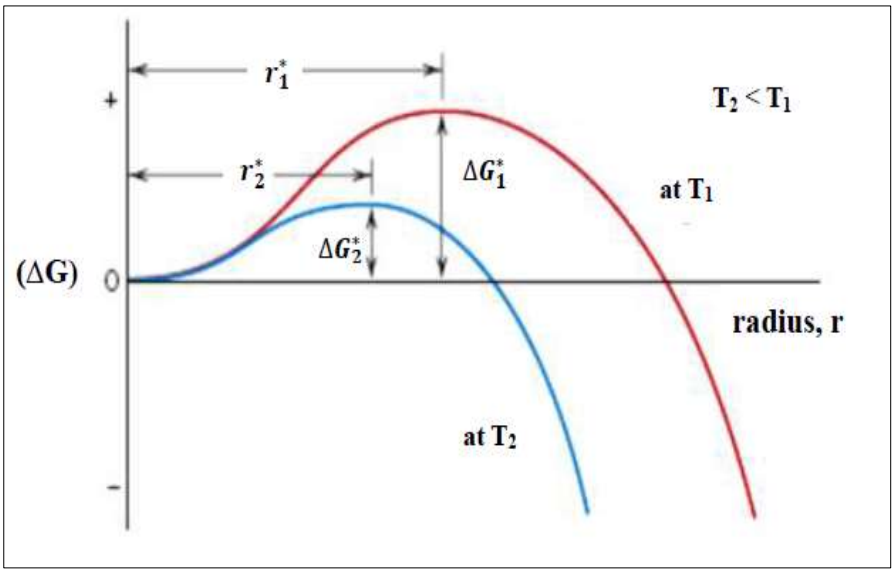

Fig 2.8: Schematic free energy-versus-embryo/nucleus-radius curves for two different temperatures. The critical free energy change (ΔG^*) and critical nucleus radius (r*) are indicated for each temperature [58].

2.7 Properties of Nanoparticles

2.7.1 Chemical Property

One of the important factors for the chemical applications of nanomaterials is the increment of their surface area which increases the chemical activity of the material. Since the electronic structure of nanoparticles depends on the size of the particle, the ability of the cluster to react with other species should depend on cluster size. This has important implications for the design of catalytic agents. High catalytic activity is observed for gold nanoparticles smaller than (3-5) nm, where

the structure is icosahedrdal instead of the bulk FCC arrangement. Multiple ionization of clusters cause them to become unstable, resulting in very rapid high-energy dissociation or explosion. The fragment velocities from this process are very high. The phenomenon is called Coulombic explosion [59].

2.7.2 Optical Properties

In small nanoclusters the effect of reduced dimensionality on electronic structure has the most profound effect on the energies of the highest occupied molecular orbital, essentially the valence band, and the lowest unoccupied molecular orbital, essentially the conduction band. Optical emission and absorption depend on transitions between these states; semiconductors and metals, in particular, show large changes in optical properties, such as color, as a function of particle size. Colloidal solutions of gold nanoparticles have a deep red color which becomes progressively more yellow as the particle size increases [60-63]. Figure (2. 9) shows the images for silver and gold nanoparticles in solution and typical absorption spectra [56].

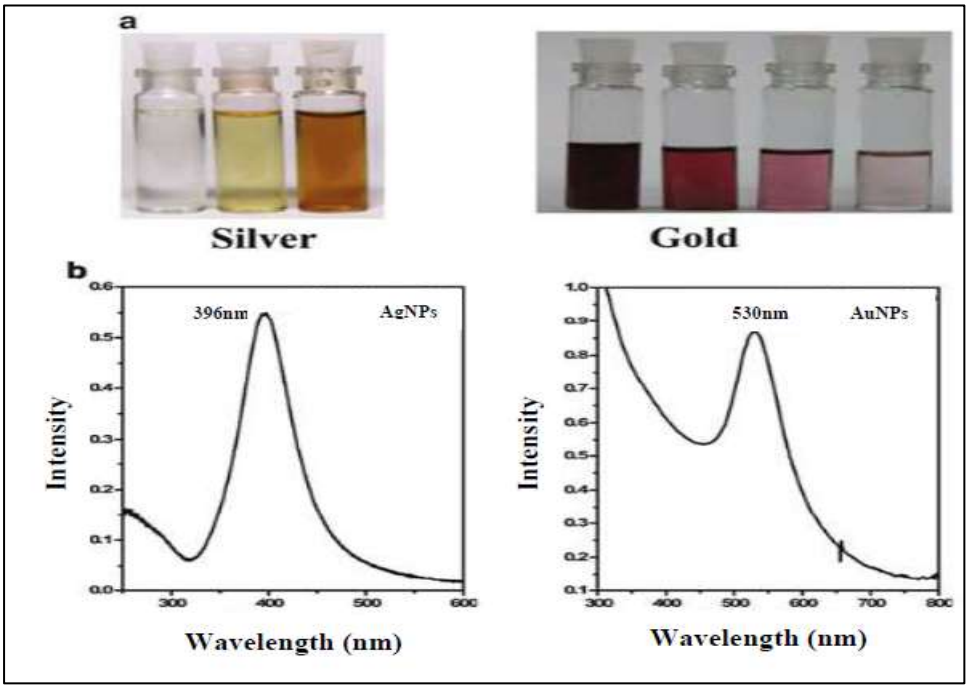

Fig 2.9: (a) Silver and gold nanoparticles in solution. (b) Typical absorption spectra of silver and gold nanoparticles [56].

2.7.2.1 Absorption and Size Dependent

According to Beer-Lambert law, for a dilute colloidal solution, if the particles are much smaller than the incident light wavelength, the electric dipole absorption is predominant [51]:

$$A = Log\ (\frac{I_o}{I}) = \mathrm{N}\ \sigma_{ext}\ \frac{1}{2.303} \quad \ldots\ldots\ldots\ldots\ldots\ (2.11)$$

Where A is the absorbance , I_0 is the incidient intensity , I is the transmit intensity, l in cm is the light path in a spectrophotometer, N is the number of the particles in cm^3 and σ is the extinction cross-section of a single particle in cm^{-2} for a bulk metal, there is [51]:

$$\omega_d = \frac{v_F}{r_\infty} \quad \ldots\ldots\ldots\ldots\ldots\ (2.12)$$

Where ω_d is scattering frequency, v_F is the electron velocity at Fermi level and r_∞ the mean free path of the electron in the bulk metal. When the particle radius, R, is smaller than r_∞, the mean free path R", becomes size-dependent with [57]:

$$\frac{1}{R"} = \frac{1}{R} + \frac{1}{r_\infty} \quad \ldots\ldots\ldots\ldots\ldots\ldots(2.13)$$

2.8 Metallic Nanoparticles

The metallic nanoparticles are used to define nanosized metals with dimensions such as thickness, width or length within the size rang (1-100) nm. The metallic nanoparticles have large surface-area-to-volume ratio as compared to other bulk materials. They have a large surface energy and number of low-co-ordination sites such as corners and edges. There are several types of metal nanoparticles such as Au, Ag, Cu, Ni, Zn, Mg, Fe and Si nanoparticles are synthesized by different chemical methods and co-precipitation methods [64].

2.8.1 Gold Nanoparticles (AuNPs)

Gold nanoparticles are defined as stable colloid solutions of clusters of gold atoms. At this nanoscale, AuNps possess different physicochemical characteristics when compared to the bulk gold, most obvious example being the color change from yellow to ruby red when bulk gold is converted into nanoparticulate gold. The surface plasmon resonance (SPR) peak is positioned at (520nm), and this peak is responsible for the ruby red color displayed by conventional gold colloids [65]. This ruby red color of AuNps is explained by a theory called "surface plasmonics". According to this theory, when the clusters of gold particles are hit by the electromagnetic field of the incoming light, the surface free electrons (6 electrons in case of AuNps) present in the conduction band of AuNps oscillate back and forth thus, creating a plasmon band which has an absorption peak in the visible region at 530-540 nm. The surface plasmon band (SPB) of AuNps is used as an indicator for formation during the synthesis of AuNps from their precursor salts. Physical properties of AuNps in turn depend on the size, shape, particle-particle distance and the nature of the stabilizer used to prevent the agglomeration of nanoparticles. According to Mie theory, Surface Plasmon Band (SPB) is absent for AuNps less than 2nm and greater than 500 nm. Gold nanorods have two SPB's, one longitudinal wavelength band at (550-600) nm and one transverse-wavelength band at 520nm. The longitudinal-wavelength band is very sensitive and changing the aspect ratio of gold nanorods changes the absorption region from visible to Near-infra red (NIR). This unique optical property of gold nanorods is used in Near-infra red ray therapy [66] and can be used as a therapeutic means to eradicate diseased cells, which forms the basis for

cancer treatment using photodynamic therapy (PDT). PDT, a minimally invasive technique for cancer therapy [67]. See Figure (2.10).

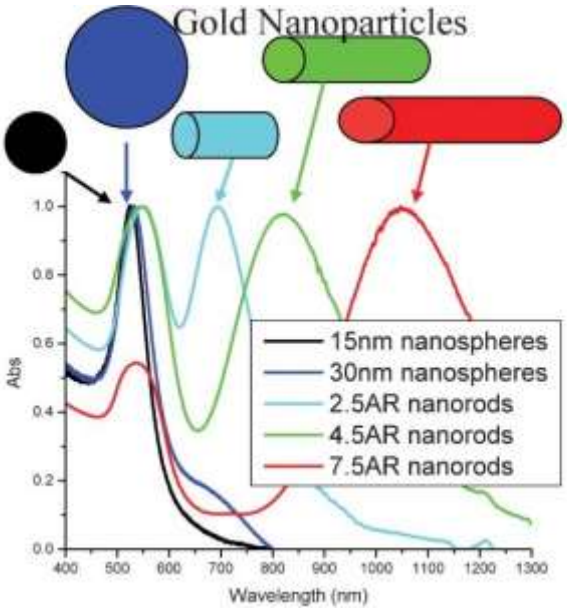

Fig 2.10: The size of AuNPs and their surface plasmon (SP) Note: AR is the standard aspect ratios for nanorods (length divided by width) [38].

2.8.2 Silver Nanoparticles (AgNPs)

Silver nanoparticles (Ag-NPs or nanosilver) have attracted increasing interest due to their unique physical, chemical and biological properties compared to their macroscale counterparts. Silver has known to be a metal that came into use even before the Neolithic revolution. Even the Greeks used it for cooking and to keep water safe. The first recorded medicinal use of silver was reported during the 8th century. Silver was known only as a metal till the recent past, and it is when the nano era came into existence that people started to believe that silver could even be produced at the nanoscale. Silver nanoparticles are nanoparticles of silver of between 1 nm and 100n min size. They have unique optical, electrical, and thermal properties and are being incorporated into products that range from photovoltaic to biological and chemical sensors. There are many consumer products and applications utilizing nanosilver in consumer

products; nanosilver-related applications currently have the highest degree of commercialization [68-70].

2.9 Synthesis of Metallic Nanoparticles

There are two methods for the synthesis of metallic nanoparticles- top-down and bottom-up approach [71]. These approaches include the attenuation of materials components with further self-assembly process which leads to the formation of nanostructures. During self-assembly the physical forces operating at nanoscale are used to combine units into large stable structures. Typical examples include quantum dot and formation of nanoparticles from colloidal dispersion. Top down approach. These approaches include macroscopic structures which can be externally controlled in the processing of nanostructures. Typical examples are ball milling, application of severe plastic deformation. Top down method V/S bottom up methods- Top down method starts with a pattern generated on a large scale, then reduced to nanoscale, quick to manufacture, slow and not suitable for large scale production. Bottom-up approach- begins with atoms or molecules and build up to nanostructures, fabrication is much less expensive. Attrition/ milling is top-down type of method and bottom-up method is production of colloidal dispersion [72].

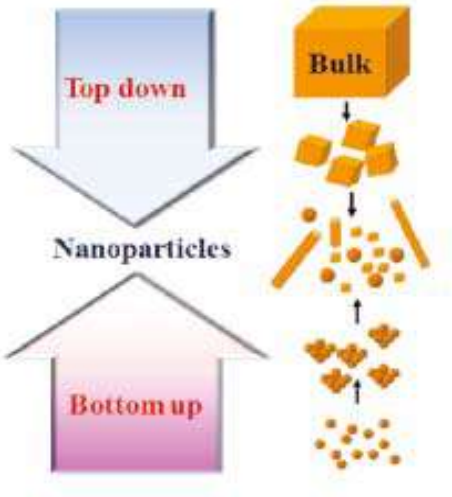

Fig 2.11: Schematic illustration of the preparative methods of nanoparticles [73].

2.9.1 Turkevich Method

Tukevich method is a bottom up method and the simplest one available where it pioneered by J. Turkevich *et al*. in 1951 and refined by G. Frens in 1970s [74-77]. Generally, it is used to produce modestly monodisperse spherical gold nanoparticles suspended in water of around 10–20 nm in diameter. Larger particles can be produced, but this comes at the cost of monodispersity and shape. It involves the reaction of small amounts of hot chlorauric acid with small amounts of sodium citrate solution. The colloidal gold will form because the citrate ions act as both a reducing agent, and a capping agent. Recently, the evolution of the spherical gold nanoparticles in the Turkevich reaction has been elucidated. Interestingly, extensive networks of gold nanowires are formed as a transient intermediate. These gold nanowires are responsible for the dark appearance of the reaction solution before it turns ruby-red [78]. To produce larger particles, less sodium citrate should be added (possibly down to 0.05%, after which there simply would not be enough to reduce all the gold). The reduction in the amount of sodium citrate will reduce the amount of the citrate ions available for stabilizing the particles, and this will cause the small particles to aggregate into bigger ones (until the total surface area of all particles becomes small enough to be covered by the existing citrate ions).

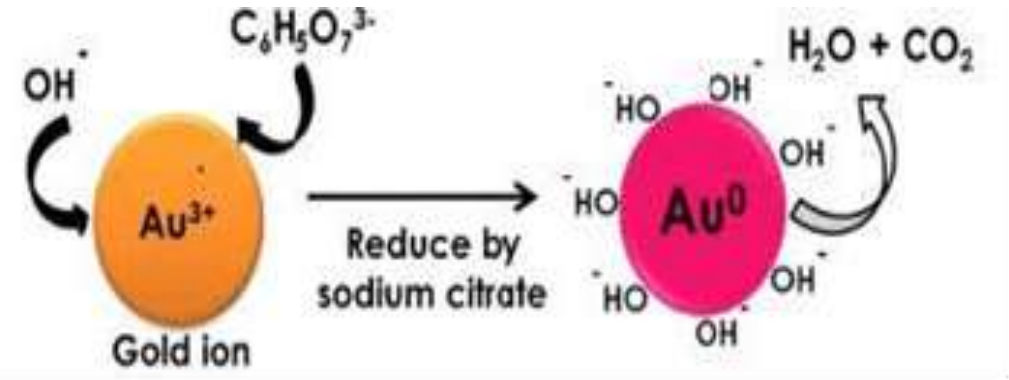

Fig 2.12: Synthesis of gold nanoparticles by the reduction of sodium citrate [79].

2.9.2 Reduction by Gallic acid

At room temperature, reduction of Ag^+ in water can be achieved by using Gallic acid (GA) whose oxidation potential is 0.5V. In benzoic acid structure the hydroxyl group at determined positions plays an important role in the synthesis of metal nanoparticles. When hydroxyl groups are located at Meta position, nanoparticles synthesis was not successful but it was achieved when hydroxyl groups are present at ortho and para positions. Here carboxylic group act as stabilizer and hydroxyl as the reactive part. To obtain silver colloids, NaOH addition is important. Then, the silver species reacting could be Ag_2O that has been reported as a good AgNps precursor by thermal decomposition [72].

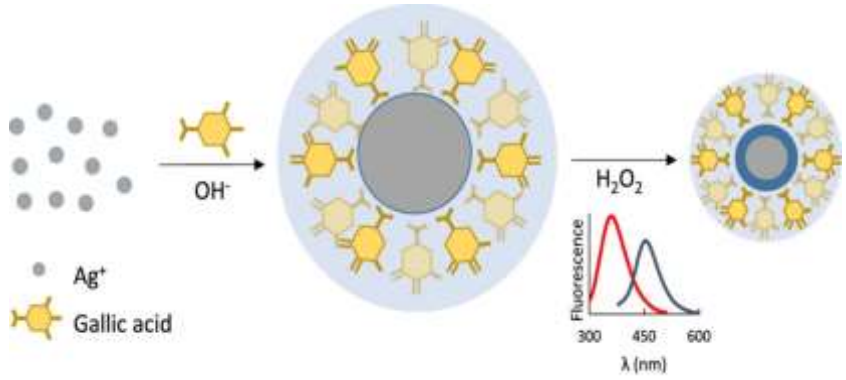

Fig 2.13: Synthesis of silver nanoparticles by the reduction of gallic acid [80].

2.10 Core -Shell Particles

Core-shell particles form a novel class of nanocomposite materials in which a thin layer of nanometer size is coated on another material by some specialized procedure. The core can be just a nanoparticle (few nanometers to tens of nanometers) with a nanometer thick coating or it can be a large core (few tens to hundreds of nanometer diameter) with nanometer thick coating as schematically shown in Figure (2.14). The properties of core-shell particles are different from core or shell material.

Their properties depend usually upon core to shell ratio. These particles are synthesized for a variety of purposes like providing chemical stability to colloids, enhancing luminescent properties, engineering band structures, sensors, drug delivery etc. These materials can be of economic interest also as precious materials can be [56].

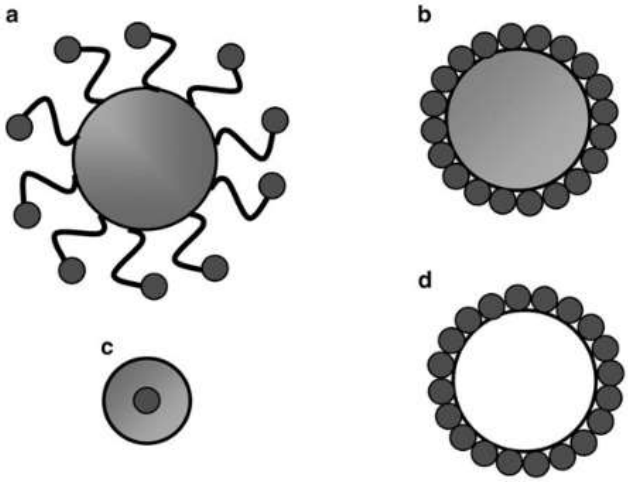

Fig 2.14: Variety of core-shell particles: (a) Surface modified core particles anchored with shell particles. (b) Smooth coating of dielectric core with shell. (c) Encapsulation of very small particles with dielectric material and (d) Quantum bubble deposited on inexpensive cores [56].

Core particles of different morphologies such as rods, wires, tubes, rings, cubes etc. also can be coated with thin shell to get desired morphology in core shell structures. Core-shell materials can be synthesized practically with all the materials, like semiconductors, metals and insulators. Dielectric materials such as silica and polystyrene are popular materials to use as core because they are soluble in water and hence can be useful in biological applications. Core-shell particles can be synthesized using variety of combinations such as dielectric-metal, dielectric-semiconductor, dielectric-dielectric, semiconductor-metal, metal-metal, semiconductor-semiconductor, semiconductor-dielectric, metal-dielectric, dyedielectric, dielectric-biomolecules etc. Although core shell particles have novel properties, these can be further assembled and utilized for creation of another class of novel materials like colloidal crystal or quantum bubbles (i.e. hollow spheres with thin shells). It is

indeed possible to create novel core shell structures having multishells and tuning optical properties from visible to infrared region of the electromagnetic spectrum. Synthesis of core-shell particles requires highly controlled and sensitive synthesis protocols to ensure complete coverage of core particles with shell. There are various methods to fabricate core-shell structures which involve precipitation, polymerization, micro emulsion, reverse micelle sol-gel condensation etc. Although these methods themselves may appear to be simple, it is rather difficult to control the thickness and homogeneity of the coating. If reaction is not controlled properly, eventually it leads to aggregation of core particles, formation of separate particles of shell material or incomplete coverage. Here we shall discuss some silica based core-shell particles as an example. Preparation of core-shell particles is a multi-step synthesis procedure. One can make coating of silica on nanoparticles or grow silica particles of large size and then anchor nanoparticles or coat thin shell around, of few nm thickness. As mentioned earlier one can use metals, semiconductors or any other dielectric material as shell or core with silica [56].

2.10.1 Advantages of Nano Thin Film Layer of Silica Coated Metal Nanoparticles

- Each particle is coated with a thin film of silicon dioxide layer which acts as a place holder between the individual spheres in the aggregate, that absorbs the light and thus generates heat [81].
- The layer of silicon dioxide thin film prevents the particles from deforming when they heat up [82].
- The SiO_2 layer thin film also dispersion and prevents the reshaping or coalescence of metal nanoparticles during laser irradiation [83].

2.11 Cell Lines

Cell culture refers to the removal of cells from an animal or plant and their subsequent growth in a favorable artificial environment [84]. Primary culture refers to the stage of the culture after the cells are isolated from the tissue and proliferated under the appropriate conditions until they occupy all of the available substrate (i.e., reach confluence) [85]. Cell lines comprise cells that are able to multiply for extended periods in vitro and can therefore be maintained by serial subculture. They can be subdivided into finite cell lines, continuous cell lines and stem cell lines [86]. Cell lines are an appropriate experimental model for mechanistic studies, because they are simpler than a complete organism [87]. Subculturing, is the removal of the medium and transfer of cells from a previous culture into fresh growth medium, a procedure that enables the further propagation of the cell line or cell strain. The growth of cells in culture proceeds from the lag phase following seeding to the log phase, where the cells proliferate exponentially as shown in Figure (2.15) [88].

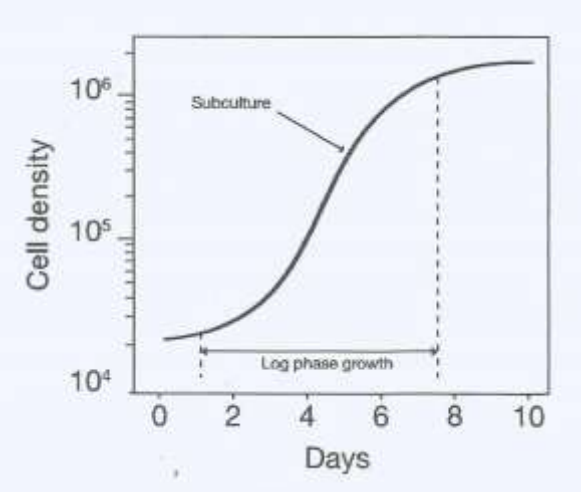

Fig 2.15: Characteristic growth pattern of cultured cells [88].

Cells in culture can be divided in to three basic categories based on their shape and appearance (i.e., morphology) [88].

❖ **Fibroblastic** (or fibroblast-like)

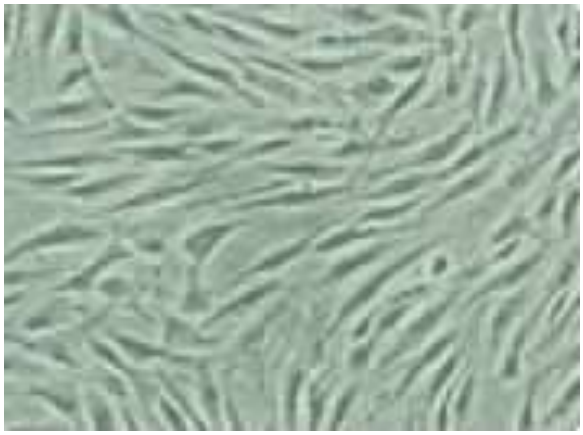

Fig 2.16: Fibroblast-like cells [88].

❖ **Epithelial-like** cells are polygonal in shape with more regular dimensions.

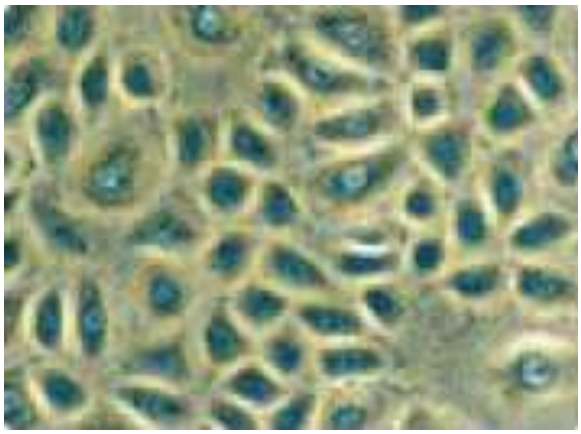

Fig 2.17: Epithelial-like cells [88].

❖ **Lymphoblast-like** cells are spherical in shape.

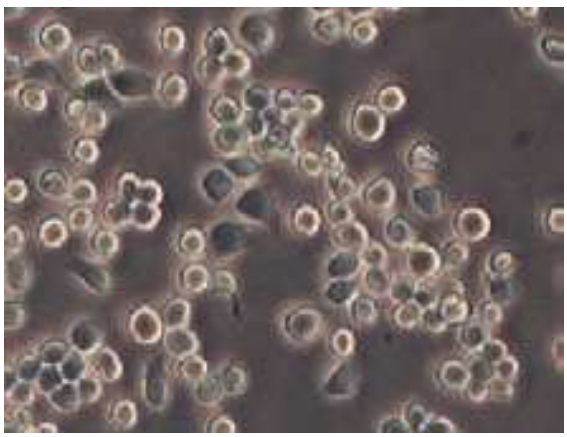

Fig 2.18: Lymphoblast-like cells [88].

2.11.1 MCF-7 Cell Line

MCF-7 is a human breast cancer cell line that was first isolated in 1970 from the malignant adenocarcinoma breast tissue of a 69-year old woman. MCF-7 is the acronym of Michigan Cancer Foundation-7, referring to the institute in Detroit where the cell line was established. MCF-7 cells are useful for in vitro breast cancer studies because the cell line has retained several ideal characteristics particular to the mammary epithelium. These include the ability for MCF-7 cells to process estrogen via estrogen receptors. MCF-7 cells are also sensitive to cytokeratin. When grown in vitro, the cell line is capable of forming domes and the epithelial like cells grow in monolayers [89].

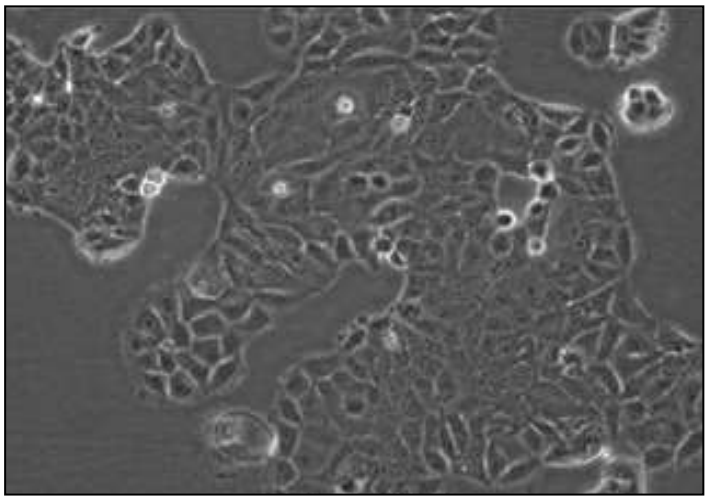

Fig 2.19: Morphological aspect of MCF-7 cells observed by phasecontrast microscopy [90].

2.11.2 HBL-100 Normal Cell Line

Holmquist and Papanicolaou (1956) described epithelial cell clusters, foam cells, leukocytes, and histocytes in smears of breast fluids obtained during both pregnancy and lactation. Buehring (1972) subsequently observed that human milk serves as a source of cells which, when cultured, form monolayer colonies without fibroblast contamination. The epithelial nature of these colony-forming cells was

later confirmed by Russo et al. (1975) and Hallowes et al. (1977). Efforts in our laboratory quantitated the distribution of cell types in fluids from all stages of lactation and showed that epithelial cell colonies observed in primary cultures originate by exfoliation from the lactating mammary gland (Gaffney et al. 1976). Ceriani et al. (1979) demonstrated that the colony-forming epithelia contain surface-differentiation antigens specific for mammary gland cells. Although cell lines from samples of malignant tissues have been established and characterized (Larsfarques and Ozello 1958; Young et al. 1974; Russo et al. 1975; Engel and Young 1978), the long term growth of cells derived from physiologically normal human mammary tissue has not been published. The current study reports the characteristics of a continuous line, designated HBL-100 (human breast lactating, donor 100), established from primary cultures of cells present in human milk [91].

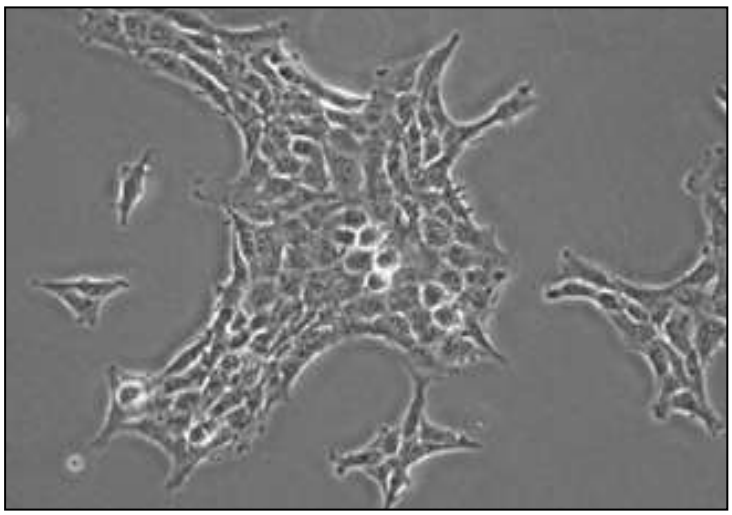

Fig 2.20: Morphological aspect of HBL-100 cells observed by phasecontrast microscopy [90].

2.12 Nanotechnology in Cancer Diagnosis and Treatment

Cancer is still one of the most dangerous diseases worldwide. The application of nanotechnology in medicine, known as nano medicine, has paved a way for introduction of nanoparticles in treating serious diseases

such as cancer. Nanotechnology differentiates cancer cells from normal cells by active and passive targeting which is essential in cancer treatment. Metal nanoparticle find application in cancer diagnosis, treatment and monitoring all in a single product enhance patient compliance and minimising potential adverse effects [92]. Metallic nanoparticles such as silver and gold are known as plasmonic materials; they have a marked ability to absorb and scatter light at a frequency that is resonant with their surface plasmon oscillation. This resonance frequency depends on particle shape, size, and the density of the particle's electron distribution and the surrounding dielectric environment. It thus provides very useful information regarding particle properties. Production and characterization of silver and gold nanoparticles have not only raised the potential for wider therapeutic application of silver and gold but it have also made them suitable for specific biomedical applications such as targeting therapy [93]. The proposed mechanism of cytotoxic effects of silver and gold nanoparticles was through their capacity to disrupt mitochondrial respiratory chain and to produce reactive oxygen species (ROS), this cause interruption of ATP synthesis and in turn initiate expression of apoptotic genes, DNA damage and cell death [94,95].

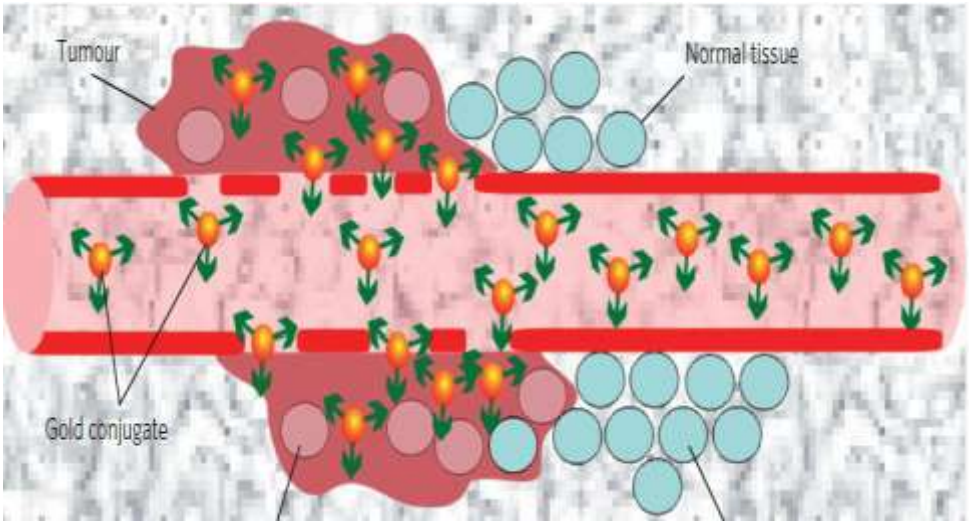

Fig 2.21: Systematic delivery of gold nanoparticles to the tumour cells via leaky blood vessels [96]

The size and shape of nanoparticles are critical factors that determine their performance: the ability to penetrate the blood vessel, reach the targeted region, affect the rate of macrophage uptake, and finally wash out from the body. For instance, nanoparticles larger than 10 nm will be too large to pull out from the normal capillaries [97,98]. In addition, the transport of smaller nanoparticles exhibits relatively higher diffusion rates, which allows them to move laterally in the blood vessel with greater ease. However, larger particles can penetrate the tumor through the gaps between the endothelial cells in leaky tumor vasculature and remain there for a long time [98]. Moreover, the surface-chemical properties of nanoparticles and their surface coating play a crucial role in further attachment to the cancer cells. Notably, the functional groups on the surface of the nanoparticle are considered as the defining factors of solubility, interaction, and attachment to the cell. Depending on the surface coating, nanoparticles can be defined as positively or negatively charged. Positively charged nanoparticles are the most beneficial in the passage of cell-membrane barriers, and concentrate in the cytosol or nucleus [99]. The control of heat delivery and dose to the cancerous cells is significant in order to meet the clinical requirements. The specific absorption rate (SAR) was found as the main factor to estimate the heating of the tissue generated by the magnetic induction. This parameter is proportional to temperature increase, which is defined as the electromagnetic energy absorption rate by a unit mass of biological material, and is defined as follows as in Equation (2.14) [100, 101].

$$\mathrm{SAR} = \frac{\Delta T \times 3\lambda}{c \times R^2} \quad \text{.....(2.14)}$$

Where:

ΔT: the required temperature increase.

λ: the thermal conductivity of the tissue.

c: the concentration of nanoparticles.

R: the radius of the spherical tumor

Chapter Three

Experimental Works

3.1 Introduction

This chapter includes a detailed explanation of the materials and method used in preparation of gold and silver nanoparticles uncoated and coated, in addition to the devices used in the study of the properties of these materials. It also includes preparation of solutions for cell culture and studying the effect of gold and silver nanoparticles uncoated and coated on both the MCF-7 and HBL-100 cell lines.

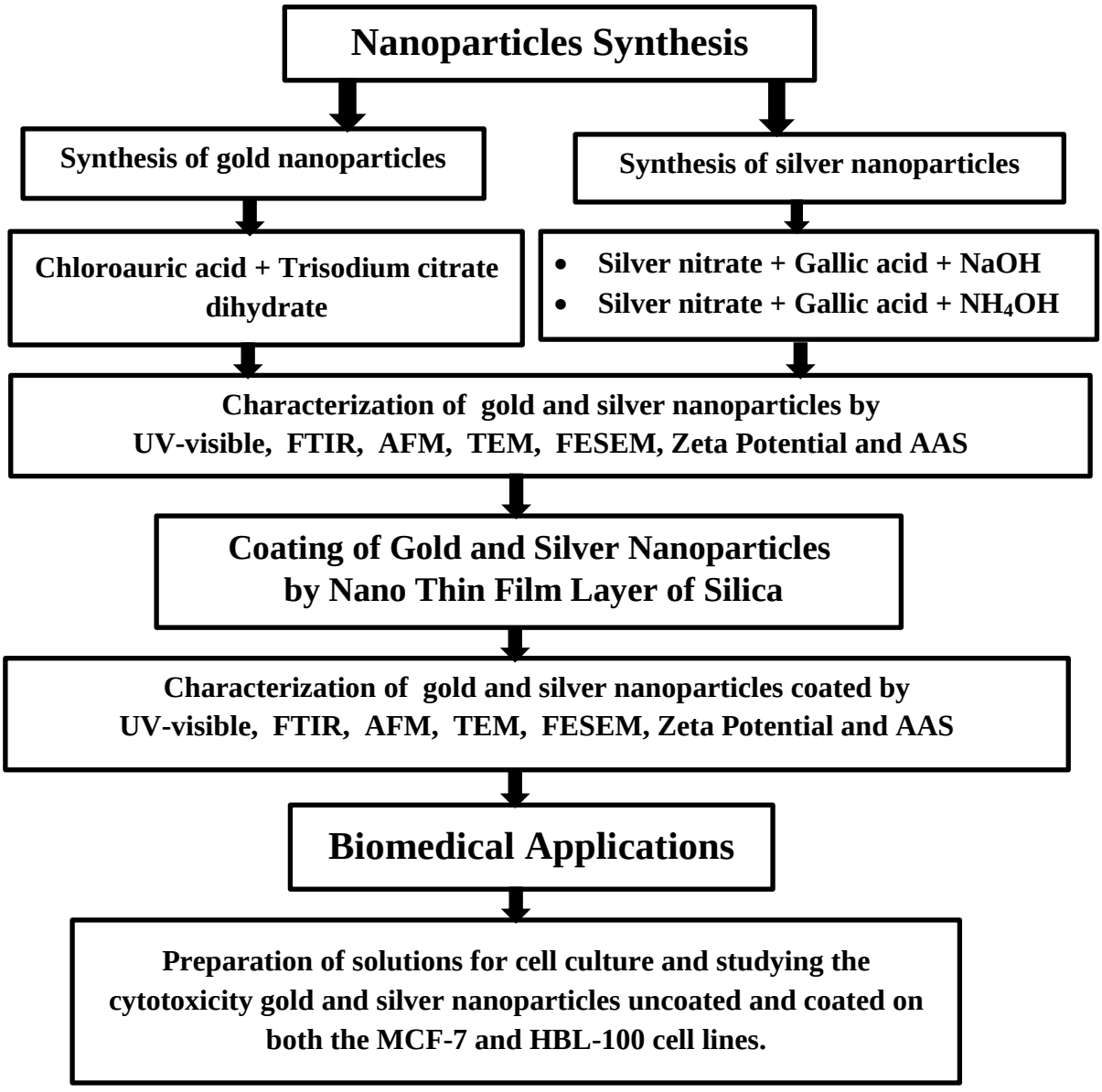

Fig 3.1: Schematic representation of experimental work.

Table 3.1:- The chemicals that used in this study.

Material	Molecular formula	Molecular weight (g/mol)	Appearance	Company and manufacturing country
chloroauric acid	$HAuCl_4$	339.79	yellow powder	Riedel Dehaenag/Seelz Hannover/ Germany
trisodium citrate dihydrate	$Na_3C_6H_5O_7$	258.07	white powder	Panreac AppliChem /Bercelona/ Spain
silver nitrate	$AgNO_3$	169.87	white powder	BDH Chemical Lit Poole
gallic acid	$C_7H_6O_5$	170.12	white powder	MAY & BAKER LTD DAGENHAM/ England
sodium hydroxide	NaOH	40	white powder	AVONCHEM/ England
ammonium hydroxide solution	NH_4OH	35.05	colourless liquid	SIGMA-ALDRICH/ Germany
Sodium silicate	Na_2SiO_3	122.063	White or grayish white	Panreac AppliChem/Bercelona/ Spain
ethanol	C_2H_5OH	46.07	colourless liquid	Scharlau/ Spain

3.2 Preparation Part

3.2.1 Gold Nanoparticles (AuNPs) Synthesis

To prepare chloroauric acid ($HAuCl_4$) stock solution, dissolve 1g of chloroauric acid in 50ml of deionized water and its molarity of (58.86mM), and to prepare trisodium citrate dihydrate ($Na_3C_6H_5O_7$) stock solution, dissolve 1g of trisodium citrate dihydrate in 100ml of deionized water with molarity of 34mM.

The appropriate weight (W_t) of the materials chloroauric acid and trisodium citrate dihydrate were determined by using the following Equation [102]:

$$M_o = \frac{W_t}{M.Wt} * \frac{1000}{V} \qquad \dots\dots\dots\dots (3.1)$$

Where

M_o: molar concentration (mol/l).

M. Wt: molecular weight of the material (g/mol).

V: volume of solution (ml).

Wt: weight (g).

The effect of the temperature, trisodium citrate dihydrate content, deionized water volume and mixing speed was determined by changed parameter ones and other fixed until reached to optimum conditions for synthesis of gold nanoparticles.

It was added 150µl of chloroauric acid ($HAuCl_4$) stock solution to optimum volume of deionized water 50ml and heating it at optimum temperature 80^{o}C on hot plate without stirring till the solution starts to evaporate, mixing the solution by magnetic bar at optimum mixing speed 1000rpm then it was added optimum content of trisodium citrate dihydrate ($Na_3C_6H_5O_7$) stock solution 700µl at once and keep heating it until the color turned to wine red, as shown in Figure (3.2).

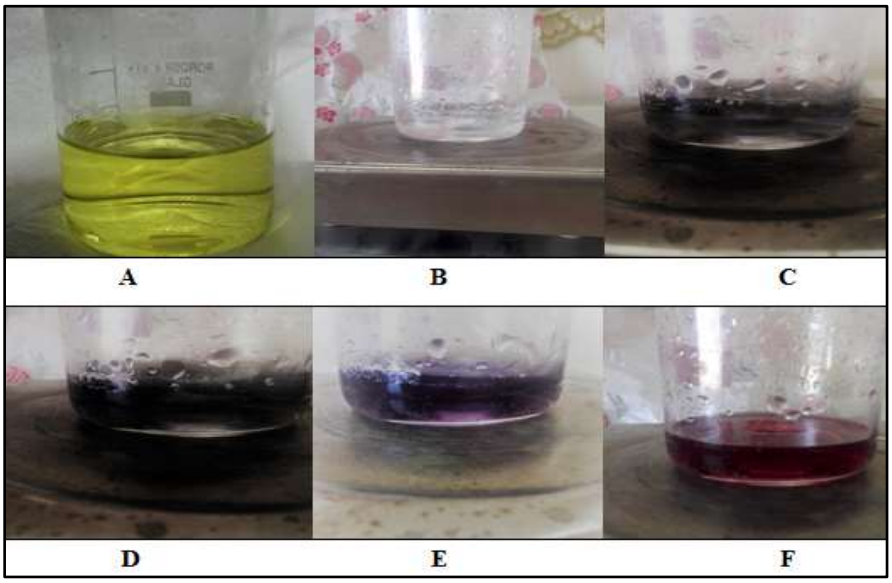

Fig 3.2: Chemically synthesis of gold nanoparticles (AuNPs). (a) Chloroauric acid stock solution. (b) After add 150µl of chloroauric acid stock solution in 50ml of deionized water without trisodium citrate dihydrate. (c) After 15 minutes of add trisodium citrate dihydrate stock solution. (e) After 30 minutes of add trisodium citrate dihydrate stock solution. (f) After 45 minutes of add trisodium citrate dihydrate stock solution.

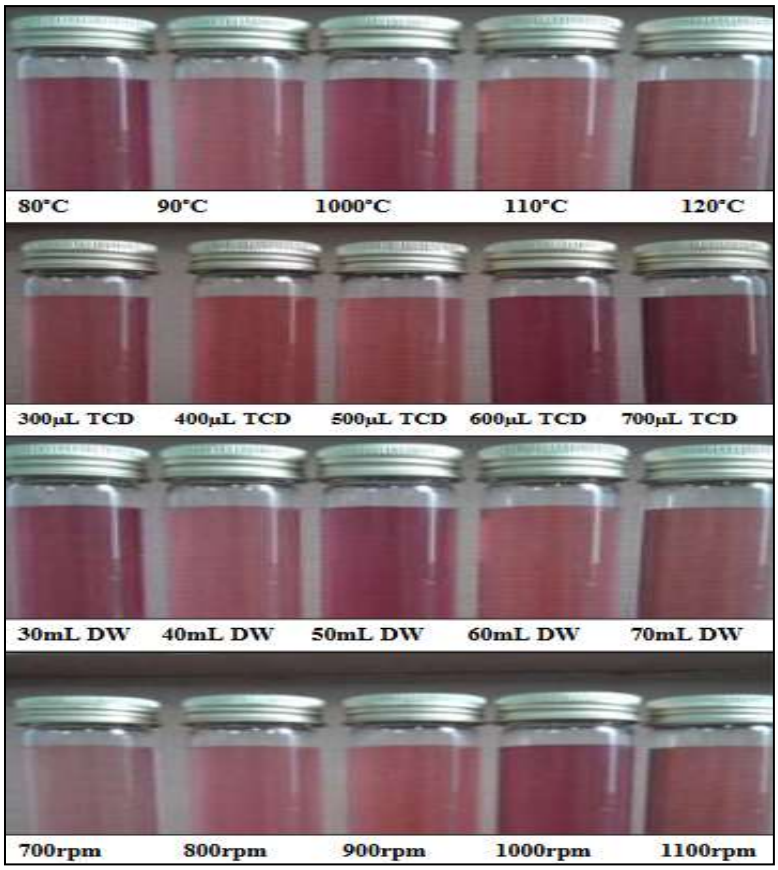

Fig 3.3: Chemically synthesis of gold nanoparticles for parameters four temperature, trisodium citrate dihydrate content, deionized water volume and mixing speed.

3.2.2 Silver Nanoparticles (AgNPs) Synthesis

The effect of the time, gallic acid weight and temperature was determined by changed parameter ones and fixed other until reached to optimum conditions for preparation of silver nanoparticles adjusted by sodium hydroxide (NaOH) and ammonium hydroxide solution (NH_4OH), as follows:-

❖ Synthesis of Silver Nanoparticles Adjusted by Sodium Hydroxide (NaOH)

0.001M of silver nitrate ($AgNO_3$) was added to 100ml of deionized water, and optimum weight of gallic acid ($C_7H_6O_5$) 0.02 g was dissolved in 10ml of deionized water. Then it was added 1M of sodium hydroxide

(NaOH) to get pH=11 turns from clear white into brown color, and heating it at optimum temperature 100 ^{o}C on hot plate for optimum time 20min, as shown in Figure (3.4).

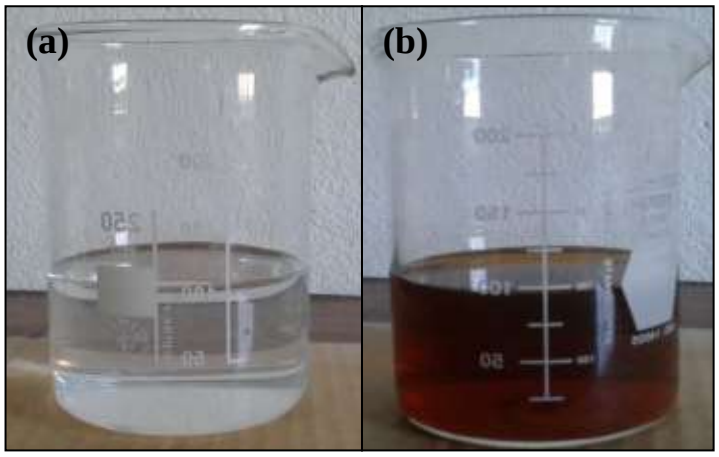

Fig 3.4: Chemically synthesis of silver nanoparticles (AgNPs). (a) Silver nitrate with gallic acid. (b) Silver nitrate with gallic acid after adjusted by NaOH.

❖ Synthesis of Silver Nanoparticles Adjusted by Ammonium Hydroxide (NH_4OH)

0.001M of silver nitrate ($AgNO_3$) was added to 100ml of deionized water, and optimum weight of gallic acid ($C_7H_6O_5$) 0.008g was dissolved in 10ml of deionized water. Then it was added 7.7M of ammonium hydroxide solution (NH_4OH) to get pH=10, and heating it at optimum temperature 80^{o}C on hot plate for optimum time 20min, as shown in Figure (3.5).

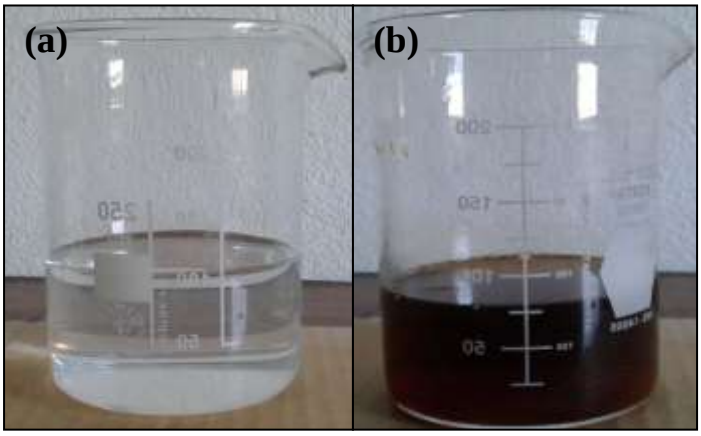

Fig 3.5: Chemically synthesis of silver nanoparticles (AgNPs). (a) Silver nitrate with gallic acid. (b) Silver nitrate with gallic acid after adjusted by NH_4OH.

The appropriate weight (W.t) of the materials silver nitrate, gallic acid, sodium hydroxide and ammonium hydroxide solution were determined also by using Equation (3.1).

Fig 3.6: Chemically synthesis of silver nanoparticles adjusted by NaOH (in left) and adjust by NH_4OH (in right), for parameters three time, gallic acid and temperature.

3.2.3 Gold and Silver Nanoparticles Coating

The effect of the SiO_2 content, deionized water volume, nanoparticles solution volume and ethanol volume was determined by changed parameter ones and fixed other until reached to optimum conditions for coating of gold and silver nanoparticles by nano thin film layer of silica, this procedure takes several steps [56,103,104].

❖ Gold Nanoparticles Coating

It was added optimum content of sodium silicate stock 600µl to optimum volume of deionized water 20ml after discard the same volume of deionized water, then it was added 2M of sodium hydroxide to get (11 < pH < 12) withdraw 1ml from this solution to optimum volume of gold nanoparticles 20ml with stirring about 10 minute then store it in a dark place a whole day, stirr optimum volume of ethanol (purity 99%) 5ml with the solution and store it again in a dark place a whole day.

Then wash the solution by centrifuge device at 13000 rpm to get residual coated gold nanoparticles with thin film layer of silica and get red of the solution [105]. In this step the coated gold nanoparticles can be used by adding deionized water for later use in applications.

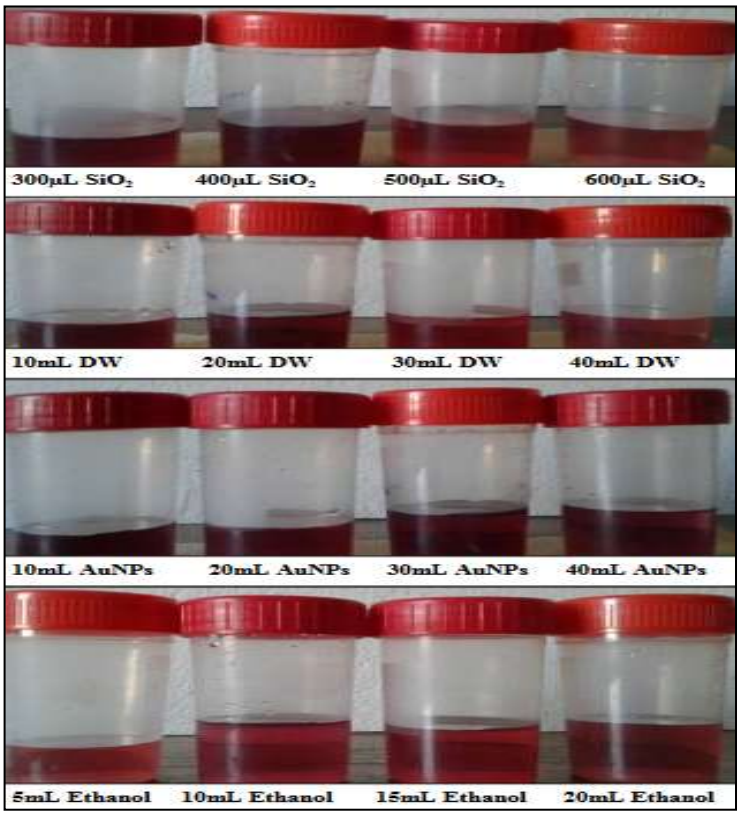

Fig 3.7: Coated gold nanoparticles under of the effect parameters four SiO_2 content, deionized water volume, gold nanoparticles solution volume and ethanol volume.

❖ Silver Nanoparticles Coating

It was added optimum content of sodium silicate stock 500µl to 20ml of deionized water after discard the same volume of deionized water, then it is added 2M of sodium hydroxide solution to get (11 < pH < 12) withdraw 1ml from this solution to volume optimum of silver nanoparticles adjusted by NaOH and NH_4OH 20ml and 30ml respectively, with stirring about 10 minute then store it in a dark place a whole day, stirr optimum volume of ethanol (purity 99%) 10 ml with the solution and store it again in a dark place a whole day.

Then wash the solution by centrifuge device at 13000 rpm to get residual silver nanoparticles coated with thin film layer of silica [105]. In this step the coated silver nanoparticles can be used by adding deionized water for later use in applications.

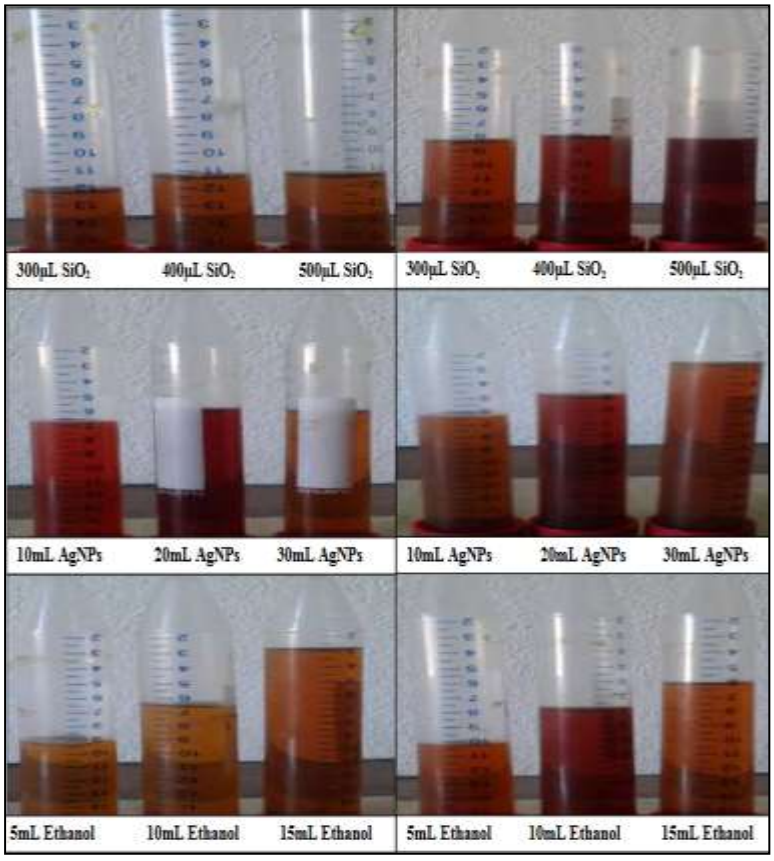

Fig 3.8: Coated silver nanoparticles under of the effect parameters three SiO_2 content, silver nanoparticles solution volume and ethanol volume.

3.3 UV-Visible Spectroscopy (UV-VIS)

Absorbance spectra of NPs solution were measured by UV-VIS double beam spectrophotometers. All spectra were measured at room-temperature in a quartz cell with 1cm optical path. Additionally, spectrophotometer was used to estimate of metals nanoparticles [106]. Samples for UV/Vis spectrophotometry are most often liquids, although the absorbance of gases and even of solids can also be measured. Samples are typically placed in a transparent cell, known as a cuvette. Cuvettes are typically rectangular in shape, commonly with an internal width of 1cm. Test tubes can also be used as cuvettes in some instruments. The type of sample container used must allow radiation to pass over the spectral region of interest. The most widely applicable cuvettes are made of high quality fused silica or quartz glass because these are transparent throughout the UV, visible and near infrared regions. Glass and plastic cuvettes are also common, although glass and most plastics absorb in the UV, which limits their usefulness to visible wavelengths [107]. UV-Vis is a type of absorption spectroscopy in the ultraviolet-visible spectral region. This technique requires a light source in the visible and adjacent ranges (near ultraviolet-visible) and a spectrometer. UV-Vis operates based on the principle that non-bonding electrons can absorb energy in the form of ultraviolet (10–380 nm) or visible (380–780 nm) light; such absorption excites these electrons to higher anti-bonding molecular orbitals and is correlated to the absorbing wavelength (easily-excited electrons are related to longer wavelength). The light source and spectrometer can be integrated into a single device or can be separate devices based on the particular application of interest. Figure (3.9) is a schematic UV–visible spectrometer works and light sources are separate devices, usually separated by a fiber optic light guide; integrated source-spectrometer devices are typically built as a single unit where the sample

is inserted into the light path. An advantage of the separate source-spectrometer arrangement in Figure (3.9) is that the sample chamber can be constructed to allow for liquid flow through it. UV-Vis spectroscopy can be used to quantitatively determine concentrations in a solution or electrolyte. This technique requires samples to be vividly colored in order to guarantee strong absorbance spectra. As a result, transition metal ions and highly conjugated organic compounds in solution are detectable using this technique. To determine the concentration of a particular species within the solution, the intensity of light transmitted through a solution can be measured relative to a clear medium [108]. UV-visible spectroscopy device was used for this purpose is Shimadzu UV-1800 made in Japan.

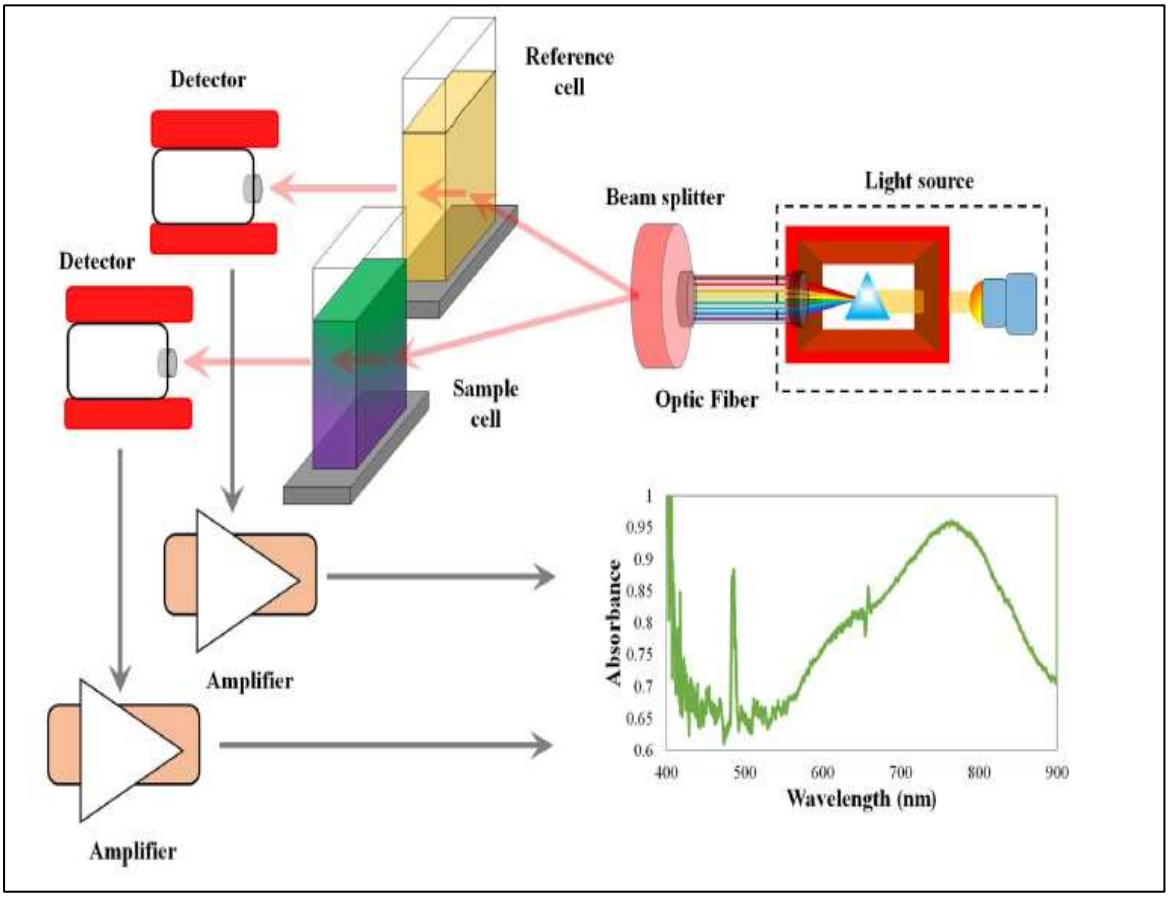

Fig 3.9: A schematic diagram shows how the UV–visible spectrometer works [108].

3.4 Fourier Transform Infrared (FTIR)

All the molecules are made up of atoms linked by chemical bonds. The atoms and their chemical bonds can be compared to that of a system comprised of springs (bonds) and balls (atoms) inconstant motion. These motions can have two components, stretching and bending. The frequencies of these vibrations are not only dependent upon the nature of particular bonds themselves, but are also affected by the entire molecule and its surroundings. The internal motion of this system can be greatly affected if energy is transferred to it. The vibrations of the bonds will increase their amplitude if an electromagnetic wave (infrared beam in the present case) strikes them. The vibrational energy levels are quantized in a molecule, therefore only those frequencies of the infrared beam will be absorbed which are exactly corresponding to that required to raise the energy level of a bond and the amplitude of vibrations increases suddenly. Thus, recording the intensity of the transmitted beam from a film or a material will give the frequencies absorbed by that material, which provides the insight about the bonding and the molecular structure of the material. The frequencies of the respective bonds that are absorbed also depend upon the whole molecular environment they are sitting in. Therefore, a particular molecule may not absorb the same exact frequency in different materials. However, certain bonds have distinguishing characteristics that can be identified by the infrared absorption spectra. An (IR) spectrum is generally displayed as a plot of the energy of the infrared radiation (expressed either as wavelength in μm or wavenumber in cm^{-1}) versus the percent of light transmitted by the sample. Within this energy range the spectrum will appear as a series of broad absorption bands of variable intensity, each giving some structural information [109,110]. FTIR spectra of prepared samples were recorded

by using Shimadzu, IRAffinity-1, Japan. A schematic of (FTIR) spectrometer is shown in Figure (3.10) [111].

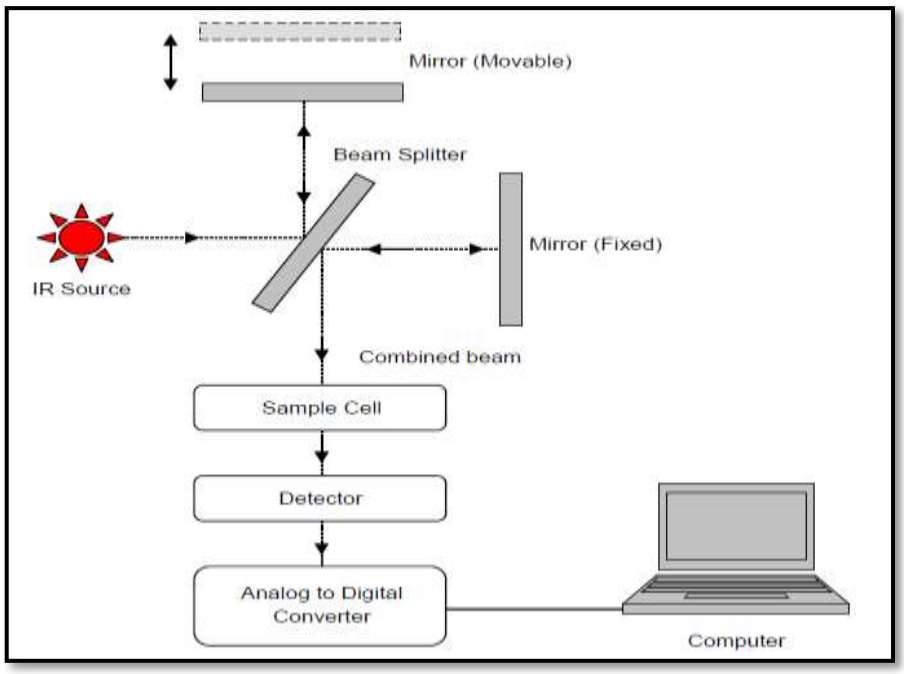

Fig 3.10: A Schematic representing FTIR spectrophotometer [111].

3.5 Atomic Force Microscope (AFM)

AFM provides topographical and elemental information. It can evaluate grain size, surface roughness, and particle size distributions. The (AFM) works by the same way as a phonograph or profilometer but on a much smaller scale. A very sharp tip is dragged across a sample surface and the change in the vertical position reflects the topography of the surface. By collecting the height data for a succession of lines, it is possible to form a three dimensional map of the surface features. The height of the tip (and therefore sample) is usually monitored using a laser beam which reflects off the backside of the cantilever (a gold coating on the cantilever makes it behave like a mirror). This reflected beam hits a multi-segment photodiode which can detect the movement of the beam, and therefore the movement of the cantilever and tip. The vertical

movement of the tip is measured as a voltage change [112-114]. Figure (3.11) shows the schematic diagram of atomic force microscopy (AFM) [115]. In this work for AFM images, (SPM-AA3000) supplied by Angstrom Advanced Inc, USA was used.

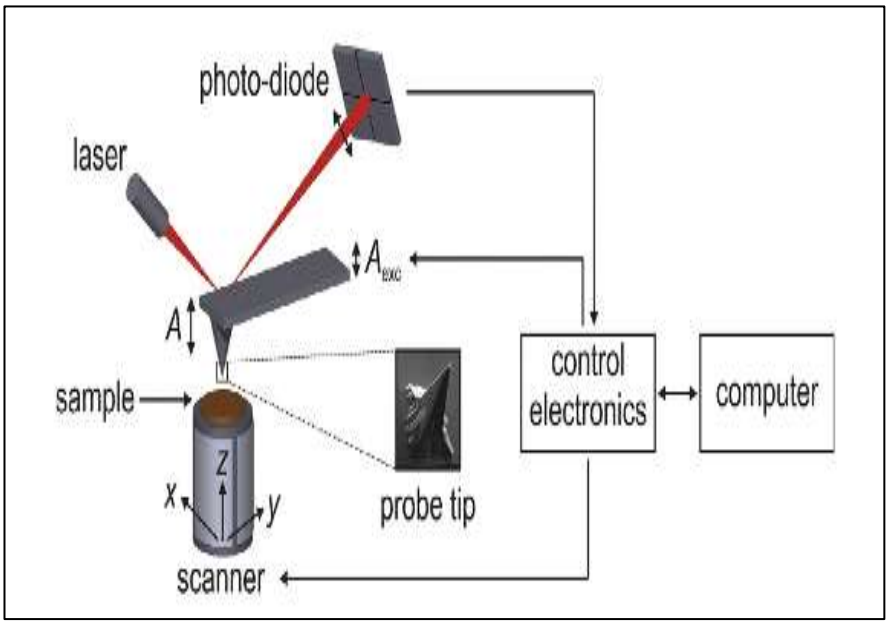

Fig 3.11: A schematic presentation of atomic force microscopy (AFM) [115].

3.6 Transmission Electron Microscopy (TEM)

Transmission electron microscopes usually have thermionic emission guns and electrons are accelerated anywhere between 40–200kV potential. However, TEM with >1000 kV acceleration potentials have been developed for obtaining higher resolutions. Owing to their brightness and very fine electron beams, field emission guns are becoming more popular as the electron guns. The test samples were prepared by placing a drop of suspension of interest on a copper mesh coated with an amorphous carbon film. The drop was dried with an infrared lamp (Philips, 100 W) until all the solvent had evaporated. This process was repeated three to four times. The TEM carbon grids were

loaded into the sample. The images were obtained at an accelerating voltage of 60 kV, with maximum magnification of 25000 x-450000 [47]. Samples of nanoparticles were identified by the transmission electron microscope TEM model CM10 pw6020, Philips-Germany.

Figure (3.12) shows the schematic diagram transmission electron microscopy (TEM) [116].

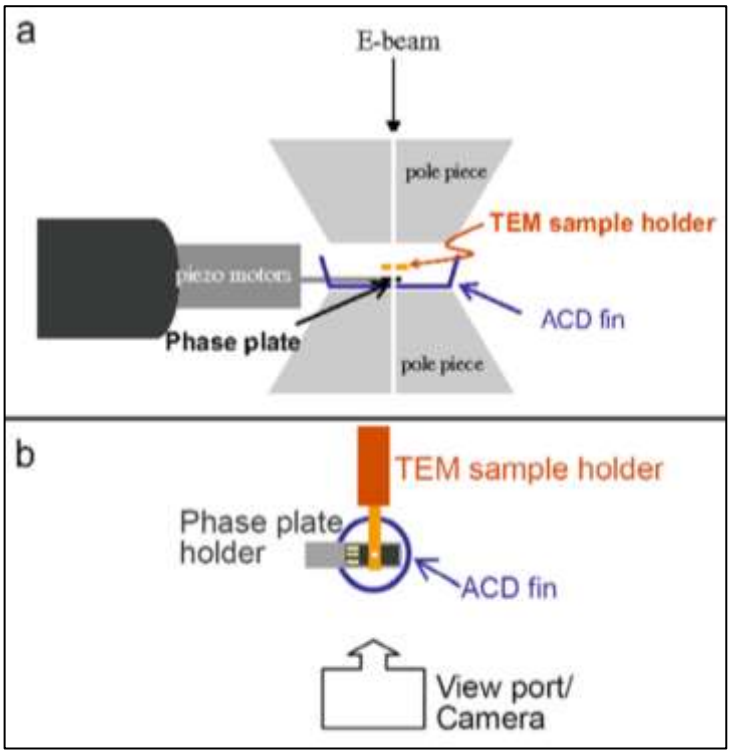

Fig 3.12: Schematic of the relative positions of various components around the pole pieces: (a) side view and (b) top view, where a monitoring set including the view port and a camera can be installed an the emptied aperture port [116].

3.7 Field Emission Scanning Electron Microscopy (FESEM)

A scanning electron microscope (SEM) is a high resolution microscope which uses a beam of electrons instead of visible light to investigate the morphological characteristics of the sample surface. The main differences between light and electron microscopy are the wavelengths of the beams which varies by a factor of many thousands

($\lambda_{visible\ light}$= 400–700 nm; $\lambda_{electron}$= Planck's constant/momentum of the electron). Electron microscopy offers a much higher resolution and thus it is possible to obtain images with a resolution of up to 2nm. The magnetic fields are used to focus the beam of electrons and to controlmagnification. It is necessary to decrease the pressure to at least 10^{-2}Pa to operate an electron microscope. An example for an electron microscope is the field emission scanning electron microscope (FESEM). The main difference in a FESEM to other electron microscopes is the production of the electron beam. The FESEM works in a high vacuum 10^{-5}-10^{-7}Pa. The electrons are generated by a field emission source and accelerated in a field gradient. The beam passes through theelectromagnetic lenses and focuses onto the specimen. As a result of this bombardment, different types of electrons are emitted from the specimen.The secondary electrons will be caught by a detector and an image of the sample surface is constructed by comparing the intensity of these secondary electrons to the scanning primary electron beam. Finally the black and white image is displayed on a monitor. For non-conductive materials it is necessary to fix the specimen on conductive tape and coat it with an electron dense material such as gold or carbon [117,118]. The surface morphology of the synthesized samples of gold and silver nanoparticles uncoated and coated by nano thin film layer of silica were observed by field emission scanning electron microscopy at room temperature, using FE-SEM model (Mira3-XMU, TESCAN, japan) the center of DeyPetronic co, Tehran, Iran. Figure (3.13) shows the schematic diagram field emission scanning electron microscopy (FE-SEM) [119].

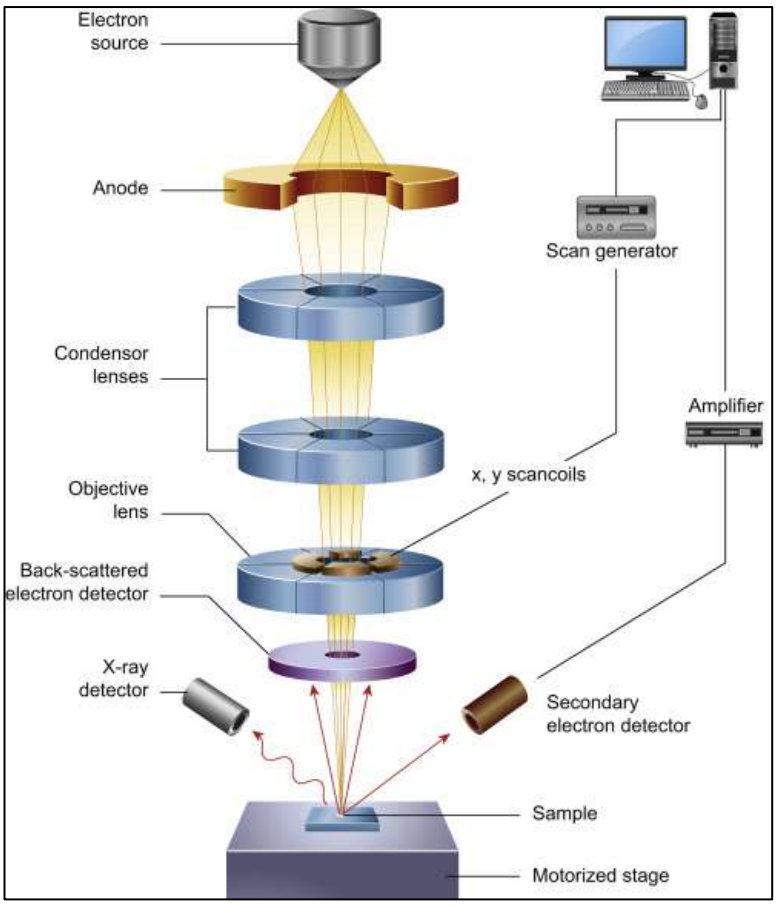

Fig 3.13: Schematic of a field emission scanning electron microscope (FESEM) [119].

3.8 Zeta Potential

The zeta potential of particles is a key indicator of the stability of a colloidal dispersion, like nanoparticles or liposomes, since it reflects the ability of particles to repulse each other electrostatically. Empirically, it is considered that absolute zeta potential values higher than ± 30 mV are indicative of stable dispersions. Only the magnitude of the zeta potential indicates the stability of the sample, whereas the sign of the zeta potential shows whether positive or negative charges are dominant at the surface. Below ±30mV processes like aggregation, sedimentation, and/or flocculation are more likely. The zeta potential (also known as electrokinetic potential) is established on the surface of any material

when it comes in contact with a liquid medium. It is thus an interfacial property. It is typically given in millivolt unit. If a material comes in contact with a liquid, the functional groups on its surface will react with the surrounding medium. This process results in a surface charge, which attracts the accumulation of oppositely charged ions. These counter ions arrange themselves spontaneously in a so-called electrochemical double layer. The zeta potential is defined as the sum of the initial surface charge and the accumulated layer. Measuring the zeta potential provides information on surface functionality, the stability of dispersed particles as well as interaction of dissolved compounds with the solid surface. The zeta potential of macroscopic surfaces is thus important for understanding the behavior of solid materials in many technical processes in which aqueous systems play a role, e.g. membranes for water treatment, biomaterials in contact with blood, or wet processing of semiconductor wafers. Knowledge of the zeta potential of a material helps you optimize specific surface modification processes for a material to perform at its best when applied [120]. The device used is zetaplus from Brooknaven company, USA. Figure (3.14) shows the schematic diagram Zeta potentia

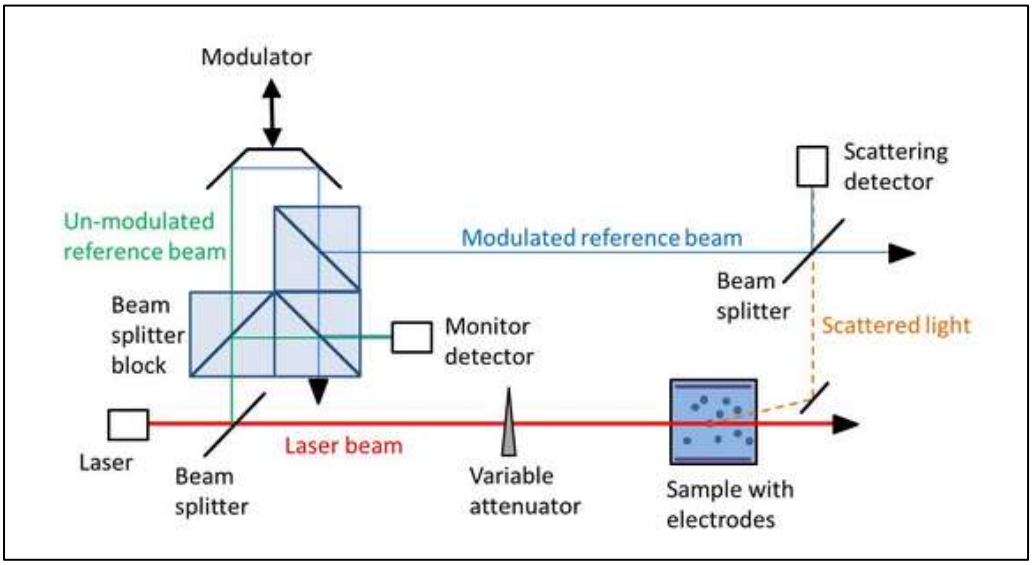

Fig 3.14: shows the schematic diagram Zeta potential [120].

3.9 Atomic Absorption Spectroscopy (AAS)

Atomic absorption spectroscopy (AAS) is a method that can be used to determine the mass concentration of an element in a liquid or solid sample. The radiation source may be continuous, emitting from visible to infrared wavelengths or from lines that emit discreet lines, specifically from each chemical element. The modulator helps to differentiate radiation emitted by radiation lamp coming from the environment and, mainly, from the atomization system. The atomization system removes analyte atoms in solution and generates atomic vapor composed of atoms in ground state, putting them between the source and the detector to absorb the radiation emitted. The monochromator is responsible for the selection of photons due to the wavelength that will reach the detector. The detector transforms the energy of photons into a proportional electronic signal and amplifies it. The signal intensity obtained is treated by systems for data acquisition and processing. At this point, it is important to stand out that the element cannot be directly determined by the atomic absorption spectrometer; even though the system provides that response. A spectrometer measures the amount of electromagnetic energy coming from the source before and after passing through a sample; this is, an indirect measurement of the absorption of energy by atoms present in the sample. To obtain a final result, a series of physical and chemical phenomenon should occur under controlled conditions and the measurement performed should be treated by an appropriate mathematical model. As each component of the equipment plays a part on this work, a more detailed study is essential to understand the performance of this analytical technique as well as its power and limitations [121]. The atomic absorption flame device model Nov AA

350 made in Germany. Figure (3.15) shows the schematic diagram atomic absorption spectroscopy (AAS) [121].

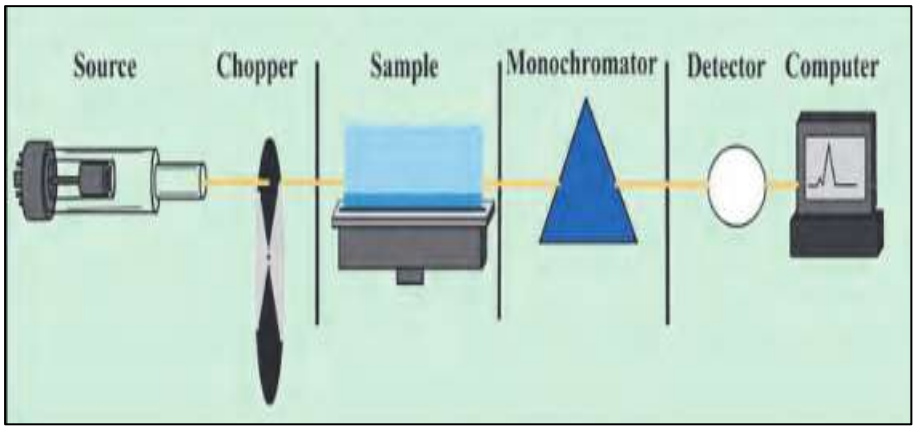

Fig 3.15: Schematic of Atomic absorption spectroscopy (AAS) [121].

3.10 Applied Part

Cell lines MCF-7 and HBL-100 were provided by the Iraqi Center for Cancer and Medical Genetic Researches (ICCMGR), experimental therapy department, cell bank unit, Al-Mustansiriyah University. All preparations were majorly done in ICCMGR laboratories.

3-10-1 Preparation of Solutions for Cell Culture:

- **Antbiotics Solutions:**

Streptomycin and Ampicillin as 100mg/µl concentration were added to all type of culture medium.

- **Sodium Bicarbonate:**

Sodium Bicarbonate Solution 2.2g were dissolved in one liter of culture medium or as recommended by manufacturing company.

- **Phosphate Buffer Saline PBS (PH 7.2)**

Ready to use powder 10.8g in one Liter, the solution was autoclaved at 121^{o}C for 15min, and then stored at 4^{o}C. Prior to any usage, PBS was warmed to 37^{o}C.

- **Fetal Bovine Serum (FBS)**

The serum is already thermally inactivated, sterile and use directly for tissue culture media.

- **Trypsin-Versene Solution**

Trypsin-Versene Solution was prepared by dissolving 10g of Trypsin-Versene powder, in one Liter PBS and stirred constantly on a magnetic stirrer at room temperature. Then solution was sterilized by Nalgen filter 0.22μm, and stored at 4^{o}C.

- **Crystal Violates Stain**

Dissolved 5g of crystal violet in 200ml of methanol and 50ml formaldehyde 37% to prepared stock solution. The added 10ml from stock solution to 90ml PBS (as 1 volume: 10 volume), filtered with an used for staining and fixation of cell culture.

3.10.2 Preparation of Tissue Culture Media

3.10.2.1 Rosswell Park Memorial Institute (RPMI) -1640 Medium

It was prepared as follows:

1. RPMI-1640 medium powder (with HEPES buffer and L-glutamine) 10.4 g. The powder was dissolved in approximately 600ml of double distilled water (DDW) and then the other components added:
2. Sodium bicarbonate powder 2.2g.
3. Benzyl penicillin 100μg/ml.
4. Streptomycin 100IU/ml.
5. Fetal Bovine Serum (FBS) 100ml.

The volume was made-up distilled water to get (1 litter), and the medium was sterilized using Nalgen filter of 0.2μm filter unit.

3.10.2.2 Minimal Essential Medium (MEM) (US Biological, USA)

It was prepared as follows:

1. MEM (with L-glutamine) 11g, the powder was dissolved in approximately 600ml of double distilled water (DDW) and then the other components added:
2. Sodium bicarbonate powder 2.2g
3. HEPES buffer (1M) 10ml
4. Benzyl penicillin 100g/ml
5. Streptomycin 100IU/ml.
6. Fetal Bovine Serum (FBS) 100 ml

The volume was made-up distilled water to get (1 litter), and the medium was sterilized using Nalgen filter of 0.2μm filter unit.

3.10.2.3 Maintenance Serum Free Medium (SFM)

MCF-7 cell line maintained in (MEM) and HBL-100 cell line maintained in (RPMI-1640) prepared as described as above but without FBS.

3.10.3 In Vitro Cytotoxic Assay

3. 10.3.1 Maintenance of Cell Lines

Cell lines used in this study were subcultured when monolayers were confluent. The growth medium was removed and the cell sheet washed twice with PBS. Two to three ml of trypsin-versene solution were added to the cell sheet and the flask rocked gently. After approximately 30 seconds most of the trypsin was poured off and the cells incubated at 30°C until they had detached from the flask. Cells were further dispensed

by pipetting in growth medium and then redistributed at the required concentration into culture flasks and re-incubated at 37°C in the presence of 5% CO_2 in air.

3.10.3.2 In vitro cytotoxicity of Gold and Silver Nanoparticles

Samples all were prepared gold and silver nanoparticles uncoated and coated filtered by 0.22µ milli pore filter. Then each sample being ready to be used as stocks, from each stock three concentrations were made 12.5, 25 and 50µg/mol.

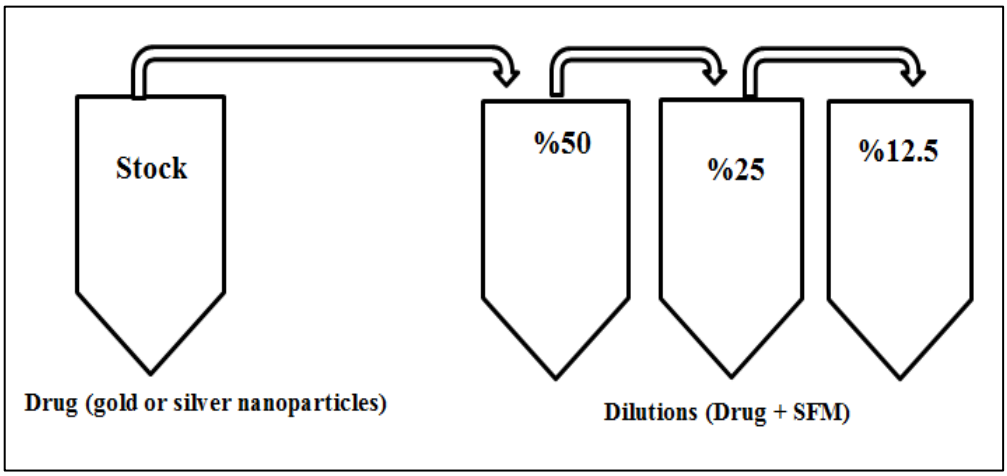

Fig 3.16: Scheme representation dilution method of gold and silver nanoparticles uncoated and coated solutions.

The cells were collected after adding trypsin/ versine 2-3ml not more than 10 min, and then concentrated into known volume with SFM. Cells were counted in order to get a final concentration of $1x10^5$ cell/well. Afterward, 0.2ml of prepared concentrations were added to the 96-well microtitration plate, as in Figure (3.17). The plate was covered with microtitration lid and sealed with adhesive film, placed in CO_2 incubator at 37°C for not more than 24hr (for cells adherence). After cells attachment, the plate was checked-out for contamination and the media were removed. Serial concentrations were added and three replicates were

used to each concentration and control (cells with SFM only). The exposure time was 72hr [122, 123].

After the exposure time was finished, the media was removed from the plate and washed with worm PBS three time. A 0.1ml of crystal violate working solution dye was added to each well and incubated at 37^{o}C for 20 min, at the end of last incubation period the dye was removed from the plate and the wells washed with tab water until the plate was become clean. Finally the plate become ready for reading after dry by FLUO star OPTIMA.

The inhibitory concentration was calculated as the drug concentration that is required to reduce absorption to half of the control. The equation was:

$$\text{The Percentage } \% = \frac{\text{control mean } - \text{test mean}}{\text{control mean}} * 100 \qquad \ldots\ldots\ldots (3.2)$$

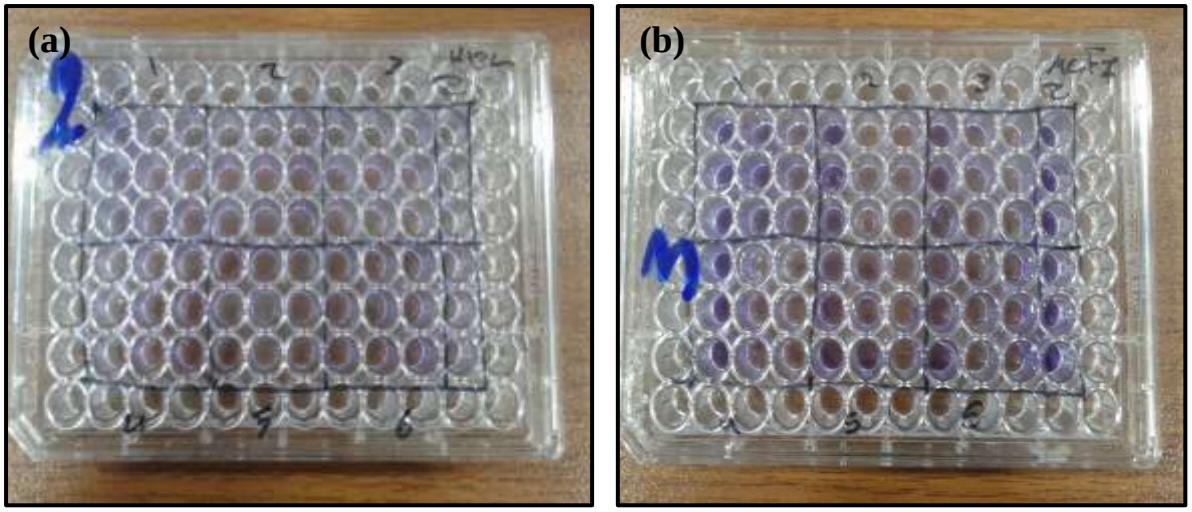

Fig 3.17: (a) Plate of contain on MCF-7 cell line with drug (gold and silver nanoparticles uncoated and coated). (b) Plate of contain on HBL-100 cell line with drug (gold and silver nanoparticles uncoated and coated).

3.11 FLUO star OPTIMA

This technique is used to assays cell toxicity. FLUO star OPTIMA device was used for this purpose is BMG LABTECH, Germany.

Fig 3.18: Image of FLUO star OPTIMA.

3.12 Inverted Microscope

This technique is used to tissue culture examination. Inverted microscope device was used for this purpose is Karl Kolb, Germany.

Fig 3.19: Image of Inverted Microscope.

Chapter Four

Results and Discussion

4.1 Introduction

This chapter includes the description and the analysis of the measurements and the discussion of the results. It focuses on the structural and optical properties of surface plasmon resonance (SPR) within high surface energy of gold and silver spherical nanoparticles uncoated and coated by nano thin film layer of silica. It will also discuss the effect of gold and silver spherical nanoparticles on cell lines MCF-7 and HBL-100.

4.2 Properties of Gold Nanoparticles

4.2.1 Absorbance of Gold Nanoparticles in Blue Shift

1. Temperature

UV–Vis spectra measurements results showed that with change temperature absorbance curve of each AuNPs sample had a single visible peak that was positioned in range of 519-524nm and it was related to spherical monodisperse AuNPs. The SPR peak shifts to shorter wavelength (more the peak shifts to left) and absorbance curve width became narrower (blue shift) at 80^{o}C this means particle size is smaller and uniformity of AuNPs. While other temperatures SPR peak shifts to longer wavelength this means particle size is larger as in Figure (4.1), also shows Figure (4.2) change of the absorbance peak position and absorbance intensity with the temperature changing. Temperature has an important role in activate the chemical reaction and the main cause of thermal oxidation of sodium citrate, that a decrease in temperature would result in a decrease in particle size. At relatively lower temperatures, the overall reduction rate and thus the nucleation rate was lower, so that fewer seed particles would be initially produced as compared to a higher

temperature and this agrees with [36]. Therefore, temperatures 80°C was selected optimum condition for synthesized gold nanoparticles.

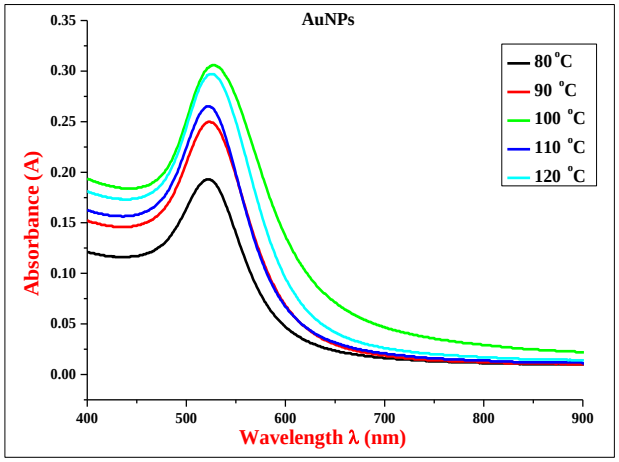

Fig 4.1: The absorbance of surface plasmon resonance (SPR) of gold nanoparticles (AuNPs) changes with the temperature changing.

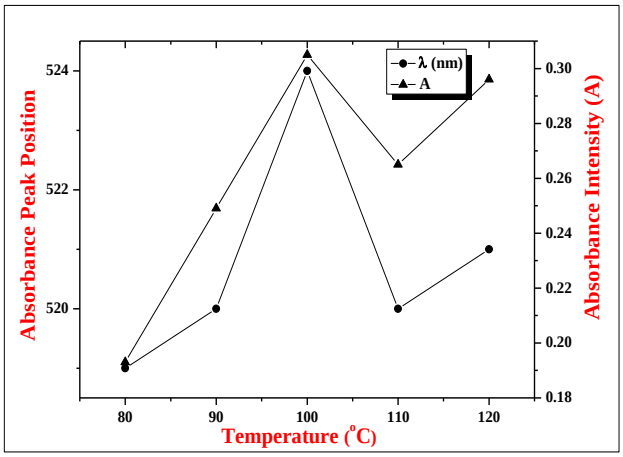

Fig 4.2: Absorbance peak position and absorbance intensity of surface plasmon resonance (SPR) of gold nanoparticles (AuNPs) changes with the temperature changing.

2- Trisodium Citrate Dihydrate (TCD) Content

UV–Vis spectra measurements results showed that with change of TCD content absorbance curve of each AuNPs sample showed a single visible peak that was positioned in range of 523-515nm and it was related to spherical of monodisperse AuNPs. The SPR peak shifts to shorter wavelength (more the peak shifts to left) and absorbance curve width became narrower (blue shift) at 700µl led to decrease the particle size and

uniformity as in Figure (4.3), also shows Figure (4.4) change of the absorbance peak position and absorbance intensity with the TCD content changing. The lower content of TCD could resultant from the binding of NPs with each other in solution due to their increased size, while using the high content of TCD led to decreasing of the size of AuNPs that formed well separated particles, also increase of TCD content works to provide the electrons necessary to reduce the gold charge and convert it into gold nanoparticle colloidal and this agrees with [20, 36]. Therefore, TCD content 700µl was selected optimum condition for synthesized gold nanoparticles.

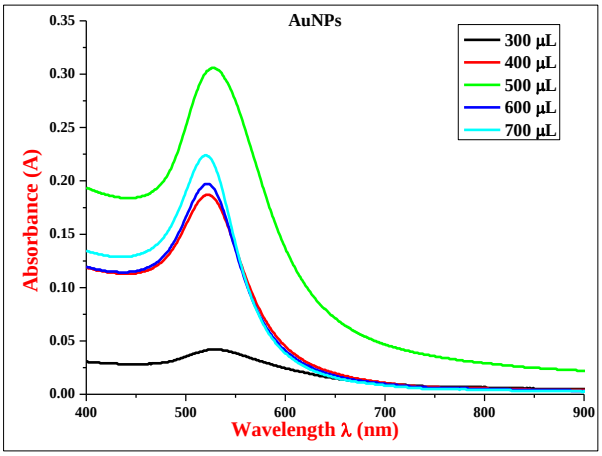

Fig 4.3: The absorbance of surface plasmon resonance (SPR) of gold nanoparticles (AuNPs) changes with the TCD content changing and a constant temperature 80°C.

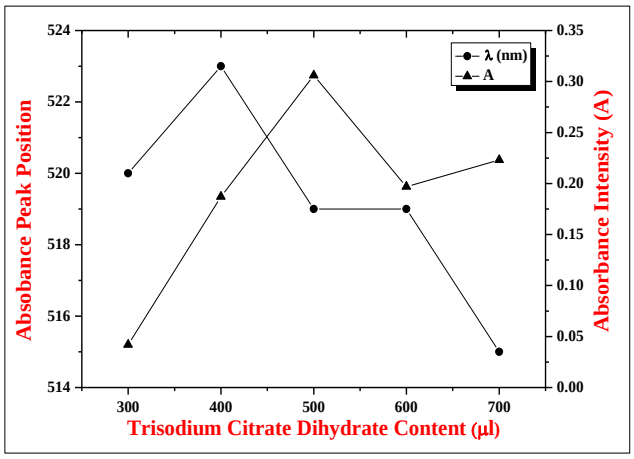

Fig 4.4: Absorbance peak position and absorbance intensity of surface plasmon resonance (SPR) of gold nanoparticles (AuNPs) changes with the TCD content changing and a constant temperature 80°C.

3- Deionized Water Volume

UV–Vis spectra measurements results showed that with change of deionized water volume absorbance curve of each AuNPs sample had a single visible peak that was positioned in the range of 517-521nm, it was related to spherical monodisperse of AuNPs. The SPR peak shifts to shorter wavelength (more the peak shifts to left) and absorbance curve width became narrower (blue shift) at 50ml this means the particle size is small and uniformity of AuNPs. While other deionized water volumes SPR peak shifts to longer wavelength this means particle size is larger as in Figure (4.5), also shows Figure (4.6) change of the absorbance peak position and absorbance intensity with the deionized water volume changing, since the SPR peak also affected by deionized water volume. Therefore, deionized water volume 50ml was selected optimum condition for synthesized gold nanoparticles.

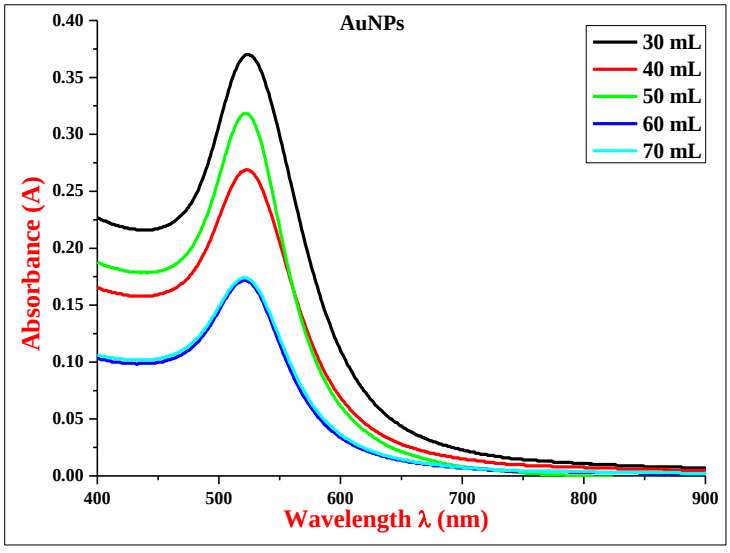

Fig 4.5: The absorbance of surface plasmon resonance (SPR) of gold nanoparticles (AuNPs) changes with the deionized water volume changing and a constant temperature 80°C and TCD content 700µl.

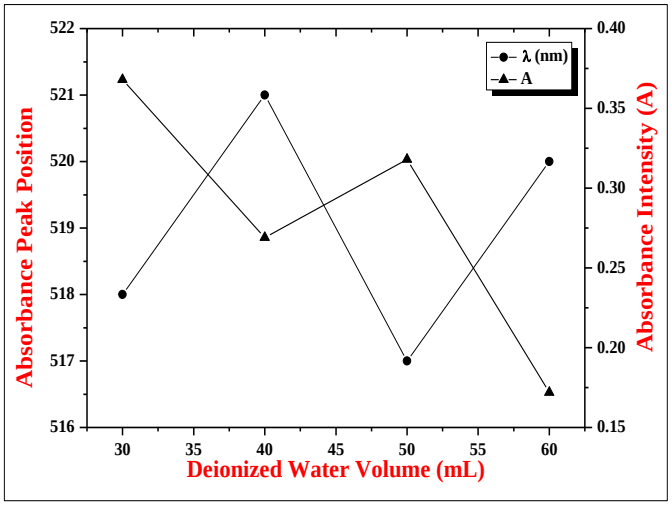

Fig 4.6: Absorbance position peak and absorbance intensity of surface plasmon resonance (SPR) of gold nanoparticles (AuNPs) changes with the deionized water volume changing and a constant temperature 80°C and TCD content 700µl.

4- Mixing Speed

UV–Vis spectra measurements results showed that with change the mixing speed absorbance curve of each AuNPs sample had a single visible peak that was positioned in range of 515-518nm and it was related to spherical monodisperse AuNPs. The SPR peak shifts to shorter wavelength (more the peak shifts to left) and absorbance curve width became narrower (blue shift) at 1000rpm led to decrease the particle size. On another hand, if the mixing speed increased more than 1000rpm the SPR peak was shifted as long wavelength that means the particle size is larger as in Figure (4.7), also shows Figure (4.8) change of the absorbance peak position and absorbance intensity with the mixing speed changing. Nanoparticle formation was observed for all mixing speeds and higher mixing speed provided a more homogenous suspension environment and hence increased the reaction surface area and high mixing speed resulted very small nanoparticle size with absorbance intensity increase, the narrow size distribution was found at the optimum rpm to gold nanoparticles was 1000rpm this means that the particle size

and size distribution were also affected by mixing speed and this agrees with [20]. Therefore, mixing speed 1000rpm was selected optimum condition for synthesized gold nanoparticles.

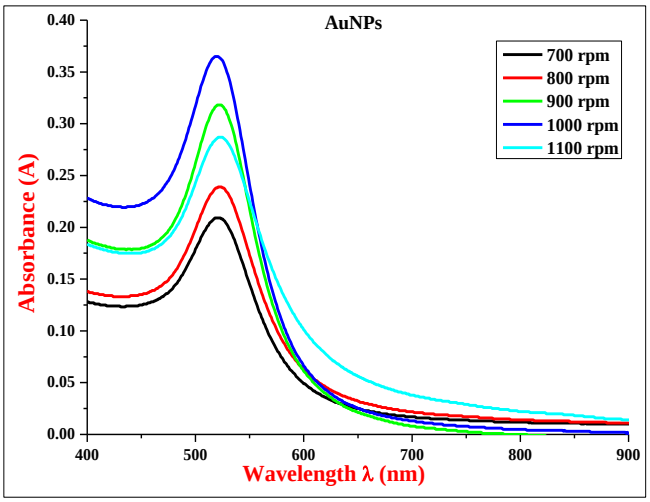

Fig 4.7: The absorbance of surface plasmon resonance (SPR) of gold nanoparticles (AuNPs) changes with the mixing speed changing and a constant temperature 80°C, TCD content 700µl and deionized water volume 50ml.

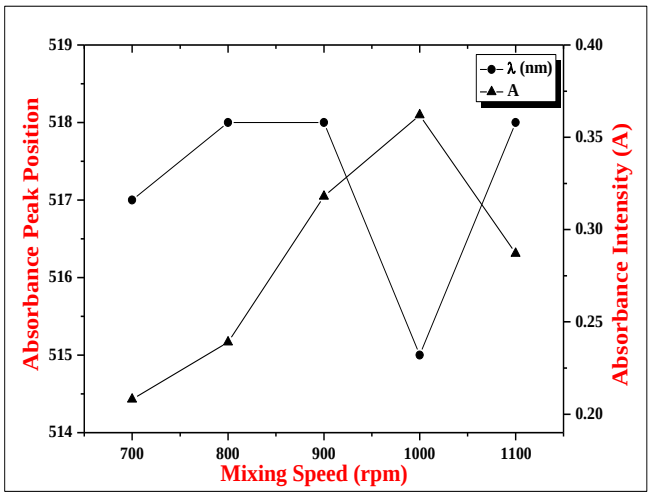

Fig 4.8: Absorbance peak position and absorbance intensity of surface plasmon resonance (SPR) of gold nanoparticles (AuNPs) changes with the mixing speed changing and a constant temperature 80°C, TCD content 700µl and deionized water 50ml.

The observation after synthesized of gold nanoparticles and evaluation of the effect different parameters such as the temperature, TCD content, deionized water volume and mixing speed. These parameters showed a strong effect on the position of SPR of gold nanoparticles (AuNPs), nanoparticle size, size distribution and the shape.

The peak SPR gives information about the size of the nanoparticle. Therefore, 80°C, 700µl of TCD, 50ml of deionized water and 1000rpm were selected optimum conditions for synthesized gold nanoparticles which SPR peak at 515nm.

Generally, gold nano colloidal displays a single absorption peak in the visible range between 515-524nm depending on the size of the particle, because of SPR and shows high absorption of visible light at 515nm, as in Figure (4.9). It is observed from the time stage of synthesizing the AuNPs the formation of gold nanowires as an intermediate step during the gold nanoparticles growth. These nanowires tend to absorb most of the visible light, giving the changing in color of the solution to the dark violet color, then they transform into spherical gold nanoparticles which only absorb light in the blue-green region, giving a red-wine color to the solution (only red light is transmitted efficiently) and this agrees with [80]. The intensity of the color and absorbance of the solution increased with the time as the reaction proceeded. The change of color of reaction mixture indicated that reduction of Au^{3+} is a rapid reaction and this agrees with [20].

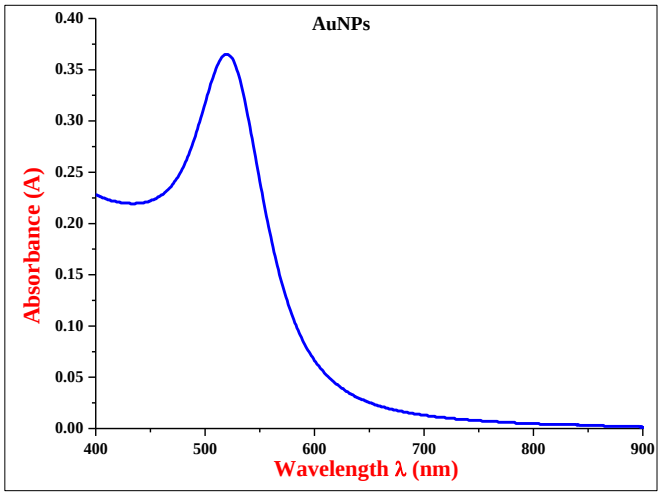

Fig 4.9: Optimum absorbance of surface plasmon resonance (SPR) of gold nanoparticles (AuNPs) in blue shift region.

Figure (4.10) shows that with the time, the gold nanoparticles were slight shift to the long wavelengths (red shift) with decreased in the absorbance intensity and also led to increasee in the particle sizes because the metal nanoparticles might undergo the transformation of thermodynamically unstable [17].

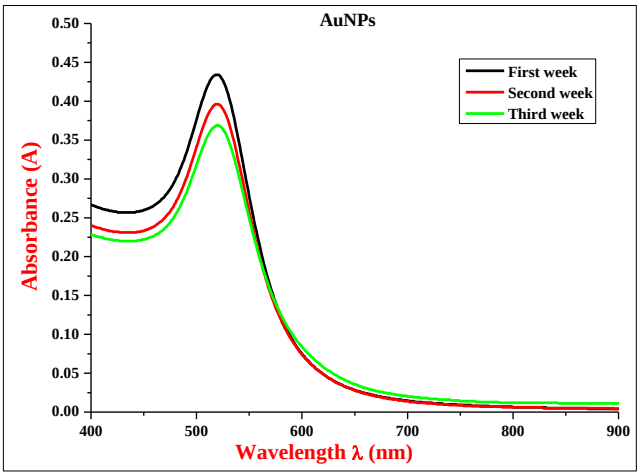

Fig 4.10: Optimum absorbance of surface plasmon resonance (SPR) of gold nanoparticles (AuNPs) in blue shift region with the time.

4.2.2 Absorbance of Gold Nanoparticles in Red Shift

1- SiO_2 Content

UV–Vis spectra measurements results showed that with change SiO_2 content absorbance curve of coated gold nanoparticles samples had a single visible peak that was positioned in range of 520-523nm it was related to spherical monodisperse AuNPs. The SPR peak shifts to shorter wavelength (less the peak shifts to the right) and absorbance curve width became narrower at 600µl of SiO_2 led to a little increase in particle size. While other SiO_2 contents the SPR peak shifts to longer wavelength (the peak shifts to more the right) this means particle size is larger as in Figure (4.11), also shows Figure (4.12) change of the absorbance peak position and absorbance intensity with SiO_2 content changing and this agrees with [31]. Coated method of gold nanoparticles by nano thin film layer of

silica has an important role in maintain on SPR position, because SiO_2 stability against and also chemically inert and optically transparent and this agrees with [56]. Therefore, SiO_2 content 600µl was selected optimum condition for coating gold nanoparticles.

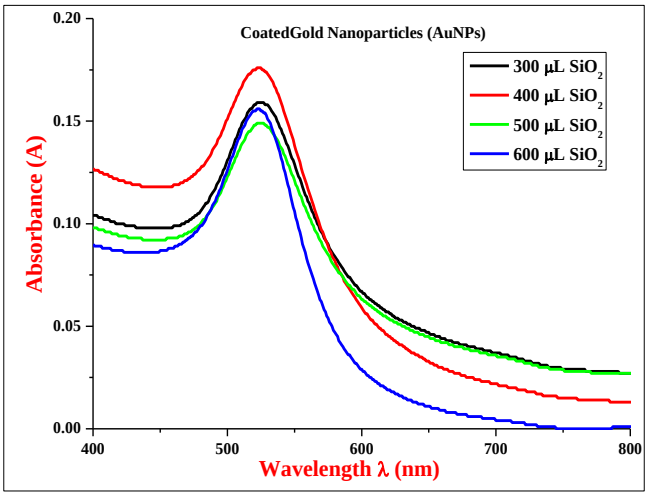

Fig 4.11: The absorbance of surface plasmon resonance (SPR) of gold nanoparticles (AuNPs) in red shift changes with the SiO_2 content changing.

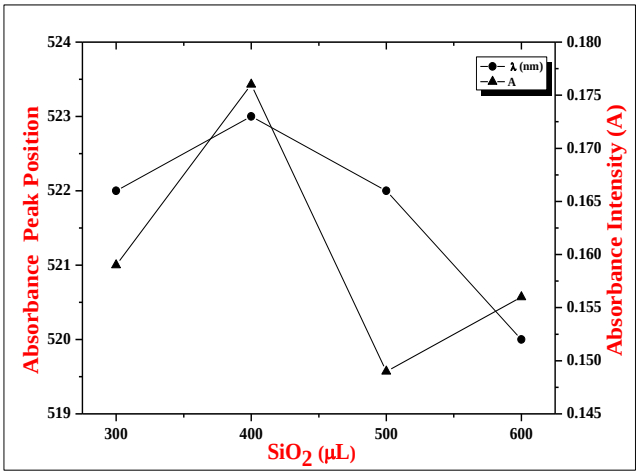

Fig 4.12: Absorbance position peak and absorbance intensity of surface plasmon resonance (SPR) of gold nanoparticles (AuNPs) changes with the SiO_2 content changing.

2- Deionized Water Volume

UV–Vis spectra measurements results showed that with change deionized water volume absorbance curve of each coated AuNPs sample had a single visible peak that was positioned in range of 524-520nm and

it was related to spherical monodisperse AuNPs, absorbance curve width became narrower and the SPR peak shifts to shorter wavelength (less the peak shifts to the right) at 20ml this means a little increase in particle size. On another hand, if the deionized water volume increased more than 20ml broadening the absorbance curve and the SPR peak was shifted as long wavelength this means the particle size is larger as in Figure (4.13), also shows Figure (4.14) change of the absorbance peak position and absorbance intensity with the deionized water volume changing. Therefore, deionized water volume 20ml was selected optimum condition for coating gold nanoparticles.

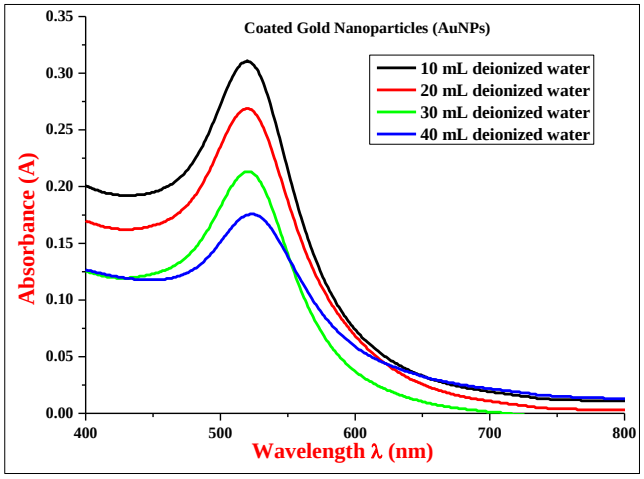

Fig 4.13: The absorbance of surface plasmon resonance (SPR) of gold nanoparticles (AuNPs) in red shift changes with the deionized water volume changing and a constant content SiO_2 600µl.

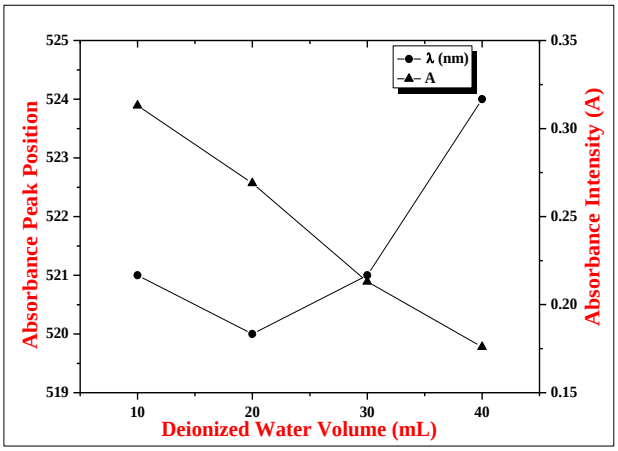

Fig 4.14: Absorbance peak position and absorbance intensity of surface plasmon resonance (SPR) of gold nanoparticles (AuNPs) changes with the deionized water volume changing and a constant SiO_2 content 600µl.

3- Gold Nanoparticles (AuNPs) Solution Volume

UV–Vis spectra measurements results showed that with change gold nanoparticles solution volume the absorbance curve of each coated AuNPs sample had a single visible peak that was positioned in range of 522-520nm and it was related to spherical monodisperse AuNPs, absorbance curve width became narrower and the SPR peak shifts to shorter wavelength (less the peak shifts to the right) at 20ml this means a little increase in particle size. While other gold nanoparticles solution volumes SPR peak shifts to longer wavelength (red shift) this means particle size is larger as in Figure (4.15), also shows Figure (4.16) change of the absorbance peak position and absorbance intensity with the gold nanoparticles solution volume changing. Therefore, gold nanoparticles solution volume 20ml was selected optimum condition for coating gold nanoparticles.

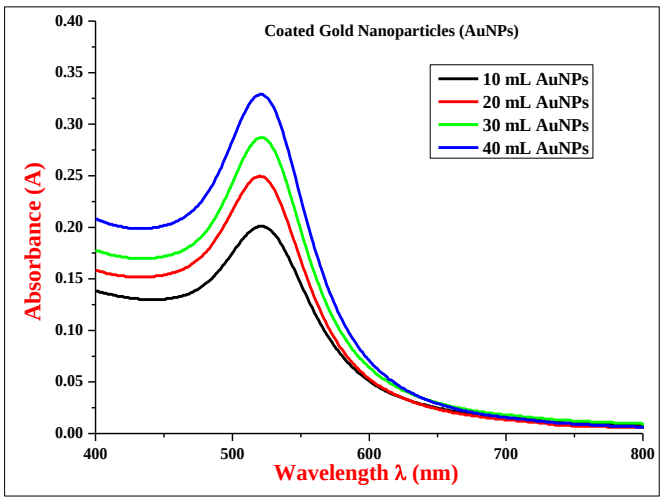

Fig 4.15: The absorbance of surface plasmon resonance (SPR) of gold nanoparticles (AuNPs) in red shift changes with the AuNPs solution volume changing and a constant SiO_2 content 600µl and deionized water volume 20ml.

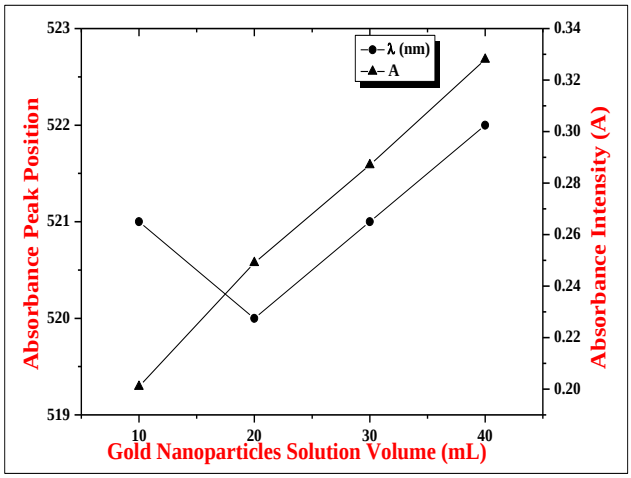

Fig 4.16: Absorbance peak position and absorbance intensity of surface plasmon resonance (SPR) of gold nanoparticles (AuNPs) changes with the AuNPs solution volume changing and a constant SiO_2 content 600µl and deionized water volume 20ml.

4- Ethanol Volume

UV–Vis spectra measurements results showed that with change the ethanol volume absorbance curve of each coated AuNPs sample had a single visible peak that was positioned in range of 521-518nm and it was related to spherical monodisperse AuNPs. The SPR peak shifts to shorter wavelength (less the peak shifts to the right) and absorbance curve width became narrower at 5ml this means a little increase in particle size. On another hand, if the ethanol volume increased more than 5ml the SPR peak shifts to longer wavelength (red shift) and broadening the absorbance curve this means particle size is larger as in Figure (4.7), also shows Figure (4.18) change of the absorbance peak position and absorbance intensity with the ethanol volume changing. Therefore, ethanol volume 5ml was selected optimum condition for coating gold nanoparticles.

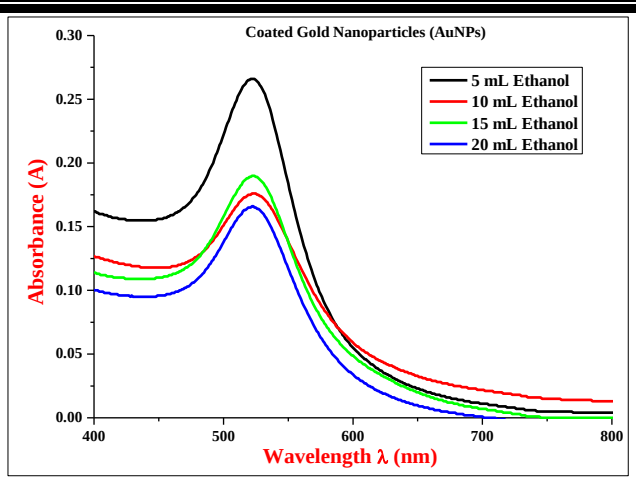

Fig 4.17: The absorbance of surface plasmon resonance (SPR) of gold nanoparticles (AuNPs) in red shift changes with the ethanol volume changing and a constant SiO_2 content 600µl, deionized water volume 20ml and AuNPs solution volume 20ml.

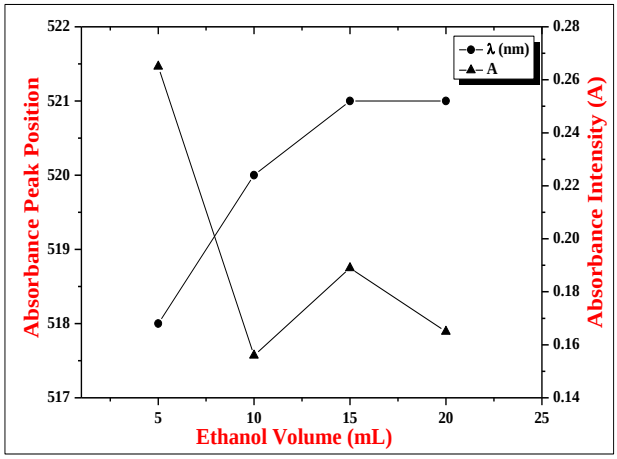

Fig 4.18: Absorbance peak Position and absorbance intensity of surface plasmon resonance (SPR) of gold nanoparticles (AuNPs) changes with the ethanol volume changing and a constant SiO_2 content 600µl, deionized water volume 20ml and AuNPs solution volume 20ml.

The observation after evaluation of the effect different parameters such as the SiO_2, deionized water volume, nanoparticles solution volume and ethanol volume. These parameters showed a strong effect in maintain on the position of SPR of coated gold nanoparticles (AuNPs). Therefore, SiO_2 600µl, 20ml of deionized water, 20ml of AuNPs solution and 5ml ethanol were selected optimum conditions for coating gold nanoparticles which SPR peak at 518nm, as Figure (4.19).

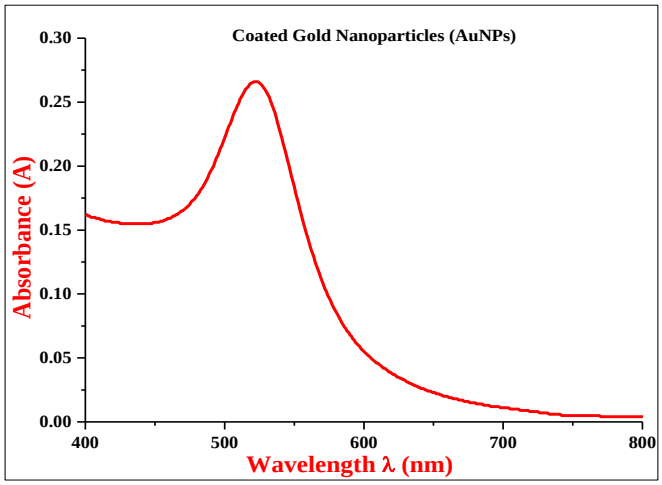

Fig 4.19: Optimum absorbance of surface plasmon resonance (SPR) of gold nanoparticles (AuNPs) in red shift region.

Figure (4.20) shows a red shift occurred to the SPR of AuNPs from 515nm to 518nm this means less increase in particle size with maintain spherical shape and this agrees with [23,33].

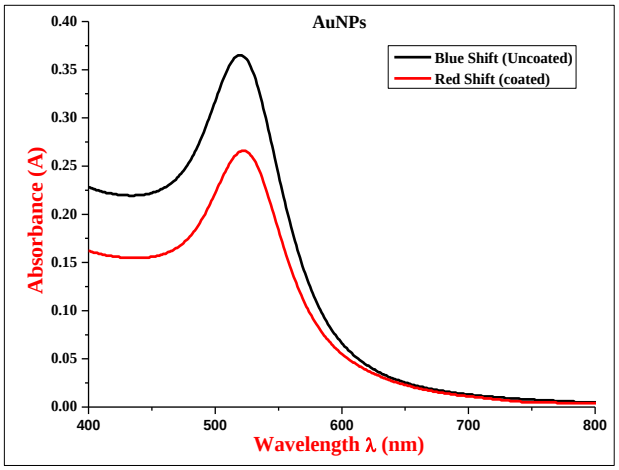

Fig 4.20: Optimum absorbance of surface plasmon resonance (SPR) of gold nanoparticles (AuNPs) in blue and red shift regions.

It is observed from Figure (4.21) that with the time position of surface plasmon resonance (SPR) of coated gold nanoparticles (AuNPs) is not changed with increasing absorbance intensity because coating method by nano thin film layer of silica which has an important role in maintaining nanoparticles stability and preventing it from agglomeration [81- 83].

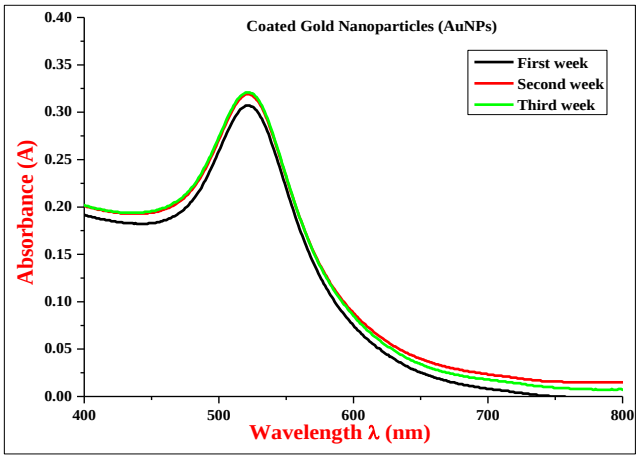

Fig 4.21: Optimum absorbance of surface plasmon resonance (SPR) of gold nanoparticles (AuNPs) in red shift region with the time.

4.2.3 Infra-Red Spectrum of Gold Nanoparticles

Figure (4.22) shows the FTIR spectrum obtained for gold nanoparticles (AuNPs) synthesized at (80°C, 700µl of TCD, 50ml of deionized water and 1000rpm) and coated at (600µl of SiO_2, 20ml of deionized water, 20ml of AuNPs and 5ml of ethanol). FTIR spectrum shown strong absorption bands at 3431cm^{-1} representing O-H stretching of carboxylic acid. The absorption peaks located at 2341 cm^{-1} correspond to C-H stretching of alkanes. The absorption peaks located at 1627 and 1506 cm^{-1} correspond to C=C stretching of alkanes and aromatics. The absorption peaks located at 1388 cm^{-1} correspond to C-O stretching of carboxylic acid. The absorption peaks located 975, 962, 632, 524 and 499 cm^{-1} correspond to O-H bend of out-level carboxylic acid. The hydroxyl groups would donate electrons to the AuNPs unoccupied molecular achieve its noble state, also it is observed that the gold nanoparticles after coating almost have the same absorption peaks with a little shift for some absorption peaks this means that the coating method led to a little increase in the size with maintaining on nanoparticles shape and prevents it from deforming, the absorption bands 524 and 499 cm^{-1} refer to

harmony happening between inorganic elements (gold) and organic compounds (Trisodium Citrate Dihydrate) and this agrees with [34].

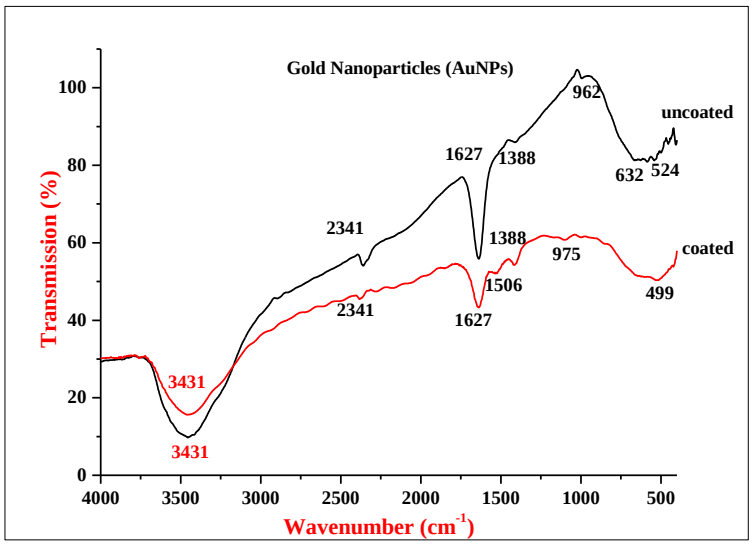

Fig 4.22: FTIR spectra obtained of gold nanoparticles (AuNPs) uncoated and coated by nano thin film layer of silica.

4.2.4 Morphology of Gold Nanoparticles

Figure (4.23) shows AFM image of gold nanoparticles (AuNPs) synthesized at (80°C, 700µl of TCD, 50ml of deionized water and 1000rpm) and coated at (600µl of SiO_2, 20ml of deionized water, 20ml of AuNPs and 5ml of ethanol). It is observed each nucleus gold nanoparticles (AuNPs) uncoated and coated by nano thin film layer of silica is spherical in geometry and has a radius r is less than critical radius r* (r < r*) this means increased surface tension and hence increased surface energy and this agrees with [55]. It is observed from Table (4.1) that surface roughness and root mean square (RMS) of gold nanoparticles (AuNPs) increase after coating and this means increase in particle size, thus the smallness of these volumes indicates the smoothness of the surface which confirms the smallness of these granules. Since the relationship between root mean square (RMS) and average grain size is a

direct relationship this led to average grain size increase and this agrees with [31].

Table 4.1: Surface roughness, root mean square (RMS) and grain size of gold nanoparticles (AuNPs) uncoated and coated by nano thin film layer of silica.

Sample	Uncoated AuNPs	Coated AuNPs
Surface Roughness (nm)	1.94	2.4
Root Mean Square (nm)	3.17	3.67
Grain size (nm)	56.32	58.46

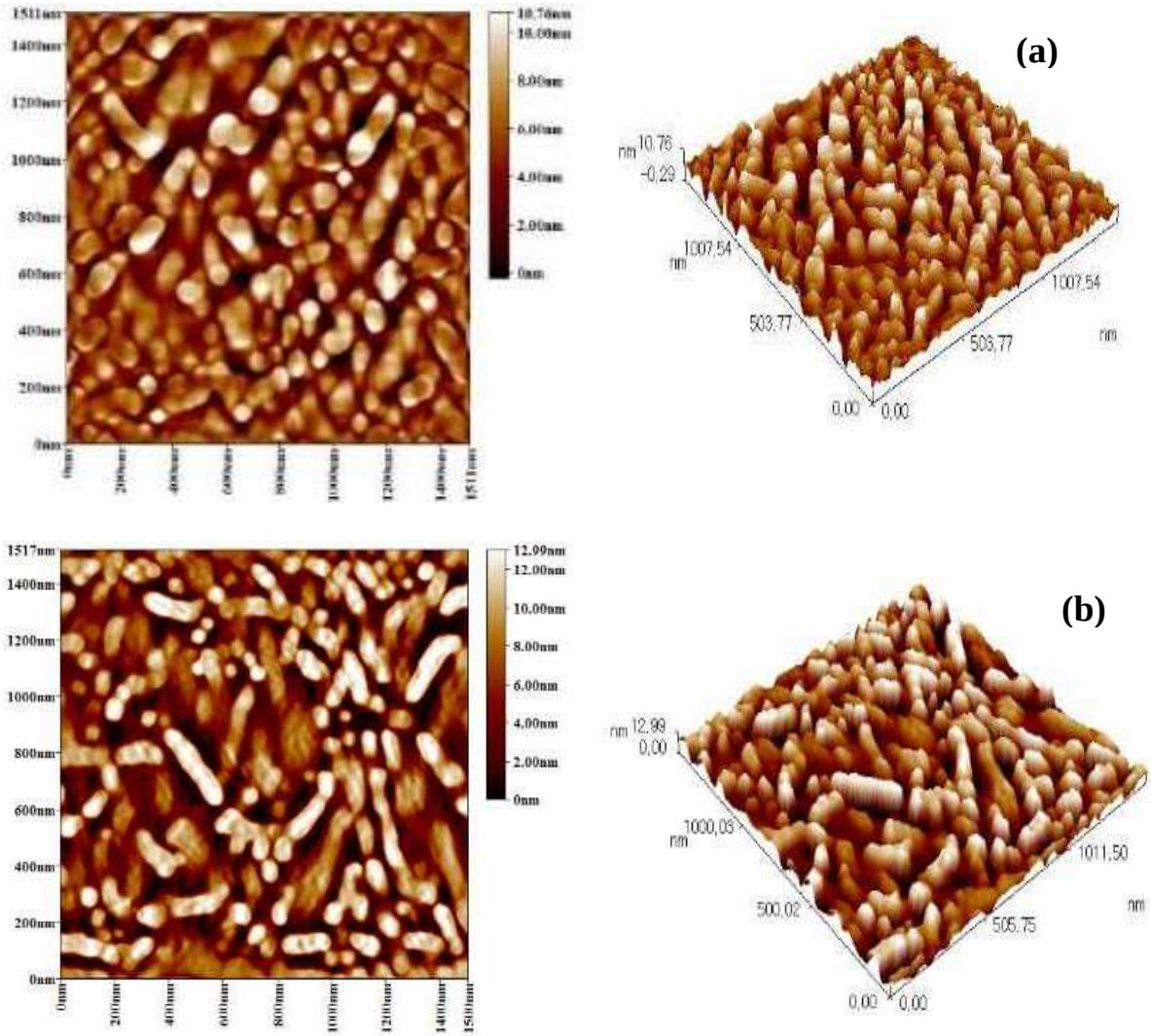

Fig 4.23: AFM images: (a) Uncoated gold nanoparticles (AuNPs). (b) Coated gold nanoparticles (AuNPs) by nano thin film layer of silica.

4.2.5 Size and Shape of Gold Nanoparticles

Figure (4.24) shows the TEM images of gold nanoparticles (AuNPs) synthesized at (80°C, 700µl of TCD, 50ml of deionized water and 1000rpm) and coated at (600µl of SiO_2, 20ml of deionized water, 20ml of AuNPs and 5ml of ethanol). TEM analysis reveal that the gold nanoparticles have a narrow size distribution and spherical shape with an average size 3-6nm. On another hand, it is observed after coating by nano silica layer that the gold nanoparticles have a narrow size distribution and spherical shape with a less increase in the particles size 9-18nm and this agrees with [21, 124].

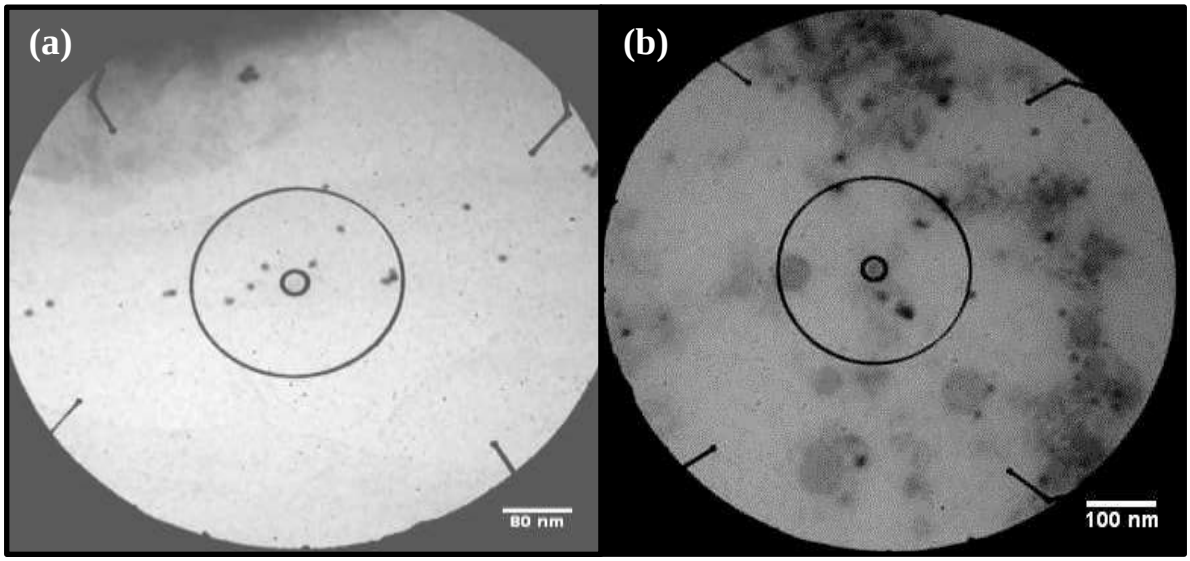

Fig 4.24: TEM images: (a) Uncoated gold nanoparticles (AuNPs). (b) Coated gold nanoparticles (AuNPs) by nano thin film layer of silica.

FESEM are the best analyzing tool for structural and morphological properties of synthesized materials. Figure (4.25) shows structure and the morphology of AuNPs investigated using FESEM analysis. The images reveal that narrow size distribution of gold nanoparticles with size < 20nm and spherical shape. On another hand, it is observe shape after coating by nano silica layer that the gold nanoparticles have a narrow size distribution and spherical shape with a less increase in the

particles size this means that coated method has an important role in maintain and control the shape and size of the nanoparticles and this agrees with [124].

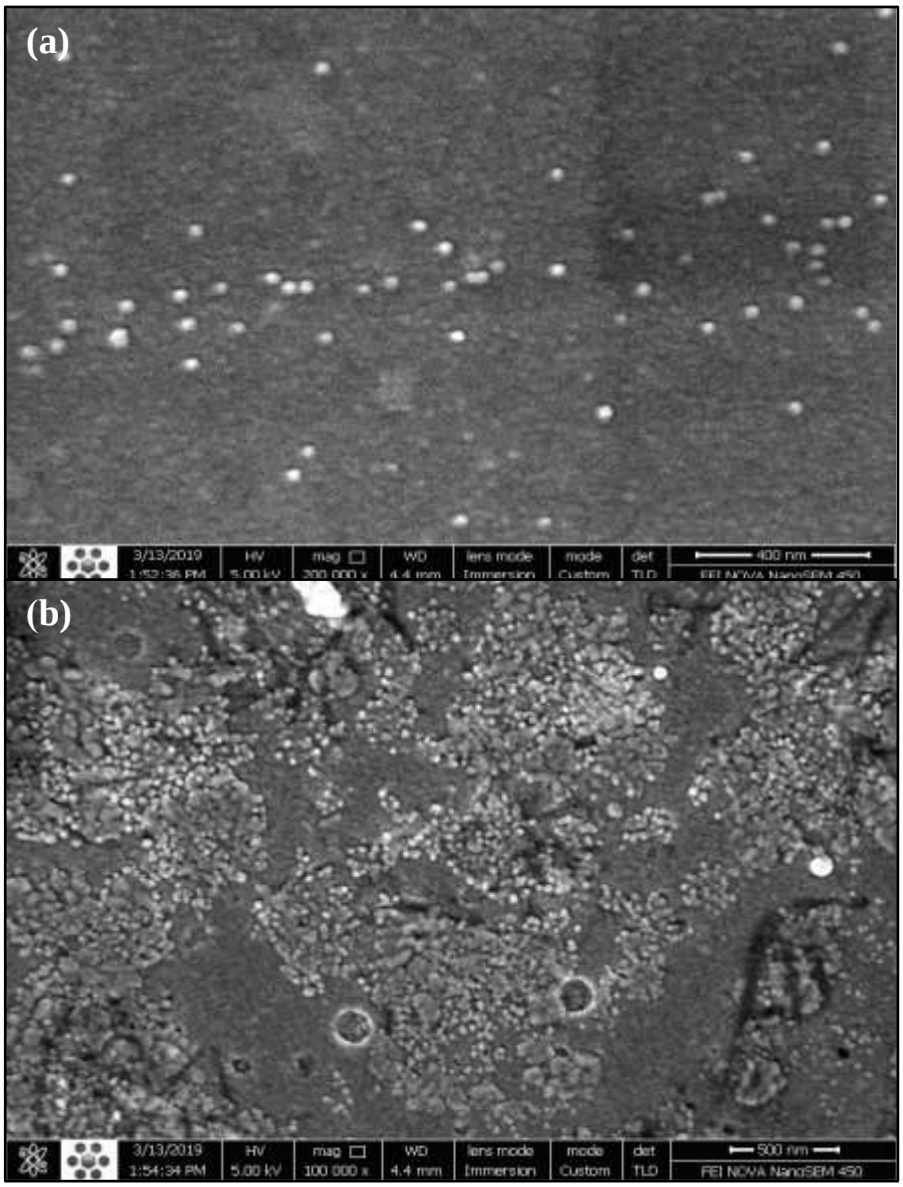

Fig 4.25: FESEM images: (a) Uncoated gold nanoparticles (AuNPs). (b) Coated gold nanoparticles (AuNPs) by nano thin film layer of silica.

4.2.6 Stability of Gold Nanoparticles

Figure (4.26) shows stability of gold nanoparticles (AuNPs) synthesized at (80°C, 700µl of TCD, 50ml of deionized water and 1000rpm) and coated at (600µl of SiO_2, 20ml of deionized water, 20ml of AuNPs and 5ml of ethanol). Zeta potential for coated with nano thin film

layer of silica (−25.92mV) is higher than the uncoated ones (−25.02 mV) and that means more stability occurred because coating method by nano thin film layer of silica which has an important role in maintaining nanoparticles stability and preventing it from agglomeration and this agrees with [21]. The negative zeta potential confirms the negative charge on the surface of colloidal nanoparticles. The columbic repulsion forces induced by surface negative charge minimize the aggregation and thus contribute to the stability of the synthesized nanoparticles and this agrees with [124].

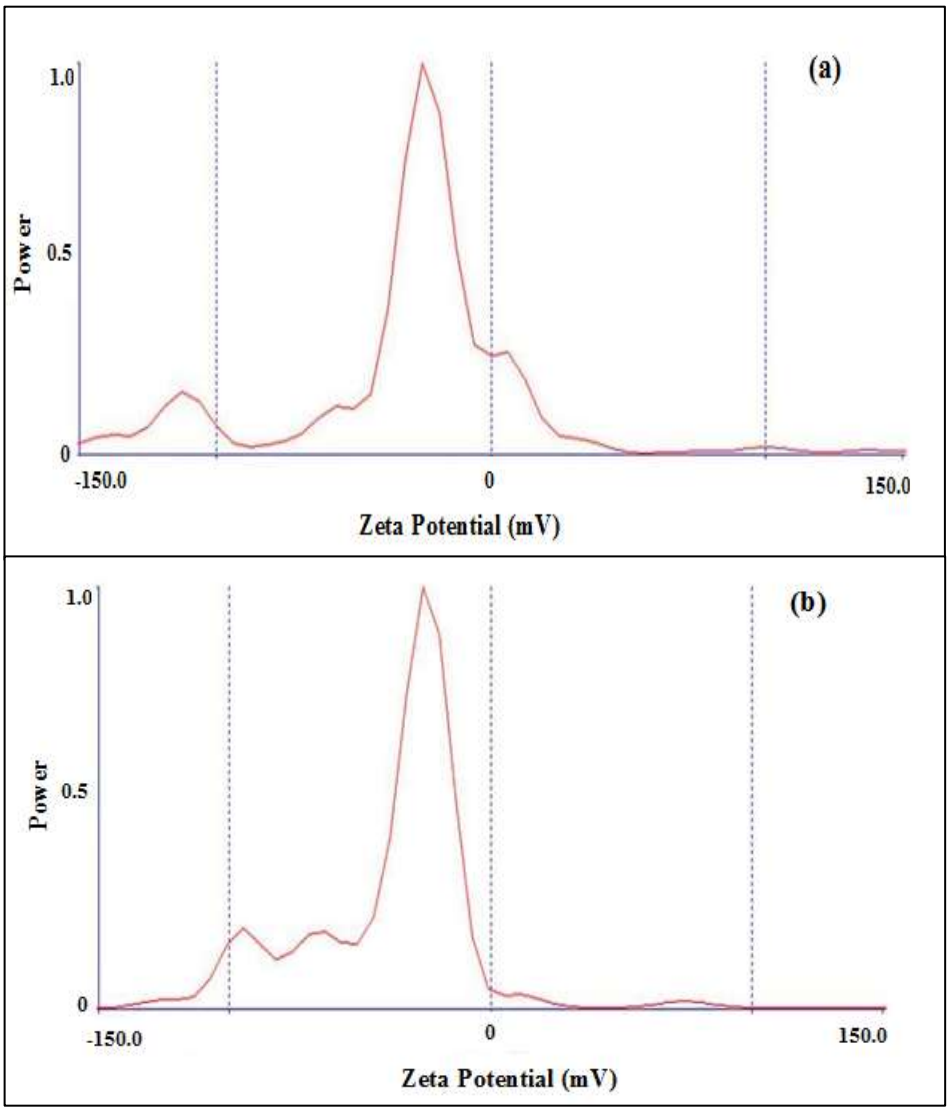

Fig 4.26: Zeta potential graphs: (a) Uncoated gold nanoparticles (AuNPs). (b) Coated gold nanoparticles (AuNPs) by nano thin film layer of silica.

4.2.7 Concentration of Gold Nanoparticles

Atomic Absorption Spectroscopy measurements results showed that the concentration of gold nanoparticles was 500μg/ml, but after coated by nano thin film layer of silica the gold nanoparticles concentration was decreased to 300μg/ml because of addition the coating solution to gold nanoparticles and this agrees with [124].

4.3 Properties of Silver Nanoparticles

4.3.1 Absorbance of Silver Nanoparticles in Blue Shift

1- Time

UV–Vis spectra measurements results showed that with change time absorbance curve of each AgNPs sample adjusted by NaOH and NH_4OH had a single visible peak that was positioned in range of 405-401nm and it was related to spherical monodisperse AgNPs. The SPR peak shifts to shorter wavelength (more the peak shifts to left) and absorbance curve width became narrower (blue shift) at 20min this means particle size is smaller and uniformity of AgNPs. While other times SPR peak shifts to longer wavelength this means particle size is larger as in Figure (4.27), also shows Figure (4.28) change of the absorbance peak position and absorbance intensity with the time changing. Time of reaction had a strong effect on size and optical property of silver nanoparticles (AgNPs). Therefore, time 20min was selected optimum condition for synthesized silver nanoparticles adjusted by NaOH and NH_4OH.

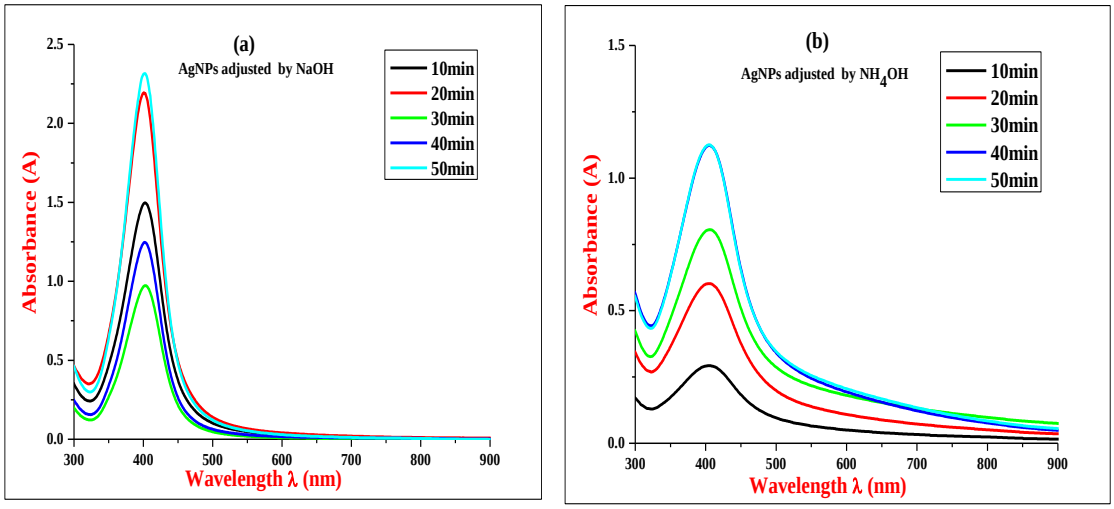

Fig 4.27: (a) and (b) The absorbance of surface plasmon resonance (SPR) of silver nanoparticles (AgNPs) adjusted by NaOH and NH_4OH respectively changes with the time changing.

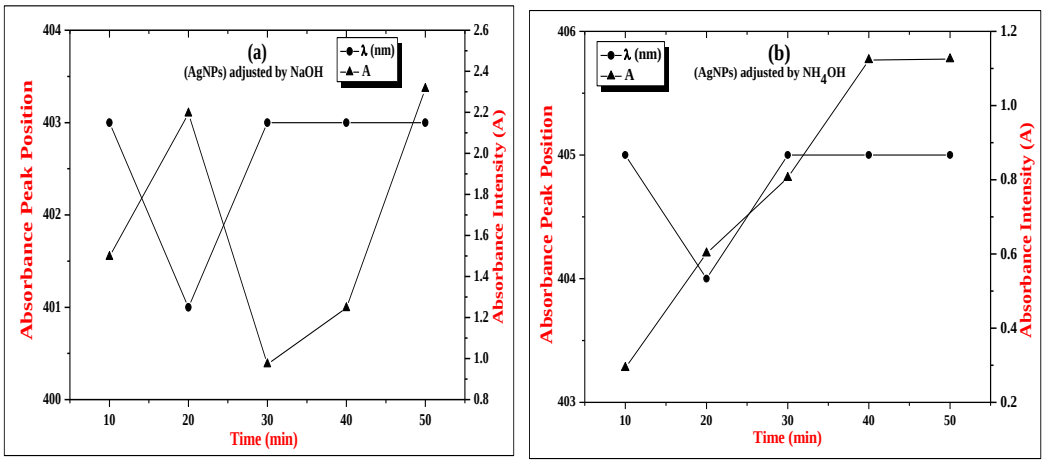

Fig 4.28: (a) and (b) Absorbance peak position and absorbance intensity of surface plasmon resonance (SPR) of silver nanoparticles (AgNPs) adjusted by NaOH and NH_4OH respectively changes with the time changing.

2- Gallic Acid (GA) Weight

UV–Vis spectra measurements results showed that with change gallic acid weight, absorbance curve of each AgNPs sample adjusted by NaOH and NH_4OH had a single visible peak that was positioned in range of 397-408nm and it was related to spherical monodisperse AgNPs. The SPR peak shifts to shorter wavelength (more the peak shifts to left) and

absorbance curve width became narrower (blue shift) at 0.02g and 0.008g for AgNPs adjusted by NaOH and NH_4OH respectively this means particle size is smaller and uniformity of AgNPs. While other weights SPR peak shifts to longer wavelength this means particle size is larger as in Figure (4.29), also shows Figure (4.30) change of the absorbance peak position and absorbance intensity with the gallic acid content changing. Gallic acid was used as reducing and stabilizing agent in the synthesis of silver nanoparticles. The NPs synthesized were observed from the presentation color of the reaction mixture to brown in less than a minute. It is obvious that the interference of phenolic group was responsible for reducing Ag^+ to Ag^0 with phenol group offering stability and this agrees with [28].Therefore, gallic acid weights 0.02g and 0.008g was selected optimum condition for synthesized silver nanoparticles adjusted by NaOH and NH_4OH respectively.

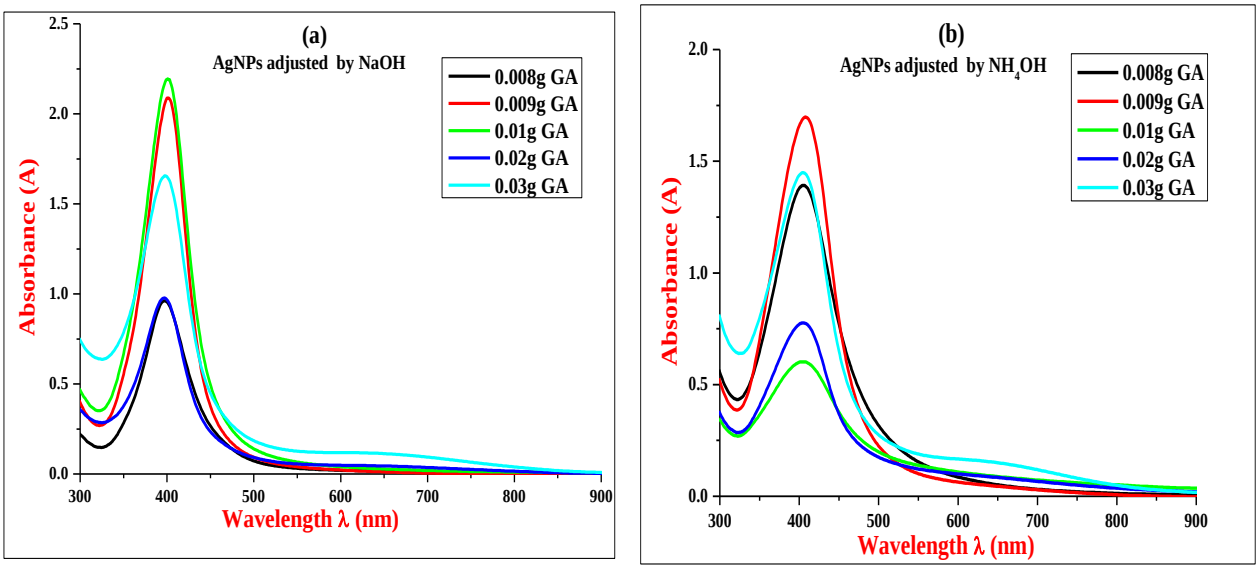

Fig 4.29: (a) and (b) The absorbance of surface plasmon resonance (SPR) of silver nanoparticles (AgNPs) adjusted by NaOH and NH_4OH respectively changes with the gallic acid weight changing and a constant time 20 min.

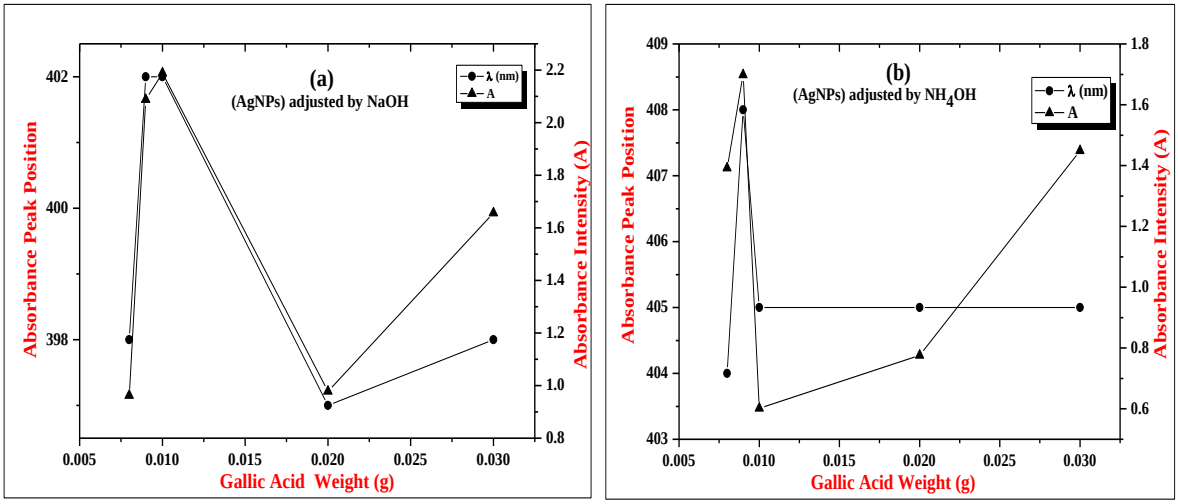

Fig 4.30: (a) and (b) Absorbance peak position and absorbance intensity of surface plasmon resonance (SPR) of silver nanoparticles (AgNPs) adjusted by NaOH and NH_4OH respectively changes with the gallic acid weight changing and a constant time at 20 min.

3- Temperature

UV–Vis spectra measurements results showed that with change temperature absorbance curve of each AgNPs sample adjusted by NaOH and NH_4OH had a single visible peak that was positioned in range of 396-418nm and it was related to spherical monodisperse AgNPs and NH_4OH had a single visible peak that was positioned in range of 396-418nm and it was related to spherical monodisperse AgNPs. The SPR peak shifts to shorter wavelength (more the peak shifts to left) and absorbance curve width became narrower (blue shift) at 100^{o}C and 80^{o}C for AgNPs adjusted by NaOH and NH_4OH respectively this means particle size is smaller and uniformity of AgNPs. While other temperatures SPR peak shifts to longer wavelength this means particle size is larger as in Figure (4.31), also shows Figure (4.32) change of the absorbance peak position and absorbance intensity with the temperature changing. Therefore, temperatures 100^{o}C and 80^{o}C was selected optimum condition for synthesized silver nanoparticles adjusted by NaOH and NH_4OH respectively.

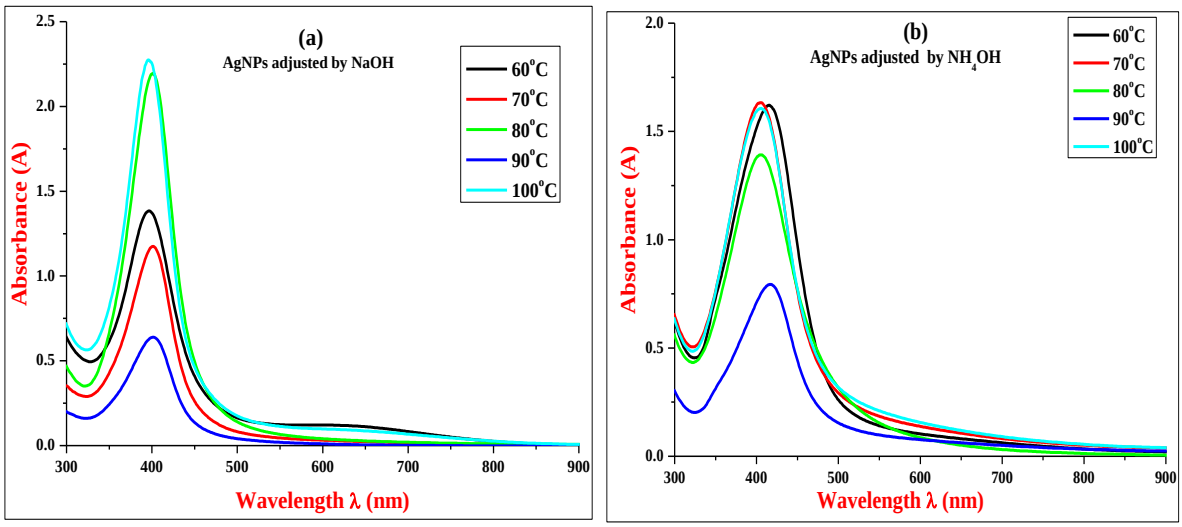

Fig 4.31: (a) and (b) The absorbance of surface plasmon resonance (SPR) of silver nanoparticles (AgNPs) changes with the temperature changing and a constant time 20 min and gallic acid weight 0.02g and 0.008g for AgNPs adjusted by NaOH and NH_4OH respectively.

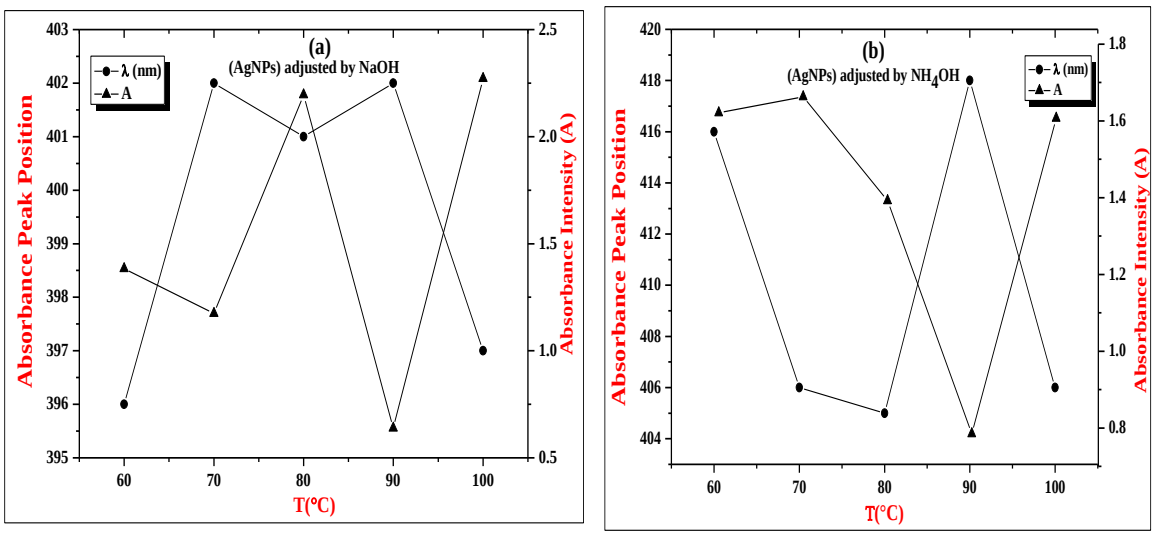

Fig 4.32: (a) and (b) Absorbance peak position and absorbance intensity of surface plasmon resonance (SPR) of silver nanoparticles (AgNPs) changes with the temperature changing and a constant time 20 min and gallic acid weight 0.02g and 0.008g for AgNPs adjusted by NaOH and NH_4OH respectively.

The observation after synthesized of silver nanoparticles and evaluation of the effect different parameters such as the time, gallic acid weight and temperature. These parameters showed a strong effect on the position of SPR of silver nanoparticles (AgNPs), nanoparticle size, size

distribution and the shape. The SPR peak gives information about the size of the nanoparticle.

Therefore, 20min, 0.02g of GA and 100°C were selected optimum conditions for synthesized of silver nanoparticles adjusted by NaOH which the SPR peak at 396nm. Whereas, 20min, 0.008g of GA and 80°C were selected optimum conditions for synthesized of silver nanoparticles adjusted by NH_4OH which SPR peak at 405nm figure (4.33).

The appearance of yellow color in the reaction mixtures which gradually changed to reddish brown tinge indicated the formation of silver nanoparticle formation. Furthermore, the nanoparticle synthesis was assured by monitoring the absorption spectra of synthesized colloidal solutions. It showed a broad absorption band and the intensity was found to increase with time the distinctive color of silver nanoparticle colloidal solution is due to the phenomenon plasmon absorbance. Incident light creates oscillations in conduction electrons on the surface of the nanoparticles. The collective oscillation of conduction electrons within metal nanoparticles, the SPR, enables scattering and absorption of light at a particular frequency, giving them the color. Owing to the SPR in the interaction of electromagnetic radiation and the electrons in the conduction band around the nanoparticles, an optical absorption band of (λ_{max}) volume which is a typical feature of the absorption of metallic silver NP's due to the (SPR), indicating the presence of AgNP's in the solutions and this agrees with [27].

The absorption spectrum of (SPR) of spherical silver nanoparticles present a maximum between 396nm and 418 nm with a blue or red shift when particle size diminishes or increases, respectively and this agrees with [19].

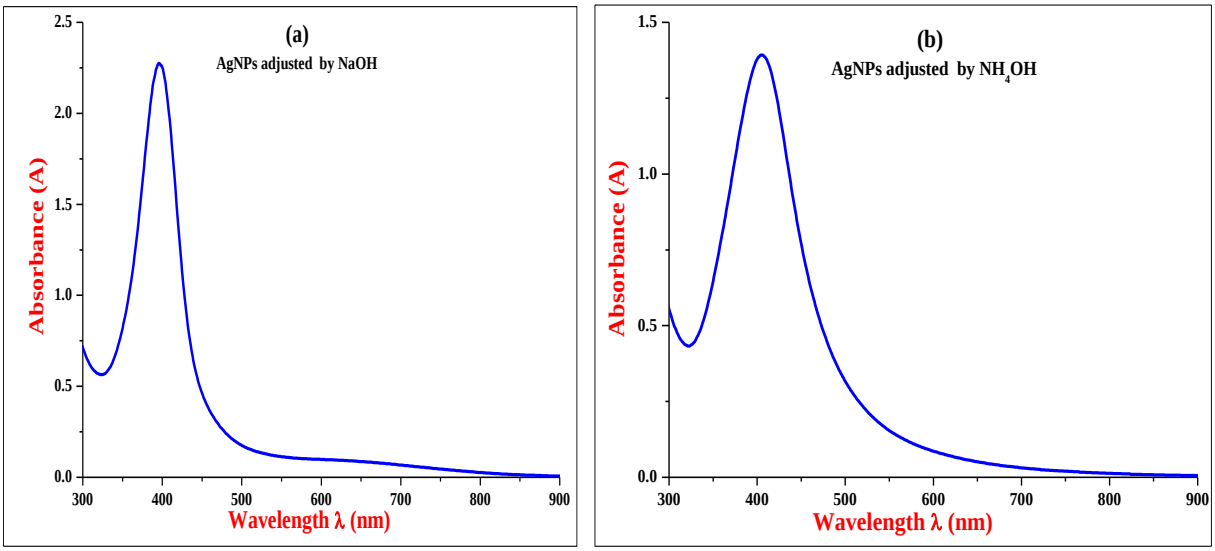

Fig 4.33: (a) and (b) Optimum absorbance of surface plasmon resonance (SPR) of silver nanoparticles (AgNPs) adjusted by NaOH and NH_4OH respectively in blue shift region.

Figure (4.34) shows that with the time, the silver nanoparticles were slight shift to the long wavelengths (red shift) with decreased in the absorbance intensity and also led to increasee in the particle sizes because the metal nanoparticles might undergo the transformation of thermodynamically unstable [17]

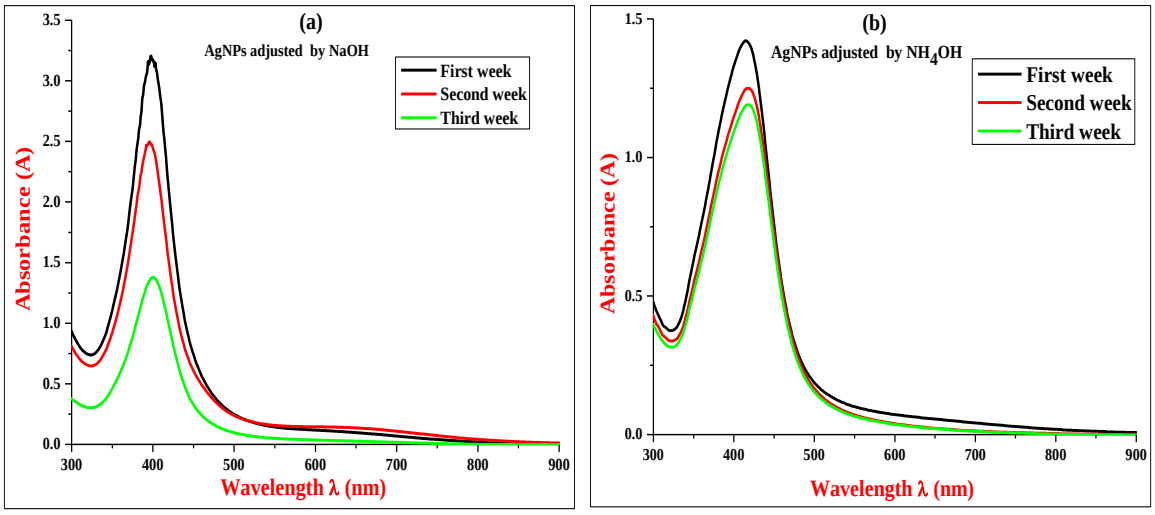

Fig 4.34: (a) and (b) Optimum absorbance of surface plasmon resonance (SPR) of silver nanoparticles (AgNPs) adjusted by NaOH and NH_4OH respectively in blue shift with the time.

4.3.2 Absorbance of Silver Nanoparticles in Red Shift

1- SiO_2 Content

UV–Vis spectra measurements results showed that with change SiO_2 content absorbance curve of coated silver nanoparticles samples had a single visible peak that was positioned in range of 417-397nm it was related to spherical monodisperse AgNPs. The SPR peak shifts to shorter wavelength (less the peak shifts to the right) and absorbance curve width became narrower at 500µl of SiO_2 led to a little increase in particle size. While other SiO_2 contents the SPR peak shifts to longer wavelength (the peak shifts to more the right) this means particle size is larger as in Figure (4.35), also shows Figure (4.36) change of the absorbance peak position and absorbance intensity with SiO_2 content changing and this agrees with [35]. Therefore, SiO_2 content 500µl was selected optimum condition for coated silver nanoparticles adjusted by NaOH and NH_4OH. Coated method of gold nanoparticles by nano thin film layer of silica has an important role in maintain on SPR position, because SiO_2 stability against and also chemically inert and optically transparent and this agrees with [56].

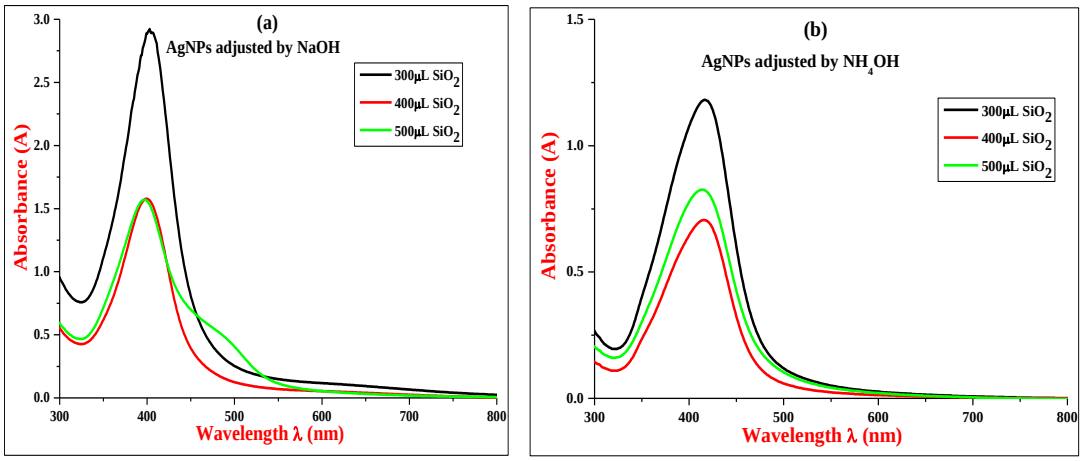

Fig 4.35: (a) and (b) The absorbance of surface plasmon resonance (SPR) of silver nanoparticles (AgNPs) adjusted by NaOH and NH_4OH respectively in red shift changes with the SiO_2 content changing.

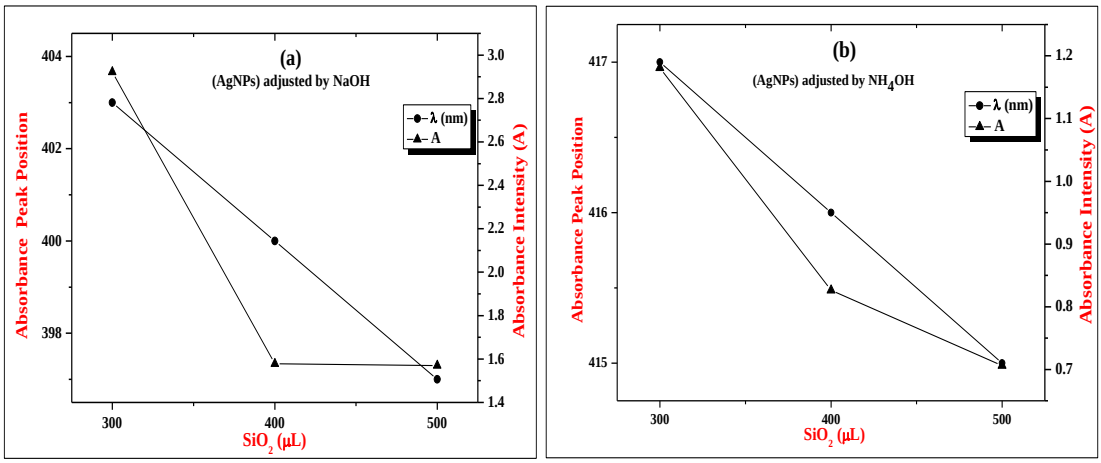

Fig 4.36: (a) and (b) Absorbance peak position and absorbance intensity of surface plasmon resonance (SPR) of silver nanoparticles (AgNPs) adjusted by NaOH and NH_4OH respectively in red changes with the SiO_2 content changing.

2- Silver nanoparticles (AgNPs) Solution Volume

UV–Vis spectra measurements results showed that with change silver nanoparticles solution volume absorbance curve of coated silver nanoparticles samples had a single visible peak that was positioned in range of 425-392nm it was related to spherical monodisperse AgNPs. The SPR peak shifts to shorter wavelength (less the peak shifts to the right) and absorbance curve width became narrower at 30ml and 20ml of solution volumes for AgNP adjusted by NaOH and NH_4OH respectively led to a little increase in particle size. While other silver nanoparticles solution volumes the SPR peak shifts to longer wavelength (the peak shifts to more the right) this means particle size is larger as in Figure (4.37), also shows Figure (4.38) change of the absorbance peak position and absorbance intensity with silver nanoparticles solution volume changing. Therefore, silver nanoparticles solution volume 30ml and 20ml was selected optimum condition for coated silver nanoparticles adjusted by NaOH and NH_4OH respectively.

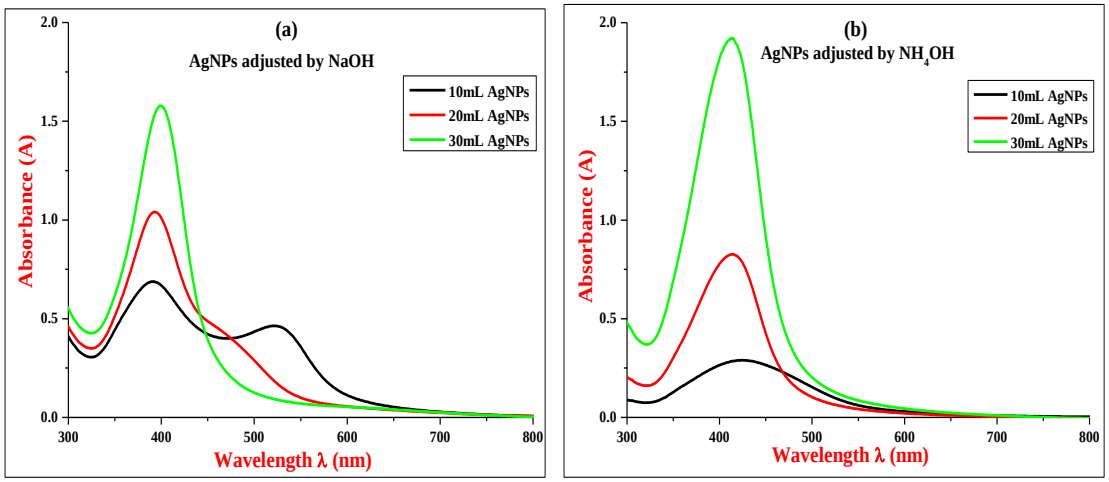

Fig 4.37: (a) and (b) The absorbance of surface plasmon resonance (SPR) of silver nanoparticles (AgNPs) adjusted by NaOH and NH_4OH respectively in red shift changes with the AgNPs solution volume changing and a constant SiO_2 content 500µl.

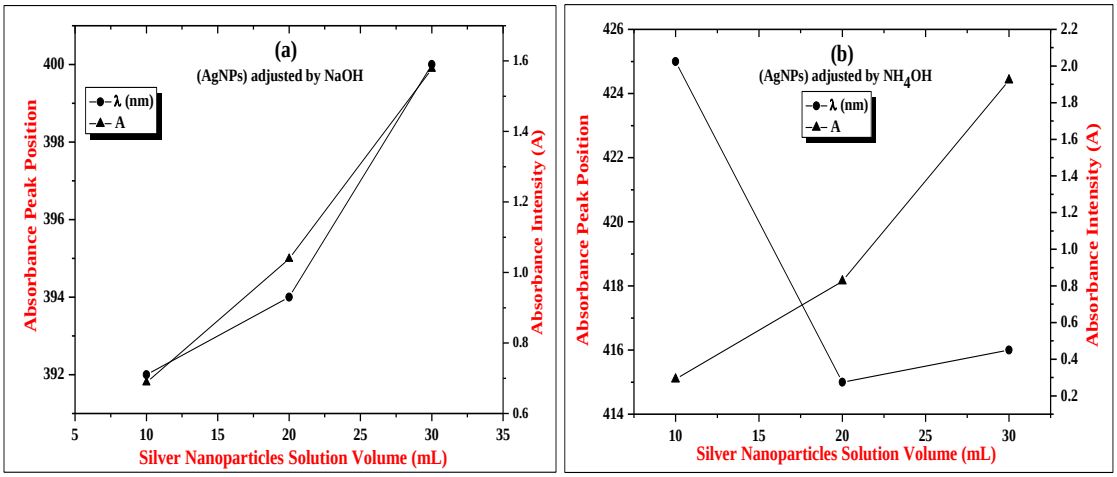

Fig 4.38: (a) and (b) Optimum absorbance of surface plasmon resonance (SPR) of silver nanoparticles (AgNPs) adjusted by NaOH and NH_4OH respectively in red changes with the AgNPs solution volume changing and a constant SiO_2 content 500µl.

3- Ethanol Volume

UV–Vis spectra measurements results showed that with change ethanol volume absorbance curve of coated silver nanoparticles samples had a single visible peak that was positioned in range of 425-395nm it was related to spherical monodisperse AgNPs. The SPR peak shifts to shorter wavelength (less the peak shifts to the right) and absorbance curve

width became narrower at 10ml of ethanol volume led to a little increase in particle size. While other ethanol volumes the SPR peak shifts to longer wavelength (the peak shifts to more the right) this means particle size is larger as in Figure (4.39), also shows Figure (4.40) change of the absorbance peak position and absorbance intensity with ethanol volume changing. Therefore, ethanol volume 10ml was selected optimum condition for coated silver nanoparticles adjusted by NaOH and NH_4OH respectively.

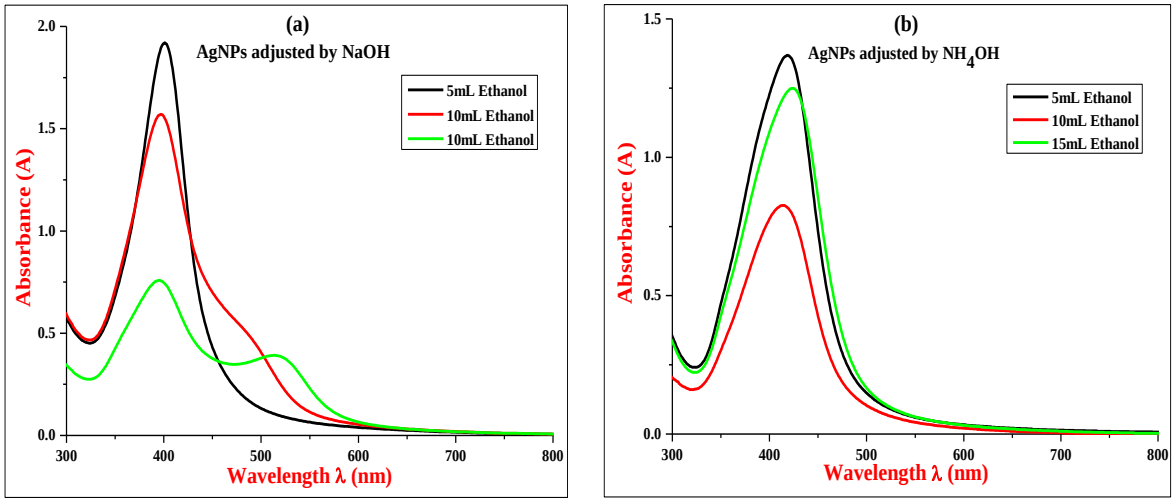

Fig 4.39: (a) and (b) The absorbance of surface plasmon resonance (SPR) of silver nanoparticles (AgNPs) changes with ethanol volume changing and a constant SiO_2 content 500µl and AgNPs solution volume 30ml and 20ml for AgNPs adjusted by NaOH and NH_4OH respectively.

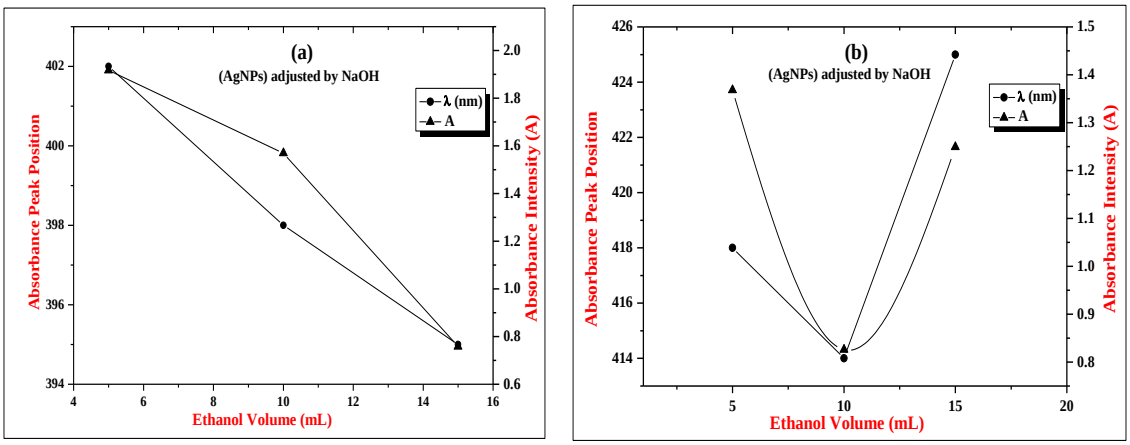

Fig 4.40: (a) and (b) Optimum absorbance of surface plasmon resonance (SPR) of silver nanoparticles (AgNPs) changes with ethanol volume changing and a constant SiO2 content 500µl and AgNPs solution volume 30ml and 20ml for AgNPs adjusted by NaOH and NH4OH respectively.

The observation after evaluation of the effect different parameters such as the SiO_2, nanoparticles solution volume and ethanol volume. These parameters showed a strong effect in maintain on the position of SPR of coated silver nanoparticles (AgNPs). Therefore, 500µl of SiO_2, 30ml of AgNPs solution and 10ml ethanol was selected optimum condition for coated s ilver nanoparticles adjusted by NaOH which SPR peak at 398nm, SiO_2 500µl, 20ml of AgNPs solution and 10ml ethanol was selected optimum condition for coated silver nanoparticles adjusted by NH_4OH which SPR peak at 414nm, Figure (4.41).

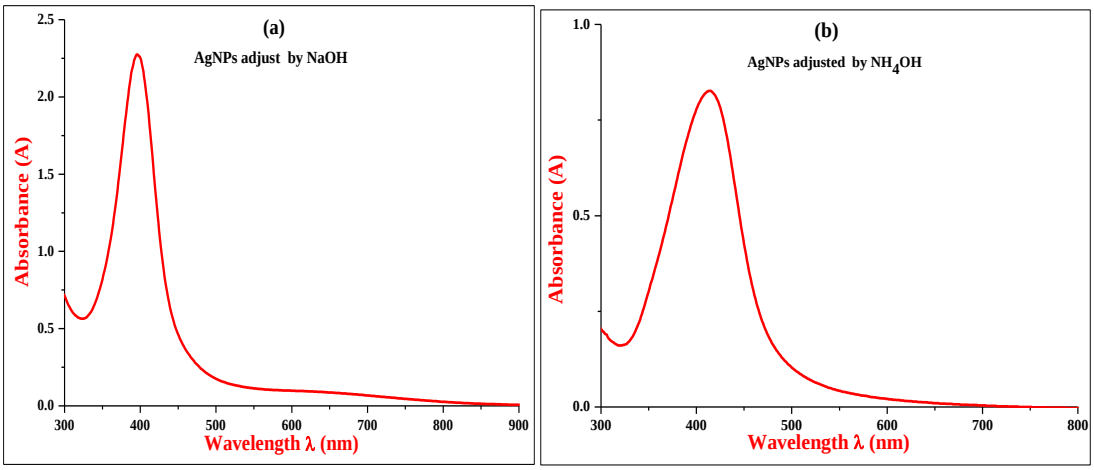

Fig 4.41: (a) and (b) Optimum absorbance of surface plasmon resonance (SPR) of silver nanoparticles (AgNPs) adjusted by NaOH and NH_4OH respectively in red shift region.

Figure (4.42) shows a red shift occurred to the SPR of AgNPs from 396nm to 398nm and from 405nm to 414nm of AgNPs adjusted by NaOH and NH_4OH respectively this means less increase in particle size with maintain spherical shape and this agrees [25,32]

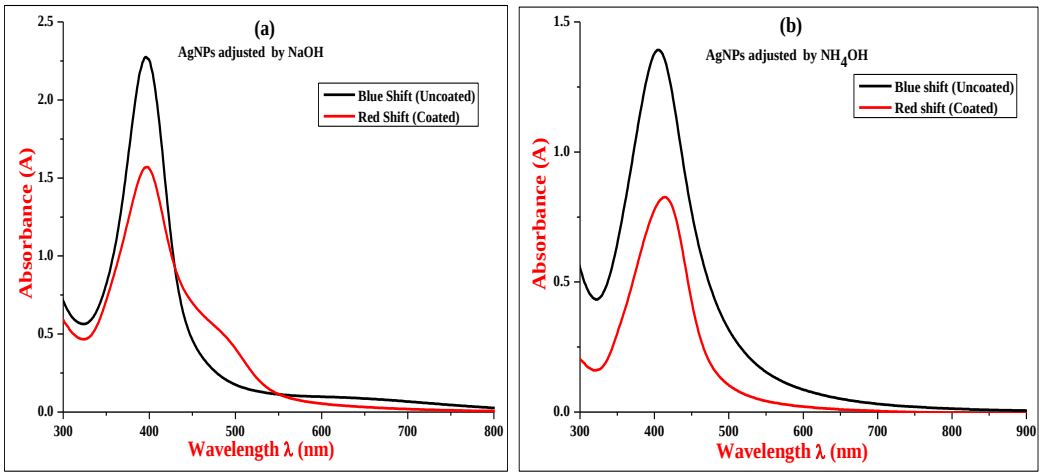

Fig 4.42: (a) and (b) Optimum absorbance of surface plasmon resonance (SPR) of silver nanoparticles (AgNPs) adjusted by NaOH and NH_4OH respectively in blue and red shift regions.

It is observed from Figure (4.43) with the time position of surface plasmon resonance (SPR) of coated silver nanoparticles (AgNPs) is not changed with increasing absorbance intensity because coating method by nano thin film layer of silica which has an important role in maintaining nanoparticles stability and preventing it from agglomeration [81- 83].

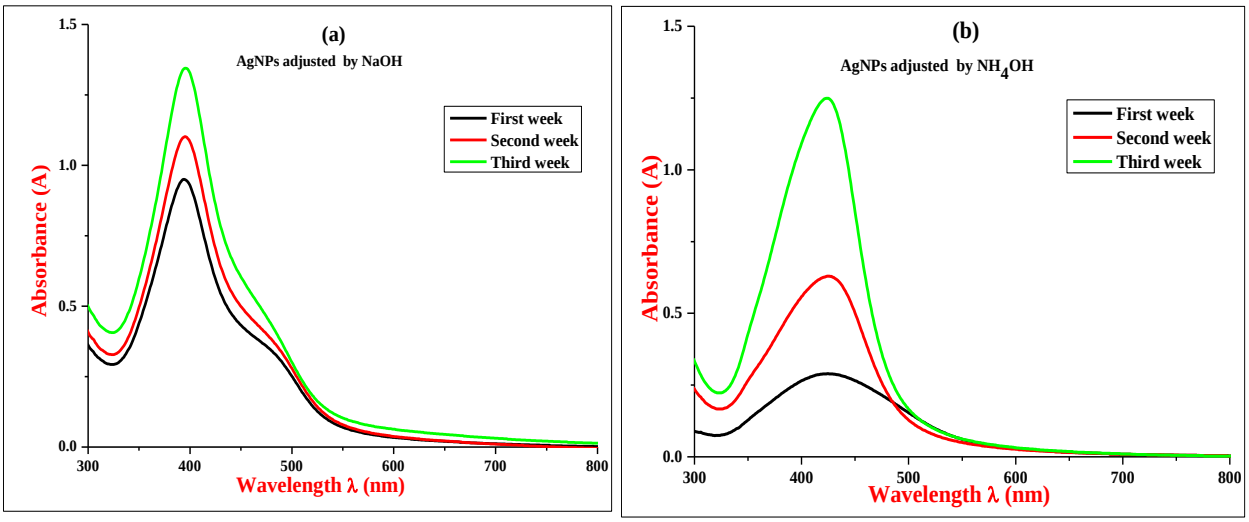

Fig 4.43: (a) and (b) Optimum absorbance of surface plasmon resonance (SPR) of silver nanoparticles (AgNPs) adjusted by NaOH and NH_4OH respectively in red shift with the time.

4.3.3 Infra-Red Spectrum of Silver Nanoparticles

Figure (4.44) shows the FT-IR spectrum obtained for silver nanoparticles (AgNPs) adjusted by N aOH synthesized at (20min, 0.02g of GA and 100°C) and coated at (500µl of SiO_2, 30ml of AgNPs and 10ml of ethanol), also silver nanoparticles (AgNPs) adjusted by NH_4OH synthesized at (20min, 0.008g of GA and 80°C) and coated at (500µl of SiO_2, 20ml of AgNPs and 10ml of ethanol). FTIR spectrum Shows strong absorption band 3431 cm^{-1} representing O-H of carboxylic acid. The absorption peaks located at 2866, 2802, 2343 and 2320 cm^{-1} correspond to C-H stretching of alkanes. The absorption peaks located at 1622, 1616, 1494 and 1489 cm^{-1} correspond to C=C stretching of alkenes and aromatics. The absorption peaks located at 1384, 1379, 1072 and 1062cm^{-1} correspond to C-O stretching of carboxylic acid. The absorption peaks located at 966, 655, 636, 543, 484 and 426 cm^{-1} correspond to O-H bend of out-level carboxylic acid, also it is observed that the silver nanoparticles after coating almost have the same absorption peaks with a little shift for some absorption peaks this means that the coating method led to a little increase in the size with maintaining on nanoparticles shape and prevents it from deforming, the absorption bands 543, 484 and 426 cm^{-1} refer to harmony happening between inorganic elements (silver) and organic compounds (Gallic acid) and this agrees with [35].

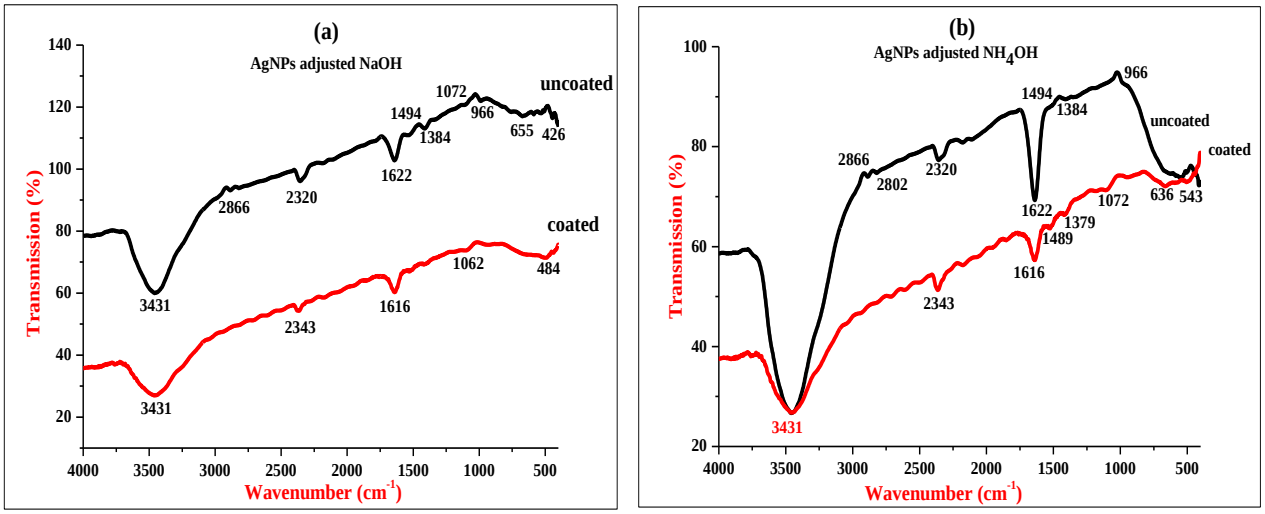

Fig 4.44: (a) and (b) FTIR spectrum obtained of silver nanoparticles (AgNPs) adjusted by NaOH and NH_4OH respectively before and after coating.

4.3.4 Morphology of Silver Nanoparticles

The morphology investigation of silver nanoparticles (AgNPs) adjusted by NaOH and synthesized at (20min, 0.02g of GA and 100°C) and coated at (500µl of SiO_2, 30ml of AgNPs and 10ml of ethanol), also silver nanoparticles (AgNPs) adjusted by NH_4OH and synthesized at (20min, 0.008g of GA and 80°C) and coated at (500µl of SiO_2, 20ml of AgNPs and 10ml of ethanol) was accomplished by using AFM. Figure (4.45) shows that each nucleus silver nanoparticles (AgNPs) adjusted by NaOH and NH_4OH without and with coated by nano thin film layer of silica is spherical in geometry and has a radius r is less than critical radius r* (r < r*) this means increased surface tension and hence increased surface energy and this agrees with [55]. It is observed from Table (4.2) that surface roughness and root mean square (RMS) of silver nanoparticles (AgNPs) adjusted by NaOH and NH_4OH increase after coating and this means increase in particle size, thus the smallness of these volumes indicates the smoothness of the surface which confirms the smallness of these granules. Since the relationship between root mean

square (RMS) and average grain size is a direct relationship this led to average grain size increase.

Table 4.2: Surface roughness, root mean square (RMS) and grain size of silver nanoparticles (AgNPs) uncoated and coated by nano thin film layer of silica.

Sample	AgNPs adjustd by NaOH (uncoated)	AgNPs adjustd by NaOH (coated)	AgNPs adjust by NH_4OH (uncoated)	AgNPs adjust by NH_4OH (coated)
Surface Roughness (nm)	1.88	1.99	1.2	2.08
Root Mean Square (nm)	2.17	2.3	2.38	2.4
Grain Size (nm)	53.03	57.23	44.1	45.74

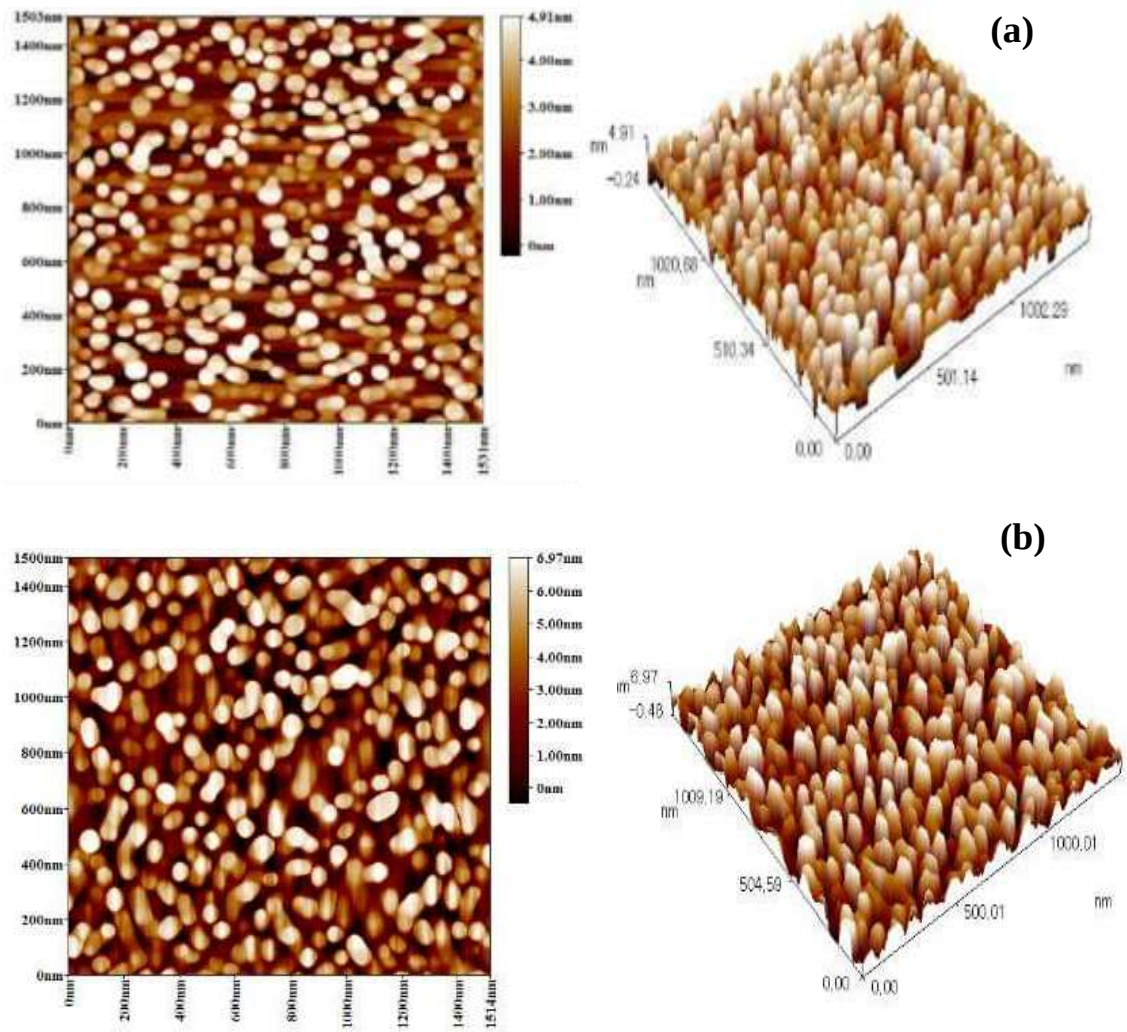

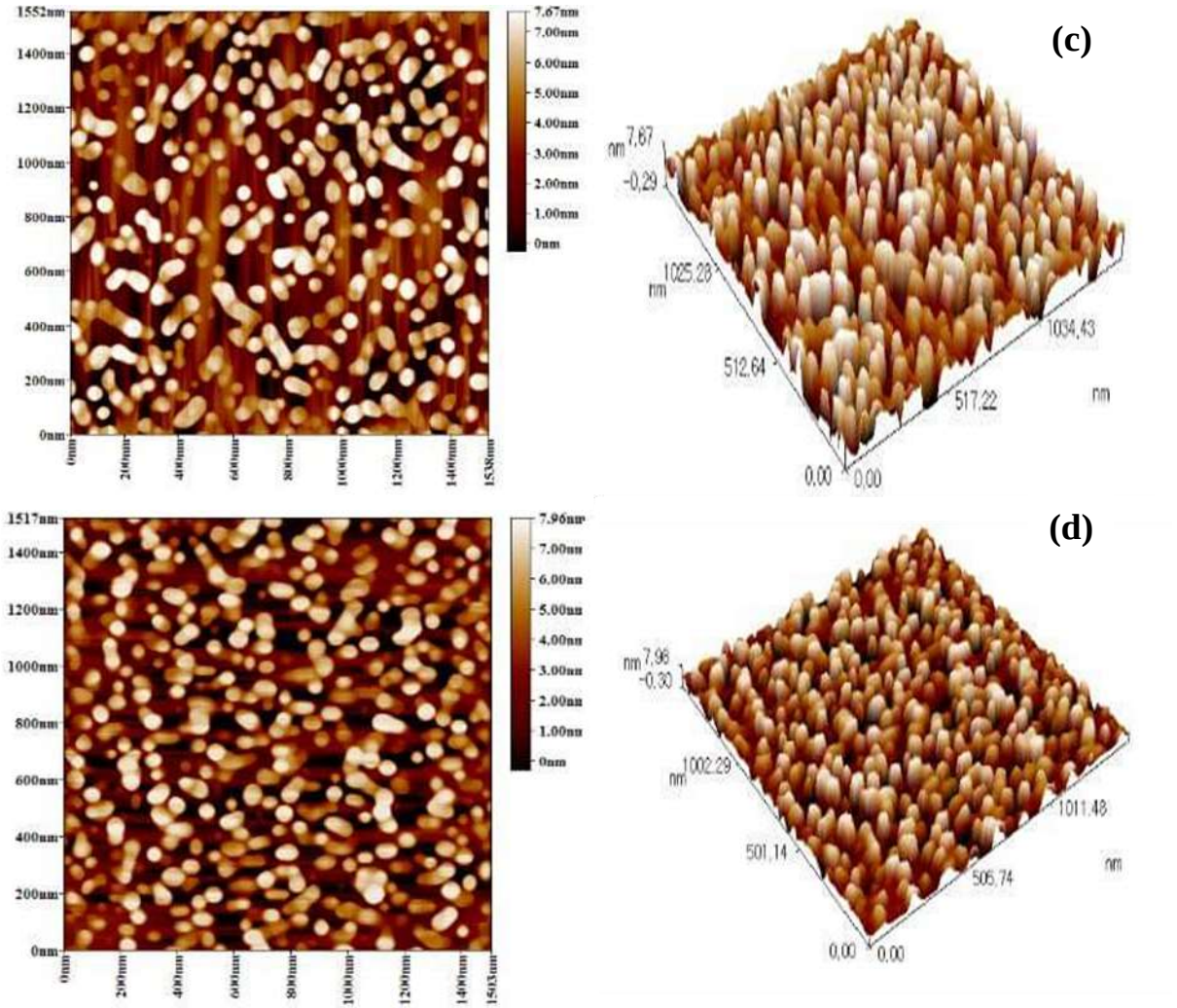

Fig 4.45: AFM images: (a) and (b) Silver nanoparticles (AgNPs) adjusted by NaOH uncoated and coated by nano thin film layer of silica respectively. (c) and (d) Silver nanoparticles (AgNPs) adjusted by NH_4OH uncoated and coated by nano thin film layer of silica respectively.

4.3.5 Size and Shape of Silver Nanoparticles

TEM and FESEM techniques have high accuracy and reliability for determining size, size distribution and shape of nanoparticles. Figure (4.46) show the TEM images of silver nanoparticles (AgNPs) adjusted by NaOH and synthesized at (20min, 0.02g of GA and 100°C) and coated at (500µl of SiO_2, 30ml of AgNPs and 10ml of ethanol), also silver nanoparticles (AgNPs) adjusted by NH_4OH and synthesized at (20min,

0.008g of GA and 80°C) and coated at (500µl of SiO_2, 20ml of AgNPs and 10ml of ethanol). TEM analysis reveal that the of silver nanoparticles adjusted by NaOH and NH_4OH have a narrow size distribution and spherical shape with an average size 6-8nm and 3-6nm respectively. On another hand, it is observe after coating by nano silica layer that the silver nanoparticles adjusted by NaOH and NH_4OH have a narrow size distribution and spherical shape with a less increase in the particles size 10-19nm and 12.9-16.7nm respectively and this agrees with [25, 32].

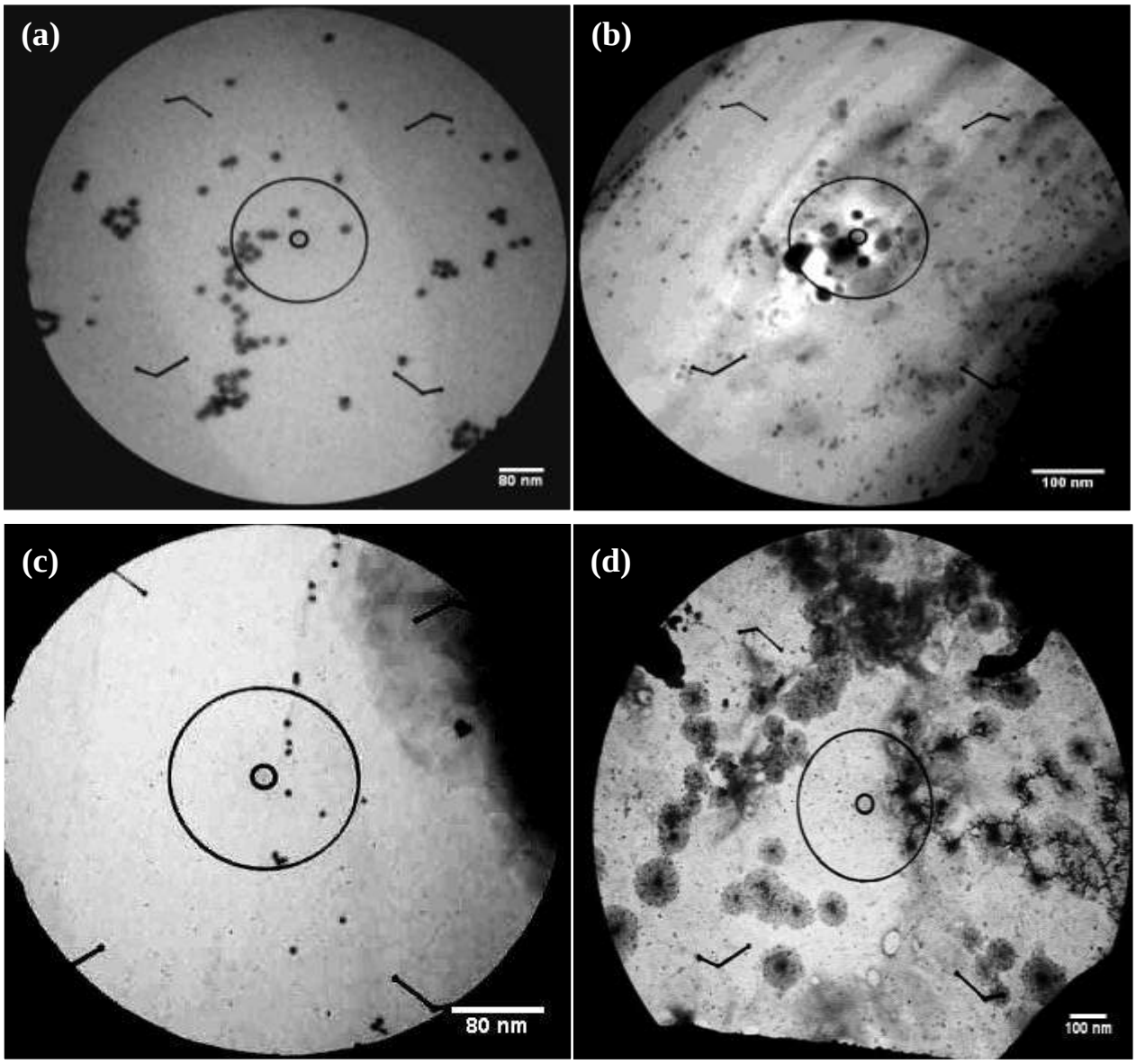

Fig 4.46: TEM images: (a) and (b) Silver nanoparticles (AgNPs) adjusted by NaOH uncoated and coated by nano thin film layer of silica respectively, (c) and (d) Silver nanoparticles (AgNPs) adjusted by NH_4OH uncoated and coated by nano thin film layer of silica respectively.

FESEM are the best analyzing tool for structural and morphological properties of synthesized materials. Figure (4.47) shows structure and the morphology of AgNPs investigated using FESEM analysis. The images reveal that narrow size distribution of silver nanoparticles with size < 20nm and spherical shape. On another hand, it is observe after coating by nano silica layer that the silver nanoparticles have a narrow size distribution and spherical shape with a less increase in the particles size this means that coated method has an important role in maintain and control the shape and size of the nanoparticles and this agrees with [28].

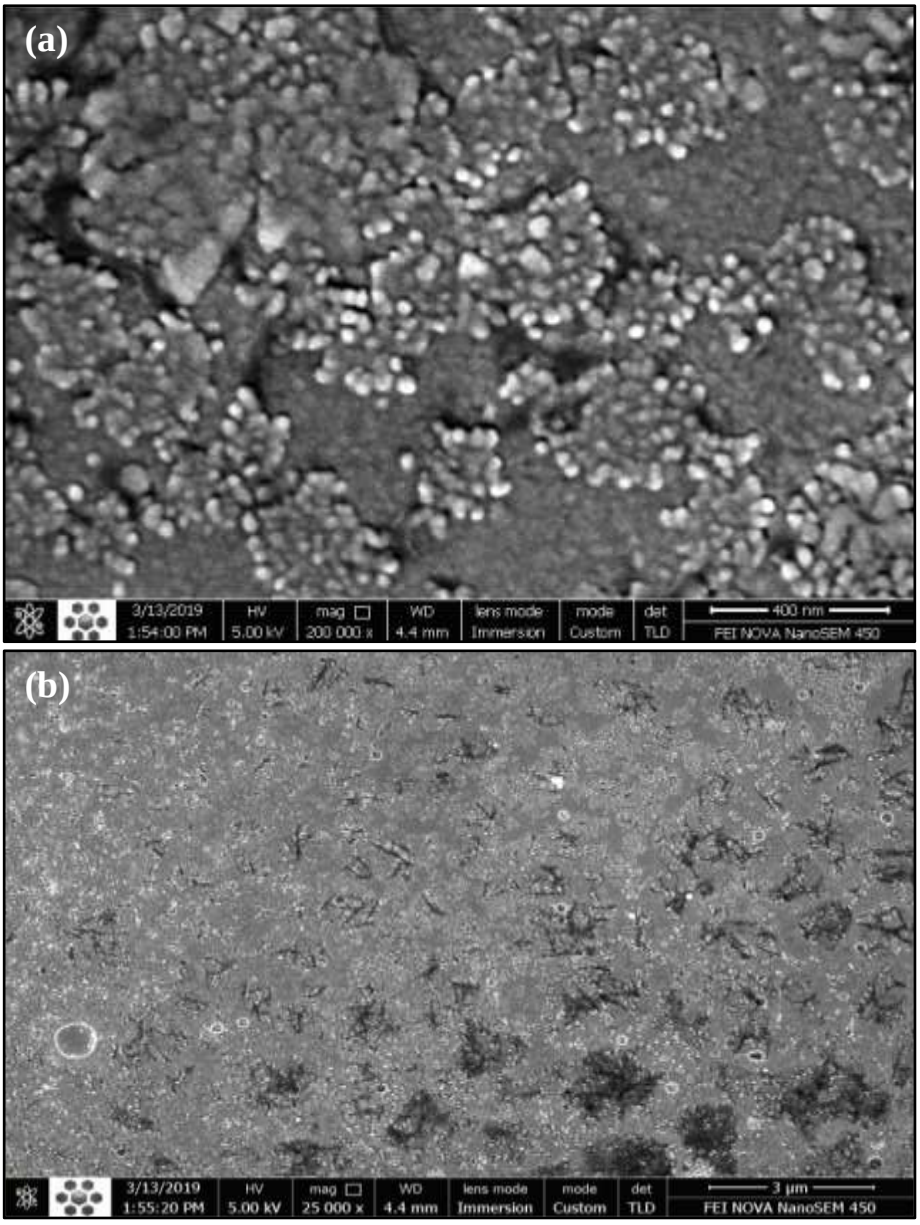

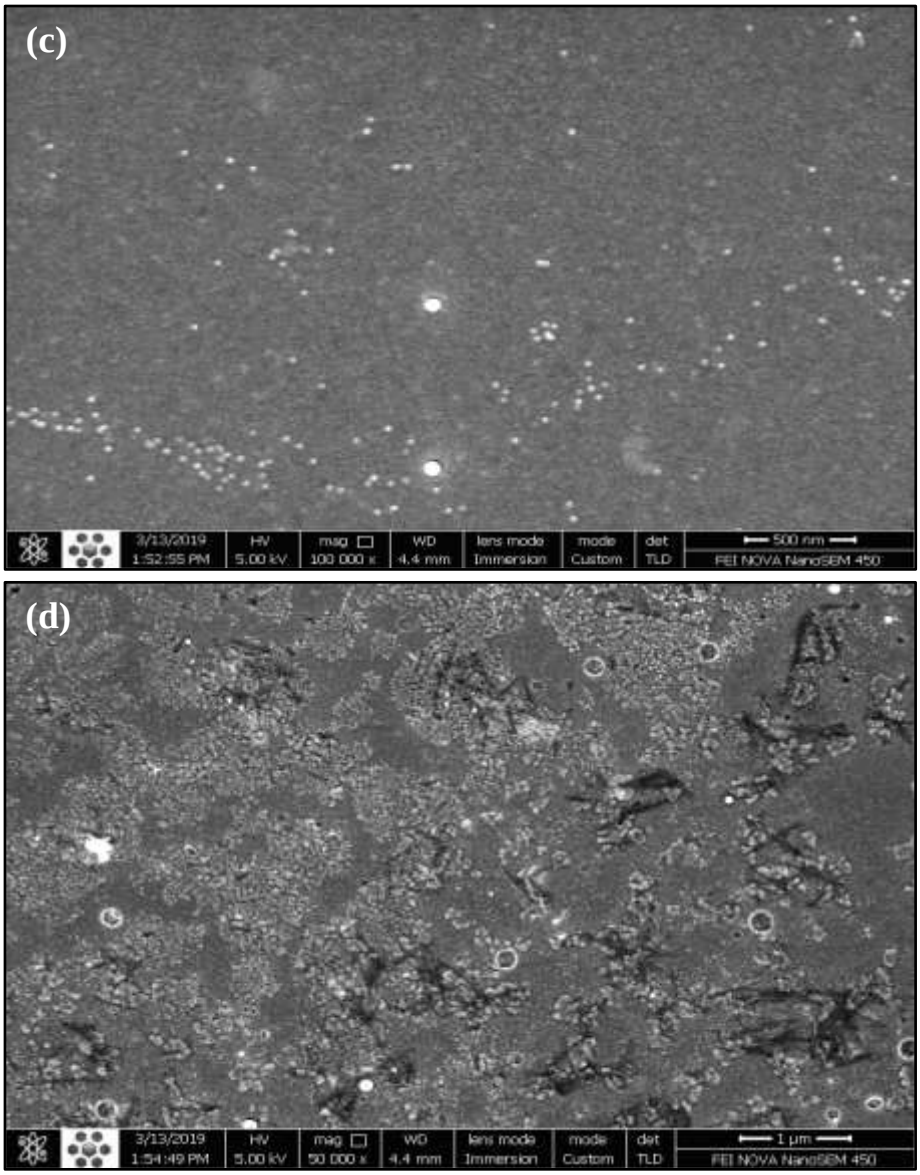

Fig 4.47: FESEM images: (a) and (b) Silver nanoparticles (AgNPs) adjusted by NaOH uncoated and coated by nano thin film layer of silica respectively. (c) and (d) Silver nanoparticles (AgNPs) adjusted by NH_4OH uncoated and coated by nano thin film layer of silica respectively.

4.3.6 Stability of Silver Nanoparticles

Figure (4.48) shows stability of silver nanoparticles (AgNPs) adjusted by NaOH and synthesized at (20min, 0.02g of GA and 100°C) and coated at (500µl of SiO_2, 30ml of AgNPs and 10ml of ethanol), also silver nanoparticles (AgNPs) adjusted by NH_4OH and synthesized at (20min, 0.008g of GA and 80°C) and coated at (500µl of SiO_2, 20ml of

AgNPs and 10ml of ethanol). Zeta potential for coated silver nanoparticles adjusted by NaOH with nano thin film layer of silica (−62.86mV) is higher than the uncoating ones (−58.17 mV), and also silver nanoparticles adjusted by NH_4OH with nano thin film layer of silica (−43.60mV) is higher than the uncoated ones (−15.68 mV) and that means more stability occurred because coating method by nano thin film layer of silica which has an important role in maintaining nanoparticles stability and preventing then from agglomeration and this agrees with [25]. The negative zeta potential confirms the negative charge on the surface of colloidal nanoparticles. The columbic repulsion forces induced by surface negative charge minimize the aggregation and thus contribute to the stability of the synthesized nanoparticles and this agrees with [124].

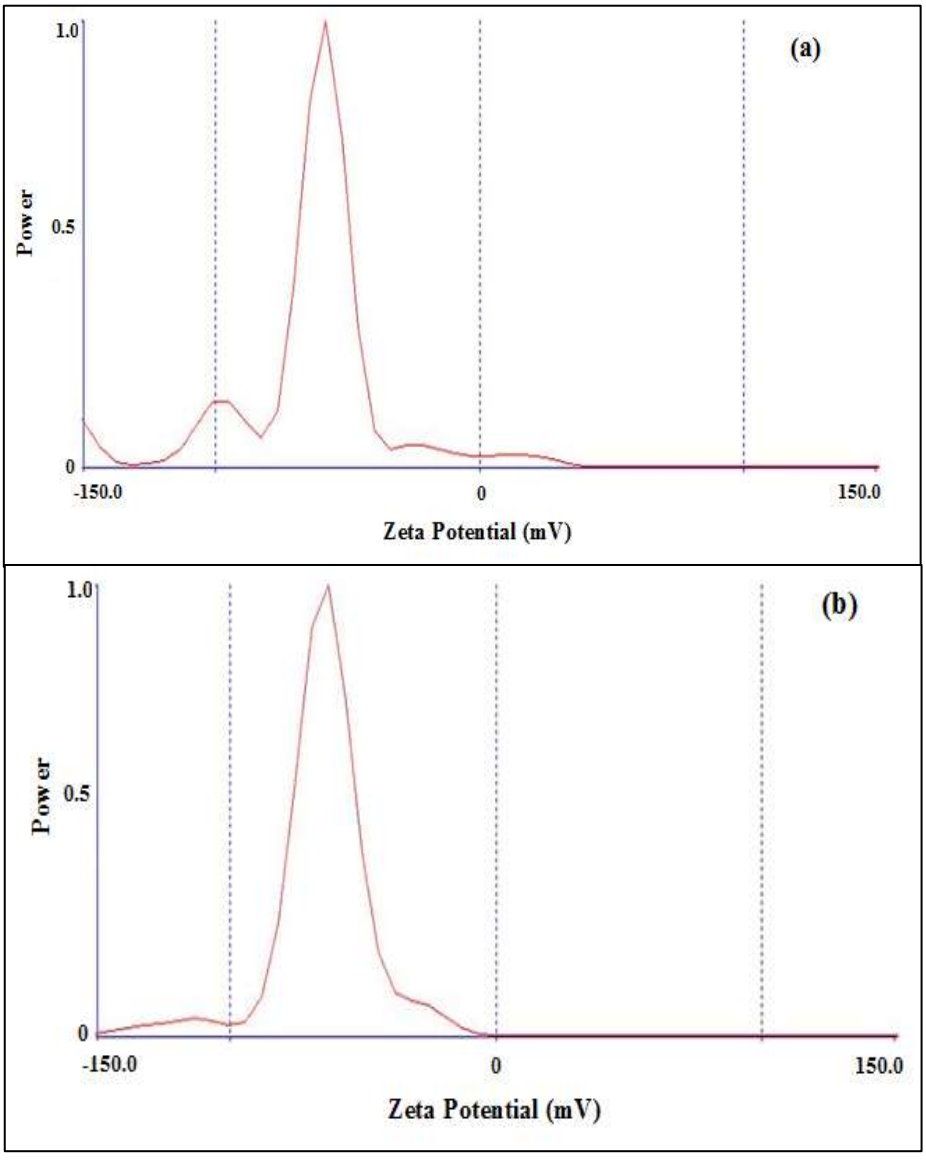

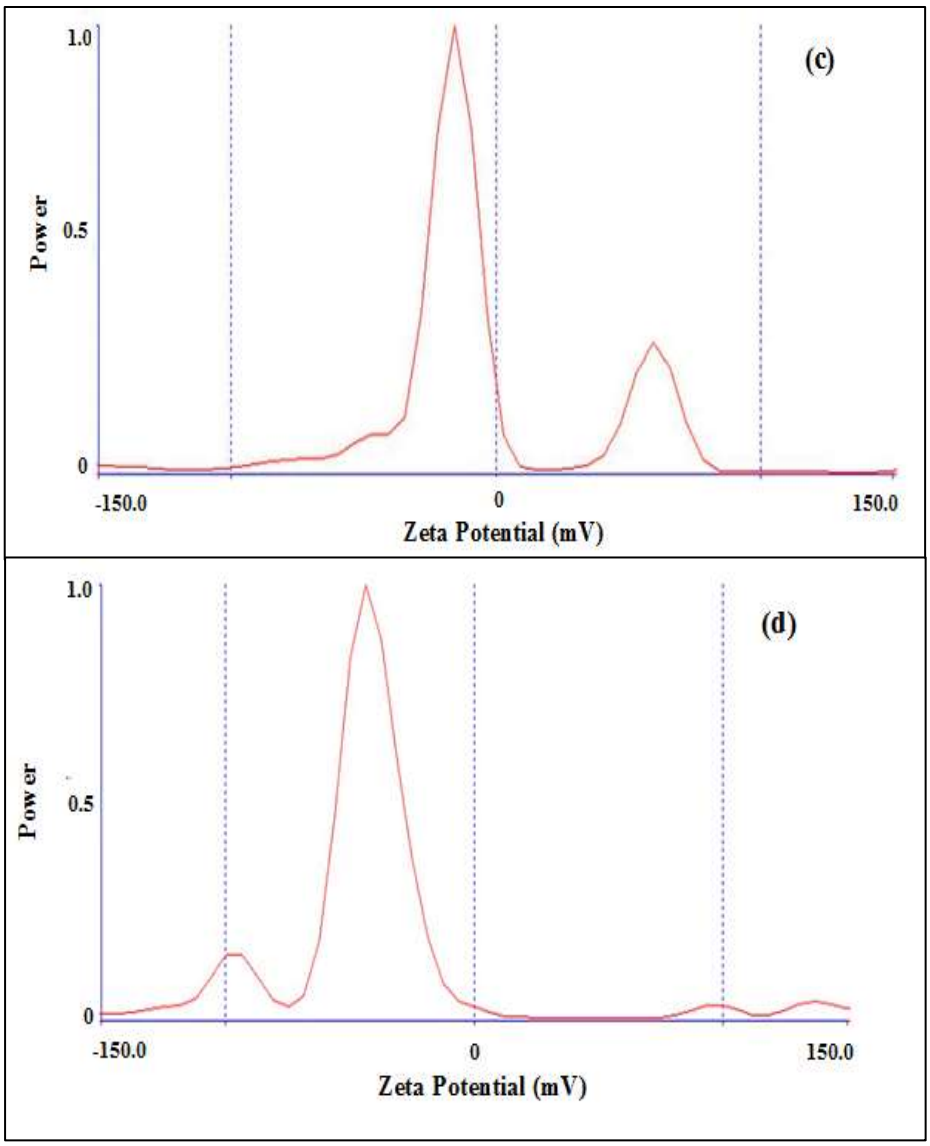

Fig 4.48: Zeta potential: (a) and (b) Silver nanoparticles (AgNPs) adjusted by NaOH uncoated and coated by nano thin film layer of silica respectively. (c) and (d) Silver nanoparticles (AgNPs) adjusted by NH_4OH uncoated and coated by nano thin film layer of silica respectively.

4.3.7 Concentration of Silver Nanoparticles

Atomic Absorption Spectroscopy measurements results showed that the concentration of silver nanoparticles adjust by NaOH was 89.3487µg/ml, but after coating by nano thin film layer of silica the silver nanoparticles concentration was decreased to 65.9056 µg/ml. While the concentration of silver nanoparticles (AgNPs) adjusted by NH_4OH 84.4728 µg/ml and was decreased after coating by nano thin film layer of

silica to 57.3969µg/ml. The concentration decrease of silver nanoparticles after coating is attributed to the addition the coating solution to it and this agrees with [124].

Table 4.3: The optimum Properties of gold and silver nanoparticles uncoated and coated by nano thin film layer of silica.

Optimum Properties	Gold Nanoparticles		Silver Nanoparticles adjusted by NaOH		Silver Nanoparticles adjusted by NH_4OH	
	uncoated	coated	uncoated	coated	uncoated	coated
SPR Peak (nm)	515	518	396	398	405	414
A	0.362	0.265	1.569	1.384	1.392	0.826
SR (nm)	1.94	3.17	1.88	1.99	1.2	2.08
RMS (nm)	2.4	3.67	9.17	2.3	2.38	2.4
Grin Size (nm)	56.32	58.46	53.03	57.23	44.1	45.74
Shape	spherical	spherical	spherical	spherical	spherical	spherical
Size (nm)	3-6	9-18	6-8	10-19	3-6	12.9-16.7
Stability (mV)	−25.02	-25.92	-58.17	-62.86	-15.68	-43.60
C (µg/ml)	500	300	89.3487	65.9056	84.4728	57.3969

4.4 Biomedical Applications Results

4.4.1 Toxicity of Gold Nanoparticles on Cell Lines

The results of AuNPs toxicity examination showed on the MCF-7 cell line there was the percentage of destroy MCF-7 cells increases with increasing concentration of gold nanoparticles (AuNPs). It is observed from the Figure (4.49) there was 70% of the MCF-7 were survived at 12.5 µg/ml concentration, 60% of MCF-7 cell line were survived at 25µg/ml and 40% MCF-7 cell line was survived at 50µg/ml at 72hr and this agrees with [29].

The results of AuNPs toxicity examination showed on the HBL-100 cell line there was increased the cells growth at 12.5µg/ml concentration. While 50% of HBL-100 cell line were survived at the concentrations 25µg/ml and 50µg/ml at 72hr, as shown in the Figure (4.49) and this agrees with [22].

Therefore, the best optimization concentration of gold nanoparticles (AuNPs) on MCF-7 and HBL-100 cell lines was 50µg/ml showed the best rate of destroy MCF-7 cell line and on same time 50µg/ml was less the destroy rate of HBL-100 cell.

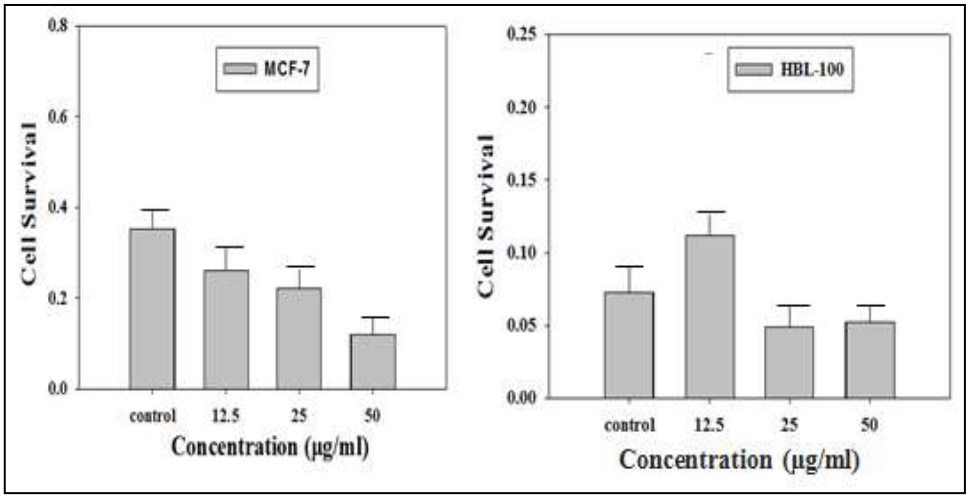

Fig 4.49: Effect of different concentrations of gold nanoparticles (AuNPs) against MCF-7 and HBL-100 cell lines.

The inverted microscope images showed the effect of gold nanoparticles (AuNPs) on the MCF-7 cell line there was the increased MCF-7 cells death with increasing concentration of gold nanoparticles (AuNPs) at 72hr and this confirmed by FLUO star OPTIMA results, as shown in the Figure (4.50).

The inverted microscope images showed the effect of gold nanoparticles (AuNPs) on the HBL-100 cell line there was increased the cells growth at 12.5 µg/ml concentration. While 50% of HBL-100 cell line were survived at the concentrations 25µg/ml and 50µg/ml at 72hr and this confirmed by FLUO star OPTIMA results, as shown in the Figure (4.50).

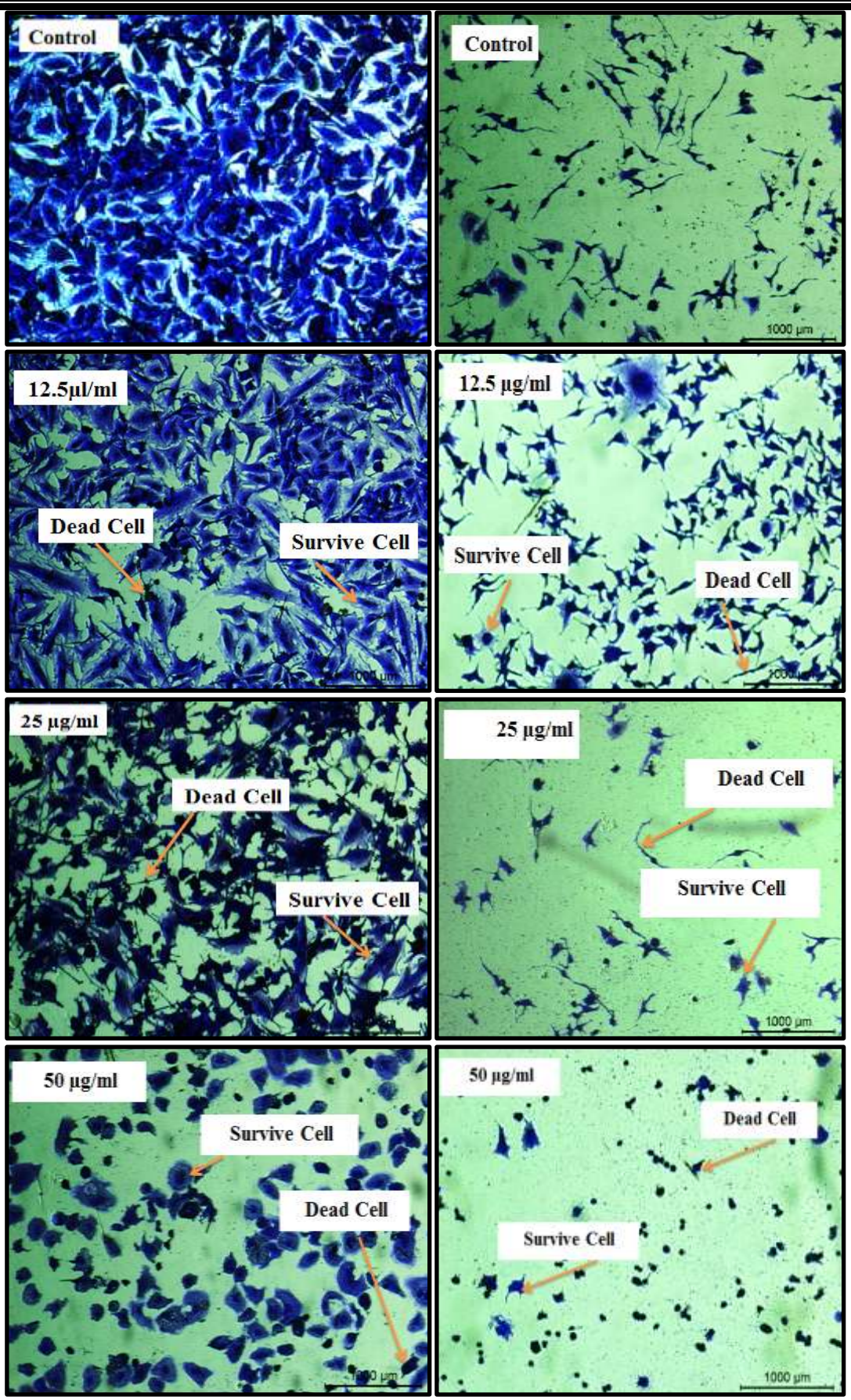

Fig 4.50: Inverted microscope images showing effect of different concentrations of gold nanoparticles (AuNPs) against (MCF-7) on left and HBL-100 on right.

The results of AuNPs toxicity examination showed after coating by nano thin film layer on the MCF-7 cell line there was the percentage of destroy MCF-7 cells increases with increasing concentration of coated gold nanoparticles (AuNPs). It is observed from the Figure (4.51) there was 70% of the MCF-7 were survived at 12.5 µg/ml concentration, 20% of MCF-7 cell line were survived at 25µg/ml and 30% MCF-7 cell line was survived at 50µg/ml at 72hr and this agrees with [29].

The results of AuNPs toxicity examination showed after coating by nano thin film layer on the HBL-100 cell line there was there was less cells death at all concentrations at 72hr, as shown in the Figure (4.51) and this agrees with [22].

Therefore, the best optimization concentration of coated gold nanoparticles (AuNPs) on MCF-7 and HBL-100 cell lines was 25µg/ml showed the best rate of destroy MCF-7 cell line and on same time 50µg/ml was less the destroy rate of HBL-100 cell.

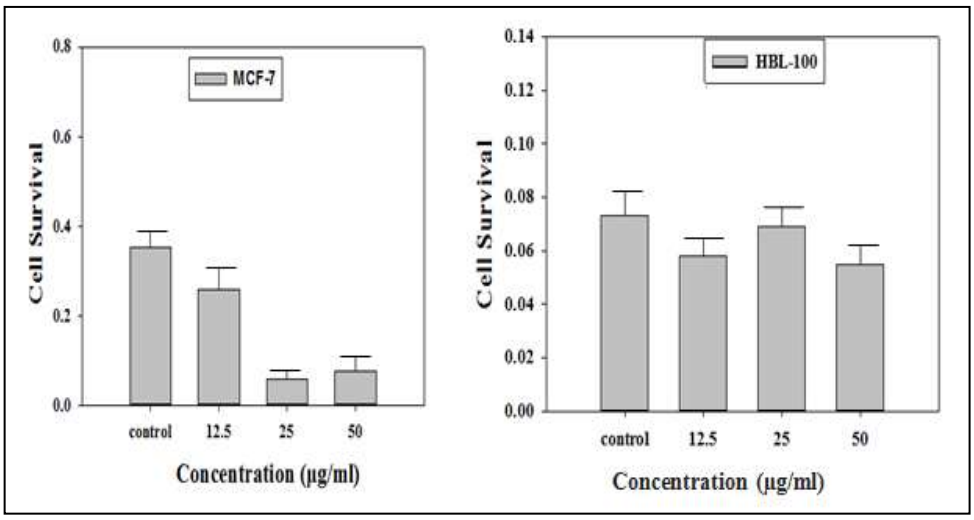

Fig 4.51: Effect of different concentration coated gold nanoparticles (AuNPs) on MCF-7 and HBL-100 cell line.

The inverted microscope images showed the effect of gold nanoparticles (AuNPs) after coating by nano thin film layer on the MCF-7 cell line there was 70% of the MCF-7 were survived at 12.5 µg/ml concentration, 20% of MCF-7 cell line were survived at 25µg/ml

and 30% MCF-7 cell line was survived at 50µg/ml at 72hr and this confirmed by FLUO star OPTIMA results, as shown in the Figure (4-52).

The inverted microscope images showed the effect of gold nanoparticles (AuNPs) after coating by nano thin film layer on the HBL-100 cell line there was less cells death at all concentrations at 72hr, as shown in the Figure (4-52).

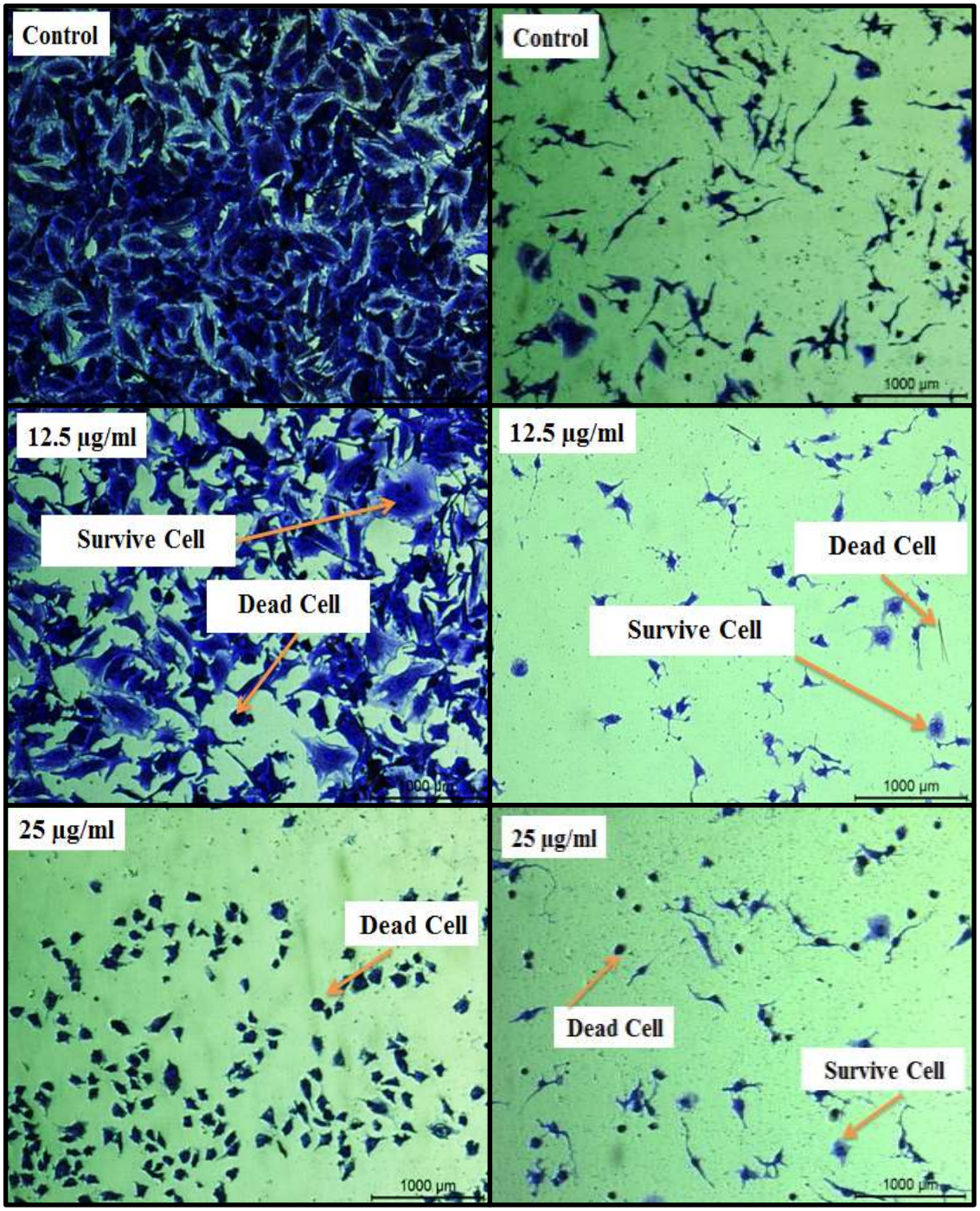

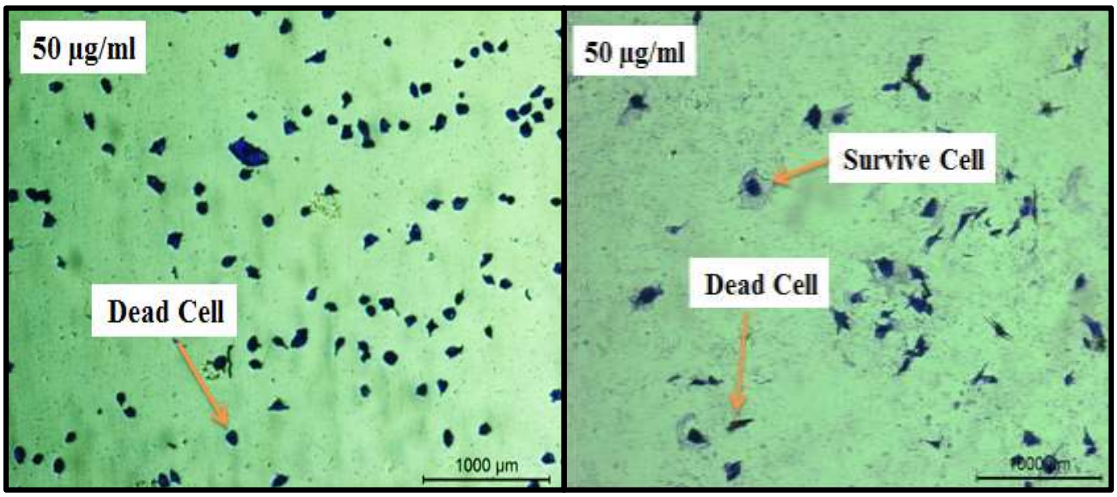

Fig 4.52: Inverted microscope image showing effect of different concentrations coated gold nanoparticles (AuNPs) against MCF-7 on left and HBL-100 on right.

4.4.2 Toxicity of Silver Nanoparticles Adjusted by NaOH on Cell Lines

The results of AgNPs adjusted by NaOH toxicity examination showed on the MCF-7 cell line there was the percentage of destroy MCF-7 cells increases with increasing concentration of silver nanoparticles (AgNPs) adjusted by NaOH. It is observed from the Figure (4.53) there was 50% of the MCF-7 were survived at 12.5 µg/ml concentration, 30% of MCF-7 cell line were survived at 25µg/ml and 20% MCF-7 cell line was survived at 50µg/ml at 72hr cell and this agrees with [23,24,26,29].

The results of AgNPs toxicity examination showed on the HBL-100 cell line there was less the destroy rate of HBL-100 cell at 12.5µg/ml and 25µg/ml concentrations. While was increased the growth rate of HBL-100 cell at 50µg/ml concentration at 72hr, as shown in the Figure (4.53) and this agrees with [23,26].

Therefore, the best optimization concentration of silver nanoparticles (AgNPs) adjusted by NaOH on MCF-7 and HBL-100 cell lines was 50µg/ml showed the best rate of destroy MCF-7 cell line and on same time 50µg/ml was increased the growth rate of HBL-100 cell.

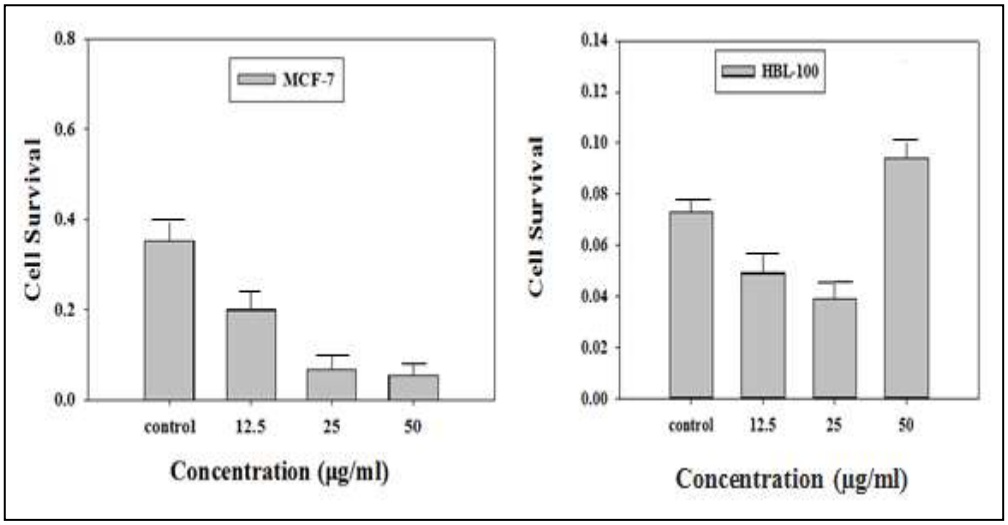

Fig 4.53: Effect of different concentration silver nanoparticles (AgNPs) adjusted by NaOH against MCF-7 and HBL-100 cell line.

The inverted microscope images showed the effect of silver nanoparticles (AgNPs) adjusted by NaOH on the MCF-7 cell line there was the increased MCF-7 cells death with increasing concentration of nanoparticles (AgNPs) adjusted by NaOH. 50% of the MCF-7 were survived at 12.5 µg/ml concentration, 30% of MCF-7 cell line were survived at 25µg/ml and 20% MCF-7 cell line was survived at 50µg/ml at 72hr and this confirmed by FLUO star OPTIMA results, as shown in the Figure (4.54).

The inverted microscope images showed the effect of nanoparticles (AgNPs) adjusted by NaOH on the HBL-100 cell line there was less the destroy rate of HBL-100 cell at 12.5µg/ml and 25µg/ml concentrations. While was increased the growth rate of HBL-100 cell at 50µg/ml concentration at 72hr and this confirmed by FLUO star OPTIMA results, as shown in the Figure (4.54).

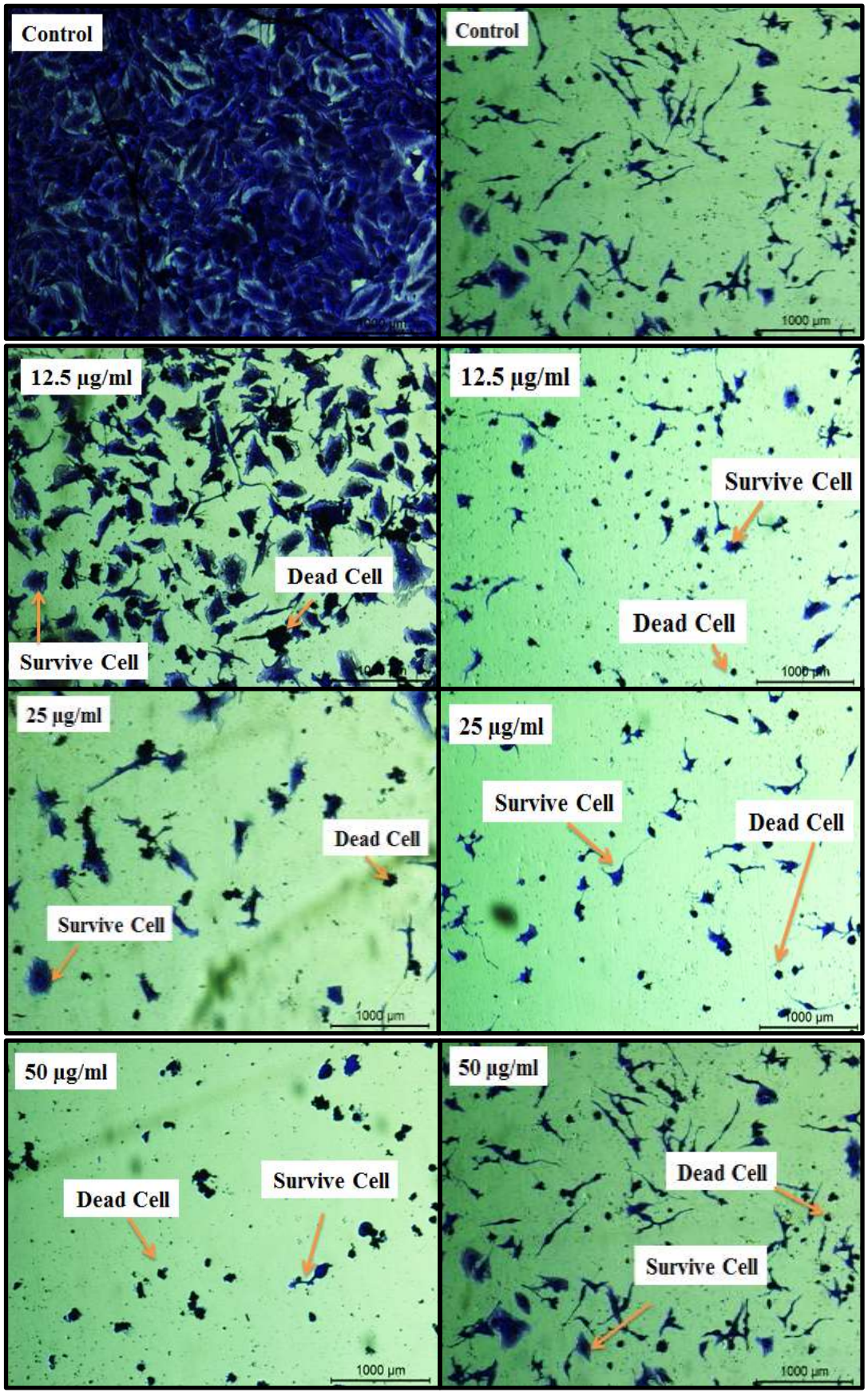

Fig 4.54: Inverted microscope images showing effect of different concentration silver nanoparticles (AgNPs) adjusted by NaOH against MCF-7 on left and HBL-100 on right.

The results of AgNPs adjusted by NaOH toxicity examination showed after coating by nano thin film layer on the MCF-7 cell line there was the percentage of destroy MCF-7 cells increases with increasing concentration of coated silver nanoparticles (AgNPs) adjusted by NaOH. It is observed from the Figure (4.55) there was 60% of the MCF-7 were survived at 12.5µg/ml concentration and 30% MCF-7 cell line was survived at 25 µg/ml and 50µg/ml concentration at 72hr and this agrees with [23,24,26,29].

The results of AgNPs adjusted by NaOH toxicity examination showed after coating by nano thin film layer on the HBL-100 cell line there was less cells death at 12.5µg/ml and 25µg/ml concentrations. While, there was increased the cells growth at 50µg/ml concentration at 72hr, as shown in the Figure (4.55) and this agrees with [23,26].

Therefore, the best optimization concentration of coated silver nanoparticles (AgNPs) adjusted by NaOH on MCF-7 and HBL-100 cell lines was 50µg/ml showed the best rate of destroy MCF-7 cell line and on same time 50µg/ml was increased the growth rate of HBL-100 cell.

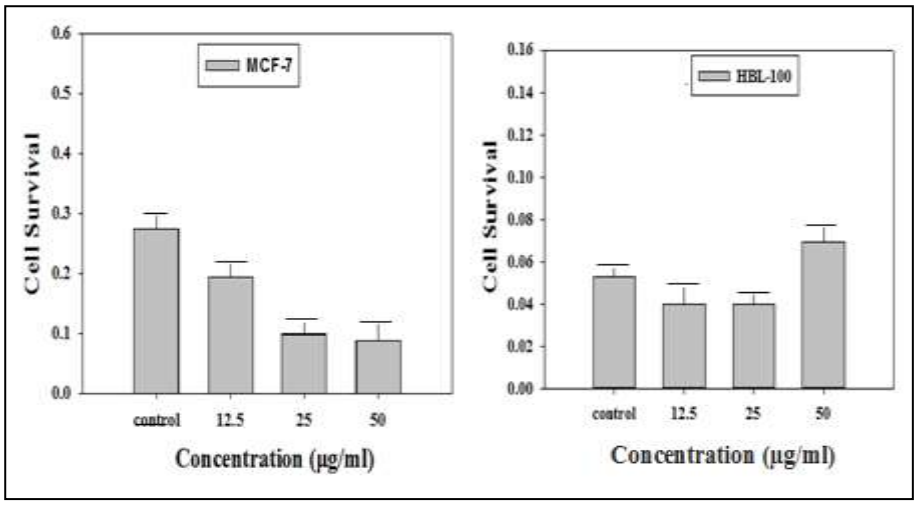

Fig 4.55: Effect of different concentration coated silver nanoparticles (AgNPs) adjusted by NaOH on MCF-7 and HBL-100 cell line.

The inverted microscope images showed the effect of silver nanoparticles (AgNPs) adjusted by NaOH after coating by nano thin film layer on the MCF-7 cell line there was the percentage of destroy MCF-7 cells increases with increasing concentration of coated silver nanoparticles (AgNPs) adjusted by NaOH. 60% of the MCF-7 were survived at 12.5µg/ml concentration and 30% MCF-7 cell line was survived at 25µg/ml and 50µg/ml concentration at 72hr and this confirmed by FLUO star OPTIMA results, as shown in the Figure (4-56).

The inverted microscope images showed the effect of silver nanoparticles (AgNPs) adjusted by NaOH after coating by nano thin film layer on the HBL-100 cell line there was less cells death at 12.5µg/ml and 25µg/ml concentrations. While, there was increased the cells growth at 50µg/ml concentration at 72hr, as shown in the Figure (4.56).

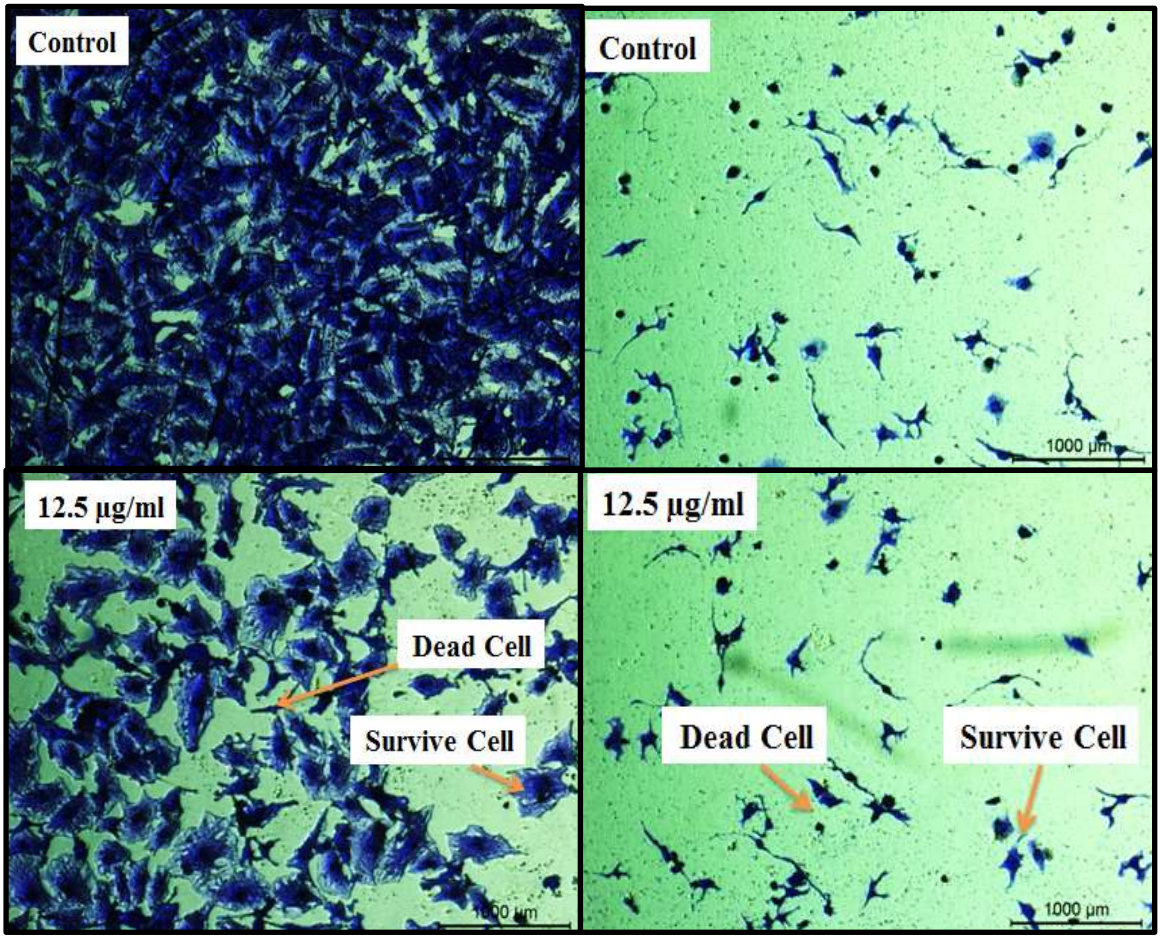

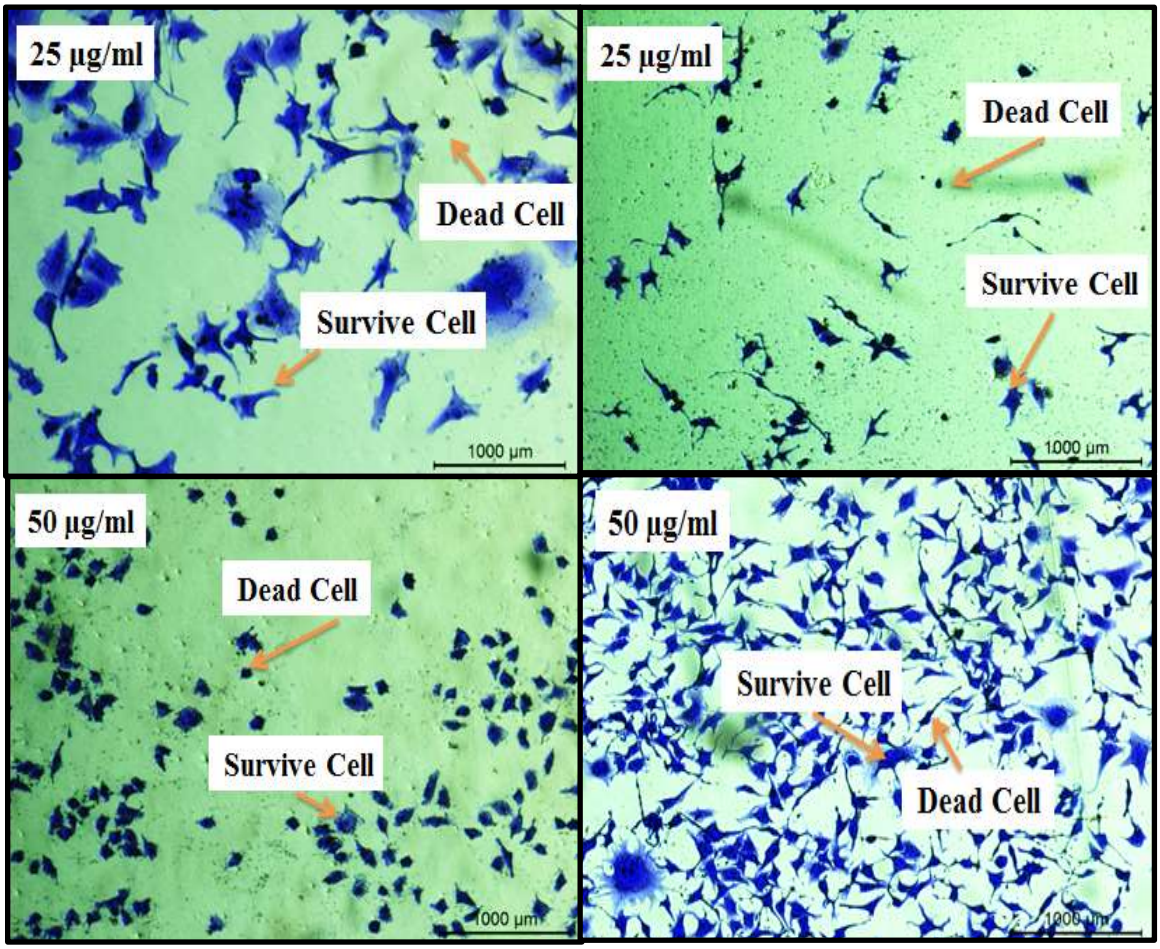

Fig 4.56: Microscopic images showing effect of different concentration coated silver nanoparticles (AgNPs) adjusted by NaOH against MCF-7 on left and HBL-100 on right.

4.4.3 Toxicity of Silver Nanoparticles Adjusted by NH_4OH on Cell Lines

The results of AgNPs adjusted by NH_4OH toxicity examination showed on the MCF-7 cell line there was the percentage of destroy MCF-7 cells increases with increasing concentration of silver nanoparticles (AgNPs) adjusted by NH_4OH. It is observed from the Figure (4.57) there was 60% of the MCF-7 were survived at 12.5 µg/ml concentration, 50% of MCF-7 cell line were survived at 25µg/ml and 40% MCF-7 cell line was survived at 50µg/ml at 72hr cell and this agrees with [23,24,26,29].

The results of AgNPs toxicity examination showed on the HBL-100 cell line there was increased the growth rate of HBL-100 cell at 12.5µg/ml, there did not affect on HBL-100 cell and 25µg/ml concentrations. While was increased the growth rate of HBL-100 cell at 50µg/ml concentration at 72hr, as shown in the Figure (4.57) cell and this agrees with [23, 26].

Therefore, the best optimization concentration of silver nanoparticles (AgNPs) adjusted by NH_4OH on MCF-7 and HBL-100 cell lines was 50µg/ml showed the best rate of destroy MCF-7 cell line and on same time 50µg/ml was increased the growth rate of HBL-100 cell.

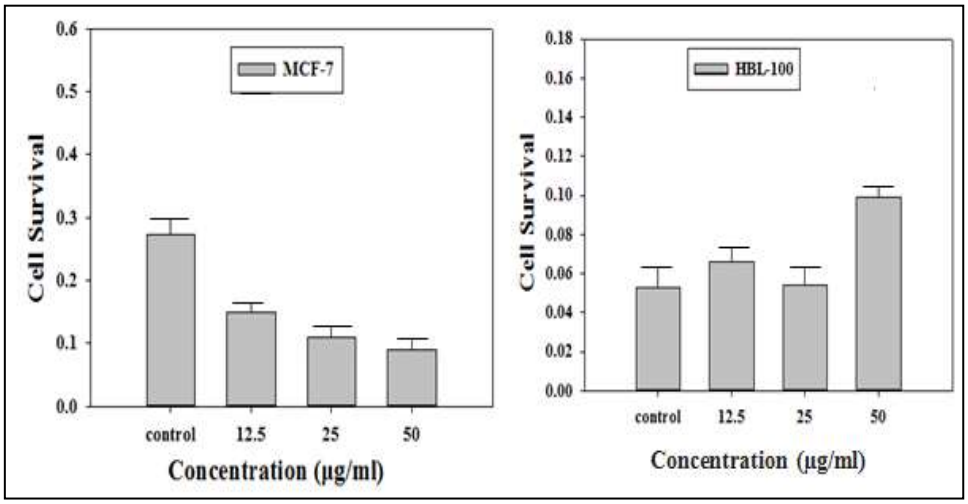

Fig 4.57: Effect of different concentration silver nanoparticles (AgNPs) adjusted by NH_4OH on MCF-7 and HBL-100 cell line.

The inverted microscope images showed the effect of silver nanoparticles (AgNPs) adjusted by NH_4OH on the MCF-7 cell line there was the increased MCF-7 cells death with increasing concentration of nanoparticles (AgNPs) adjusted by NH_4OH. 60% of the MCF-7 were survived at 12.5 µg/ml concentration, 50% of MCF-7 cell line were survived at 25µg/ml and 40% MCF-7 cell line was survived at 50µg/ml at 72hr and this confirmed by FLUO star OPTIMA results, as shown in the Figure (4.58).

The inverted microscope images showed the effect of nanoparticles (AgNPs) adjusted by NH_4OH on the HBL-100 cell line there was increased the growth rate of HBL-100 cell at 12.5µg/ml, there did not affect on HBL-100 cell and 25µg/ml concentrations. While was increased the growth rate of HBL-100 cell at 50µg/ml concentration at 72hr, as shown in the figure at 50µg/ml concentration at 72hr and this confirmed by FLUO star OPTIMA results, as shown in the Figure (4.58).

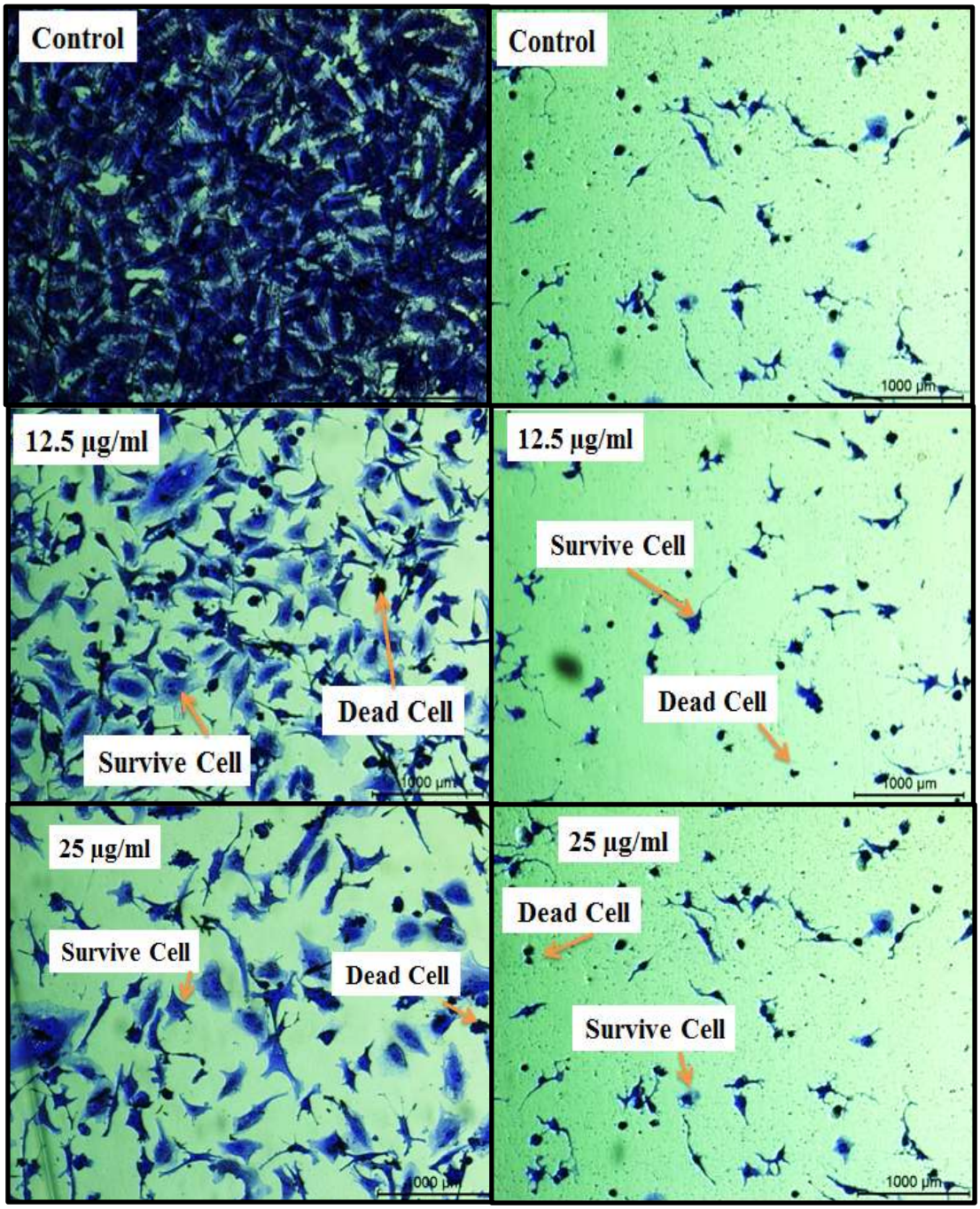

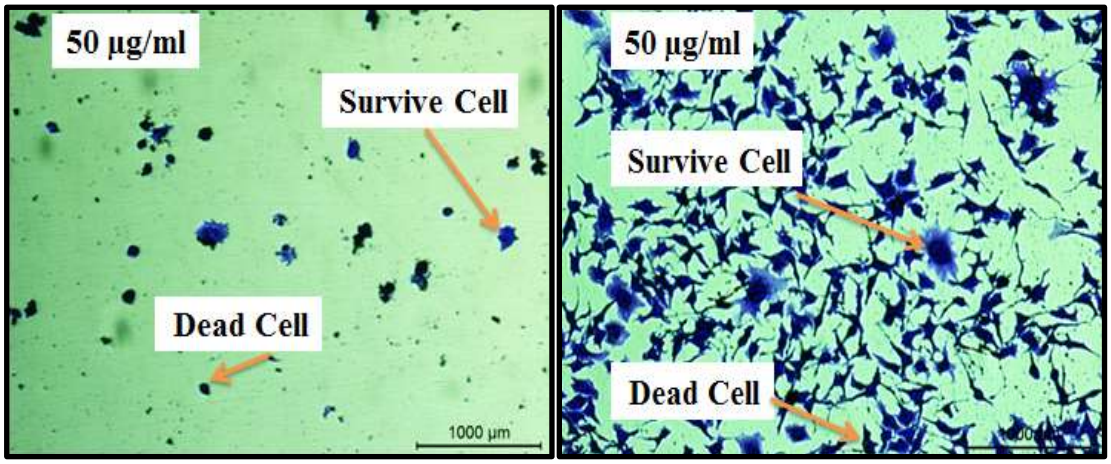

Fig 4.58: Microscopic images showing the effect of different concentration silver nanoparticles (AgNPs) adjusted by NH_4OH against MCF-7 on left and HBL-100 on right.

The results of AgNPs adjusted by NH_4OH toxicity examination showed after coating by nano thin film layer on the MCF-7 cell line there was the percentage of destroy MCF-7 cells increases with increasing concentration of coated silver nanoparticles (AgNPs) adjusted by NH_4OH. It is observed from the Figure (4.59) there was 60% of the MCF-7 were survived at 12.5µg/ml concentration and 30% MCF-7 cell line was survived at 25 µg/ml and 50µg/ml concentration at 72hr and this agrees with [23,24,26,29].

The results of AgNPs adjusted by NH_4OH toxicity examination showed after coating by nano thin film layer on the HBL-100 cell line there was less rate of destroy at 12.5µg/ml and 25µg/ml concentrations. While, there was increased the cells growth at 50µg/ml concentration at 72hr, as shown in the Figure (4.59) and this agrees with [23, 26].

Therefore, the best optimization concentration of coated silver nanoparticles (AgNPs) adjusted by NH_4OH on MCF-7 and HBL-100 cell lines was 50µg/ml showed the best rate of destroy MCF-7 cell line and on same time 50µg/ml was increased the growth rate of HBL-100 cell.

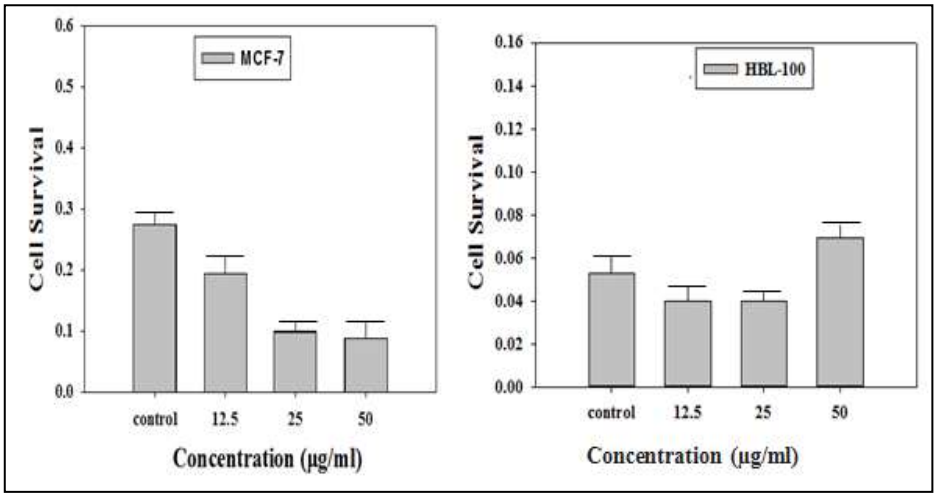

Fig 4.59: Effect of different concentration coated silver nanoparticles (AgNPs) adjusted by NH_4OH on MCF-7 and HBL-100 cell line.

The inverted microscope images showed the effect of silver nanoparticles (AgNPs) adjusted by NH_4OH after coating by nano thin film layer on the MCF-7 cell line there was the percentage of destroy MCF-7 cells increases with increasing concentration of coated silver nanoparticles (AgNPs) adjusted by NH_4OH. 60% of the MCF-7 were survived at 12.5µg/ml concentration and 30% MCF-7 cell line was survived at 25µg/ml and 50µg/ml concentration at 72hr and this confirmed by FLUO star OPTIMA results, as shown in the Figure (4.60).

The inverted microscope images showed the effect of silver nanoparticles (AgNPs) adjusted by NH_4OH after coating by nano thin film layer on the HBL-100 cell line there was less rate of destroy at 12.5µg/ml and 25µg/ml concentrations. While, there was increased the cells growth at 50µg/ml concentration at 72hr and this confirmed by FLUO star OPTIMA results, as shown in the Figure (4.60).

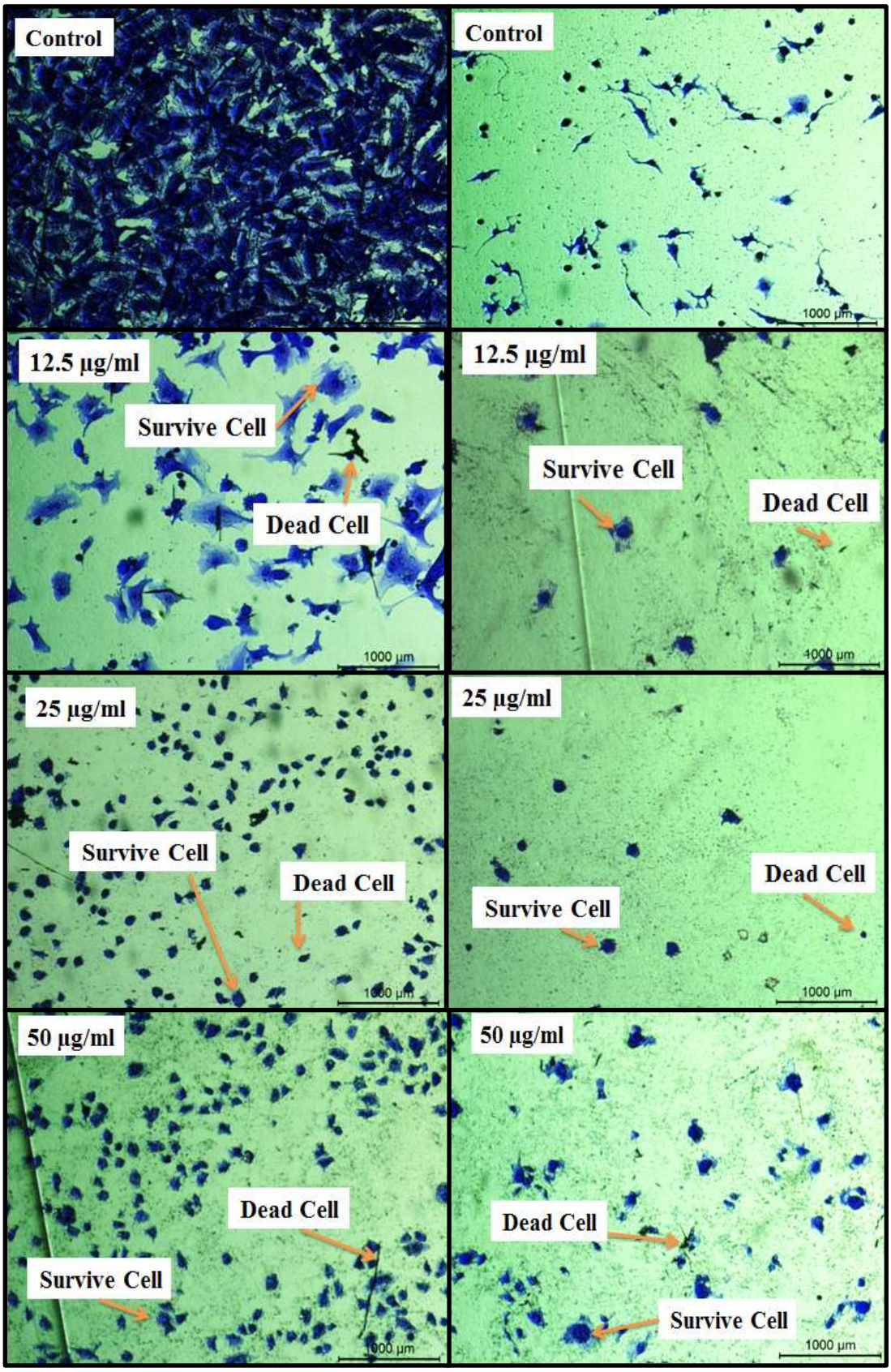

Fig 4.60: Microscopic images showing effect of different concentrations coated silver nanoparticles (AgNPs) adjusted by NH_4OH against MCF-7 on left and HBL-100 on right.

The results of this study showed the surface plasmon resonance (SPR) of gold and silver nanoparticles without and with coating have ability to destroy for MCF-7 cells at all concentrations accordingly. While, the effect against normal HBL -100 cells appeared less percentage of destroy cells at some concentration. While, the effect of SPR on the normal HBL -100 cells showed different effects on the normal HBL -100 cell line, it is less percentage of destroy cells at some concentration, and other concentrations appeared increased the cells growth.

The high surface energy of the nanoparticles possess were injected into the body or tissue culture that led to increase the local heating, this heating might cause to cancer cells injury, increasing their temperature significantly and thus destroying the cancerous tumor without compromising the normal cells and this agrees with [97-101]. Further studies are required to elucidate the precise molecular mechanism involved in cell growth inhibition thereby permitting the synthesized chemically AuNPs and AgNPs of cancer chemopreventive and/or therapeutic agents. The results of this study also provides the conclusive evidence for cytotoxic effect of AgNPs and AuNPs against breast cancer MCF-7 cell line compared with HBL-100 normal breast cell line, this agrees with a large number of in vitro studies indicated that the AgNPs and AuNPs are destroy to the mammalian cells [22,23,24,26,29].

Chapter Five

Conclusions and Future Works

5.1 Conclusions

- The parameters of temperature, TCD content, deionized water volume and mixing speed, SiO_2 content, deionized water volume, gold nanoparticles solution volume and ethanol volume have an important roles in the detection of localized the surface plasmon resonance (SPR) of gold nanoparticles (AuNPs) in blue and red shifts. The parameters of time, galic acid weight, temperature SiO_2 content, silver nanoparticles solution volume and ethanol volume have an important roles in the detection of localized the surface plasmon resonance (SPR) of silver nanoparticles (AgNPs) in blue and red shifts.
- Optical measurements results showed peak band surface plasmon resonance (SPR) of gold nanoparticles (AuNPs) at 515nm and this peak shifted to 518nm after coating. In same time, the optical measurements of silver nanoparticles (AgNPs) adjusted by NaOH and NH_4OH showed that the peak band surface plasmon resonance (SPR) was shifted from 396nm to 398nm and from 405nm to 414nm respectively.
- FTIR spectrum measurements results showed strong absorption peaks of the gold nanoparticles at 3431, 2341, 1627, 1506, 1388, 975, 962,632, 524 and 499 cm^{-1}, also strong absorption peaks showed at 3431, 2866, 2802, 2343, 2320 ,1622, 1616, 1494 1489 ,1384, 1379, 1072, 1062, 966, 655,636 543, 484 and 426 cm^{-1} of silver nanoparticles adjusted by NaOH and NH_4OH, also it is observed that the gold and silver nanoparticles after coating almost have the same absorption peaks with a little shift for some absorption peaks this means that the coating method led to a little increase in the size with maintaining on nanoparticles shape and prevents it from deforming,

the absorption bands 524 and 499 cm^{-1} of gold nanoparticles refer to harmony happening between inorganic elements (gold) and organic compounds (Trisodium Citrate Dihydrate), while refer the absorption bands 543, 484 and 426 cm^{-1} of silver nanoparticles to harmony happening between inorganic elements (silver) and organic compounds (Gallic acid).

- Gold nanoparticles all before and after coating by nano silica layer have a narrow size distribution and spherical shape with a little increase in the size after coating from 3-6nm to 9-18nm respectively. Also, silver nanoparticles all before and after coating by nano silica layer have a narrow size distribution and spherical shape with a little increase in the size from (6-8)nm and (3-6)nm to (10-19)nm and (12.9-16.7)nm for silver nanoparticles (AgNPs) adjusted by NaOH and NH_4OH respectively.
- Stability of gold and silver nanoparticles increase after coating by nano silica layer this means coating method led to maintain and control on the shape and size of nanoparticles and preventing it from agglomeration and this earns great importance in the use of any application.
- The surface plasmon resonance (SPR) of gold and silver nanoparticles without and with coating by nano thin film layer of silica have ability to destroy for MCF-7 cells at all concentrations. While, surface plasmon resonance (SPR) of gold and silver nanoparticles showed different effects on the normal HBL -100 cell line.
- The best optimization concentration of surface plasmon resonance (SPR) of gold nanoparticles (AuNPs) before and after coating by nano thin film layer of silica on MCF-7 and HBL-100 cell lines was 50µg/ml and 25µg/ml respectively showed the best rate of destroy MCF-7 cell line and on same time 50µg/ml and 25µg/ml was less the

destroy rate of HBL-100 cell. The best optimization concentration of surface plasmon resonance (SPR) of silver nanoparticles (AgNPs) adjusted by NaOH and NH_4OH before and after coating by nano thin film layer of silica on MCF-7 and HBL-100 cell lines was 50μg/ml showed the best rate of destroy MCF-7 cell line and on same time 50μg/ml was increased the growth rate of HBL-100 cell. Therefore, this study also provides the conclusive evidence of surface plasmon resonance (SPR) of gold and silver nanoparticles has toxic effect against breast cancer MCF-7 cell line at all concentrations compared with HBL-100 normal breast cell line.

5.2 Future Works

- Synthesis of gold nanoparticles (AuNPs) of Gallic acid ($C_7H_6O_5$) and synthesis of silver nanoparticles (AgNPs) of Trisodium Citrate Dihydrate ($Na_3C_6H_5O_7$).
- Studying the effect of different pH on the size, shape and size distribution of gold and silver nanoparticles.
- Studying the effect of Surface plasmon resonance (SPR) of silver nanoparticles with contentious output power of laser and x-ray on human breast cancer cells (MCF-7) and the normal cells (HBL- 100).
- Studying time different effect in treatment human breast cancer cells (MCF-7) and the normal cells (HBL- 100) by using gold and silver nanoparticles.

REFERENCES

References

[1] K. D. Sattler, "Handbook of Nanophysics", CRC press, (2011).

[2] A. K. H. Zaree, "Nanophysics & Nanotechnology (Book review) ISM", 15(4), pp. 339-340, (2013).

[3] Zanichelli "The Feynman Lectures on Physics", (2008).

[4] D. L. Schodek, P. Ferreira and M. F. Ashby, "Nanomaterials, nanotechnologies and design: an introduction for engineers and architects", Butterworth-Heinemann, (2009).

[5] R. Psaro, M. Guidotti and M. Soboba, "Nanosystems, Inorganic and Bioinorganic Chemistry", 2, pp. 1-10, (2008).

[6] M. D. Cheng, D. Lowndes and D. B. Geohegan, "Generation and Characterization Engineered Nanoparticles for Environmmental and Billogical Exposure Research, International Symposium on Envirnomental Nanotechnology", Taiwan, pp.1-12, (2004).

[7] Z. P. Xu, Q. H. Zeng, G. Q. Lu and A. B. Yu, "Inorganic nanoparticles as carriers for efficient cellular delivery", Chemical Engineering Science, 61(3), pp.1027-1040, (2006).

[8] P Sen, J. Ghosh, Al. Abdullah, P. Kumar and Vandana, "Preparation of Cu, Ag, Fe and Al nanoparticles by the exploding wire technique", Proc. Indian Acad. Sci. (Chem. Sci.), 115(5), pp. 499–508, (2003).

[9] A. R. Siekkinen, J. M. McLellan, J. Chen, and Y. Xia,"Rapid synthesis of small silver nanocubes by mediating polyol reduction with a trace amount of sodium sulfide or sodium hydrosulfide", Chemical Physics Letters, 432 (4-6), pp. 491–496, (2006).

[10] J. Prikulis, F. Svedberg, M. Kall, "Optical spectroscopy of single trapped metal nanoparticles in solution", Nano Letters 4 , pp. 115-118, (2004).

[11] M. S. Chargot, A. Gruszecka, A. Smolira, J. Cytawa and L. Michalak, "Mass spectrometric investigations of the synthesis of silver nanoparticles via electrolysis", Vacuum, 82(10) , pp. 1088–1093, (2008).

[12] V. Kattumuri, "Gold nanoparticles for biomedical applications: synthesis, characterization, in vitro and in vivo studies", PhD thesis, University of Missouri–Columbia, (2006).

[13] J. A. Scholl, A. L. Koh and J. A. Dionne, "Quantum plasmon resonances of individual metallic nanoparticles", 483 (7390) , pp. 421-7, (2012).

[14] Sh. Zeng, K. T. Yong, I. Roy, X. Q. Dinh, X. Yu and F. Luan, "A review on functionalized gold nanoparticles for biosensing applications", Plasmonics 6 (3), pp. 491-506, (2011).

[15] M. Rycenga, C. M. Cobley, J. Zeng, W. Li, C. H. Moran, Q. Zhang, D. Qin and Y. Xia , "Controlling the synthesis and assembly of silver nanostructures for plasmonic applications", Chemical Reviews, 111(6), pp. 3669-712, (2011).

[16] Cuncheng Li, K. L. Shuford, Q. H. Park, W. Cai, Y. Li, E. J. Lee and S. O. Cho, "High-yield synthesis of single-crystalline gold nano-octahedra", Angewandte Chemie, 46(18), pp. 3264-3268. (2007).

[17] C. G. Granqvist and R. A. Buhrman, "Ultrafine metal particles",]Journal of applied Physics, 47, pp. 2200-2219, (1976).

[18] D. Mirela,"Metallic nanoparticles", university of Nova Gorica, doctoral study, programme physics, (2009).

[19] G. A. M. Castanon, N. N.Martinez, F. M. Gutierrez, J. R. M. Mendoza and F. Ruiz, "Synthesis and antibacterial activity of silver nanoparticles with different sizes", Nanopart Res, 10, pp. 1343-1348, (2008).

[20] A. Tabrizi, F. Ayhan and H. Ayhan, "Gold nanoparticle synthesis and characterization", Hacettepe J. Biol. & Chem., 37 (3), pp. 217-226, (2009).

[21] N. M. Bahadur, Sh. Watanabe, T. Furusawa, M. Sato, F. Kurayama, I. A. Siddiquey, Y. Kobayashi and N. Suzuki, "Rapid one-step synthesis, characterization and functionalization of silica coated gold

nanoparticles", Colloids and Surfaces A: Physicochem. Eng, pp. 137-144, (2011).

[22] K. Amarnath, N. L. Mathew, J. Nellore, Ch. R.V. Siddarth and J. Kumar, "Facile synthesis of biocompatible gold nanoparticles from Vites vinefera and its cellular internalization against HBL-100 cells", Cancer Nano, 2, pp. 121-132, (2011).

[23] R. Vivek, R. Thangam, K. Muthuchelian, P. Gunasekaran, K. Kaveri and S. Kannana, " Green biosynthesis of silver nanoparticles from Annona squamosa leaf extract and its in vitro cytotoxic effect on MCF-7 cells", Process Biochemistry, 47, pp. 2405–2410, (2012).

[24] M. Jeyaraj, G. Sathishkumar, G. Sivanandhan, D. M. Ali, M. Rajesh, R. Arun, G. Kapildev, M. Manickavasagam, N. Thajuddin, K. Premkumar and A. Ganapathi, "Biogenic silver nanoparticles for cancer treatment: An experimental report", Colloids and Surfaces B: Biointerfaces, 106 , pp. 86-92, (2013).

[25] F. M. Britto and I. Química, "Virucidal activity of silver-silica functionalized nanoparticles", relatório final de bolsista – 22º programa bolsas de verão do cnpem, (2013).

[26] Ch. Rejeeth, B. Nataraj , R. Vivek and M. Sakthivel, "Biosynthesis of silver nanoscale particles using spirulina platensis induce growth-inhibitory effect on human breast cancer cell line MCF-7", Med Aromat Plants, 3(4), pp.1-7, (2014).

[27] A. P. Sulthana, J. M. Rathi and K. Sahayaraj, " Terminalia chebula Retz. gallic acid–biased silver nanoparticles and their antiphytopathogenic activity", Nanoparticles antiphytopathogenic activity, J Biopest 7(Supp.) , pp.1-6 (2014)

[28] M. Lakshmipathy and A. Nanda, "Assessment of in vitro prophylactic efficacy of gallic acid fabricated silver nanoparticles", J. Chem. Pharm. Res., 7(1), pp. 356-361, (2015).

[29] S. A Loutfy, N. A. Al-Ansary, N.T A. Ghani, A. R. Hamed, M. B. Mohamed, J. D. Craik, T. A. S. Eldin, A. M. Abdellah, Y. Hussein, M. T. M. Hasanin and S. E. I. Elbehairi," Anti-proliferative activities of metallic nanoparticles in an in vitro breast cancer model" , Asian Pac J Cancer Prev, 16 (14), pp. 6039-6046, (2015).

[30] S. Rahman,"Size and concentration analysis of gold nanoparticles with ultraviolet-Visible", Undergraduate Journal of Mathematical Modeling: One + Two, 7(1), (2016).

[31] Z. Yahia and R. M. S. Al-Haddad, "The effect of silica concentrations on the absorbance of gold nanoparticles", International Journal of ChemTech Research,10(3), pp. 448-455, (2017).

[32] D. Acharya, B. Mohanta, P. Pandey and F. Nasiri, "Antibacterial properties of synthesized Ag and Ag@SiO_2 Core-shell nanoparticles: A Comparative Study, Canadian Journal of Physics, pp. 1-13, (2017).

[33] Z. B. afrapoli, R. F. majidi, B. Negahdari and G. Tavoosidana, "Inversed Turkevich' method for tuning the size of gold nanoparticles: evaluation the effect of concentration and temperature", Nanomed Res J, 3(4), pp. 190-196, (2018).

[34] J. Yadav, "Synthesis and characterization of gold nanoparticles", International Journal on Future Revolution in Computer Science & Communication Engineering, 4(4), pp. 220-230, (2018).

[35] A. Thapliyal and A. Chandra, " Antibacterial and anticancer potential of silver nanoparticles synthesized using gallic Acid in bentonite/starch bio-nanocomposites", Int J App Pharm, 10 (5), pp. 178-189, (2018).

[36] J. Dong, P. L. Carpinone, G. Pyrgiotakis, Ph. Demokritou and B. M. Moudgil, "Synthesis of precision gold nanoparticles using Turkevich method", KONA Powder and Particle Journal, 11(1), (2019).

[37] D. B. Sanchez ,"The surface plasmon resonance of supported noble metal nanoparticles: characterization, laser tailoring, and SERS application", PhD thesis, Madrid University, (2007).

[38] E. Susie and M. A. El-Sayed, " Why gold nanoparticles are more precious than pretty gold: noble metal surface plasmon resonance and its enhancement of the radiative and nonradiative properties of nanocrystals of different shapes", Chemical Society Reviews, 35(3), pp.209-217, (2006).

[39] M. A. Garcia, "Surface plasmons in metallic nanoparticles: fundamentals and applications", Journal of Physics D: Applied Physics, IOP Publishing, 44(28), pp. 283001, (2011).

[40] D. Th. Gangadharan, Z. Xu, Y. Liu, R. Izquierdo and D. Ma, "Recent advancements in plasmon-enhanced promising third-generation solar cells", Nanophotonics, 6(1), pp. 23, (2017).

[41] N. Zhou, V. L. Puente, Q. Wang and Q. H. Xu, "Plasmon-enhanced light harvesting: applications in enhanced photocatalysis, photodynamic therapy and photovoltaics", RSC Adv, 5(37), pp. 29076- 29097, (2015).

[42] P. Jain., I. El-Sayed, M. El-Sayed , "AuNPs target cancer", Nano Today, 2, pp. 18-29, (2007).

[43] G. Mie, "Beitrage zur optik truber medien, speziell kolloidaler metallosungen", Ann. Phys, 330(3), (1908).

[44] R. L. Lee, "Mie theory, Airy theory, and the natural rainbow", Applied Optics, 37(9), pp. 1506-1519, (1998).

[45] L. Strasak , V. Vetterl and J. Smarda, "Effects of low-frequency magnetic fields on bacteria escherichia coli", Bioelectrochemistry, 55, pp. 161-164, (2002).

[46] Y. Fang and X. Tian, "Resonant surface plasmons of a metal nanosphere can be considered in the way of propagating surface plasmons", arXiv preprint arXiv : 1412. 2664 (2014).

[47] A. K. Ali, "Preparation of Ag and Au nanoparticles by pulsed laser ablation in liquids", PhD thesis, University of Technology, Baghdad, (2010).

[48] G. E. J. Poinern, "A Laboratory course in nanoscienc and nanotechnology", CRC. press, London, (2014).

[49] Amsh, "Chemical properties of nanomaterials", Science Articles for Winners, 21 September (2012).

[50] Amsh, "Surface area to volume ratio in nanoparticles", Science Articles for Winners, 28 May (2012).

[51] S. Chaturvedi, Pr. N. Dave and N.K. Shah, "Applications of nano-catalyst in new era", Journal of Saudi Chemical Society,16 (3), pp.307-325, (2012).

[52] C. Altavilla and E. Ciliberto, " Inorganic Nanoparticles: Synthesis, Applications, and Perspectives", CRC Press, (2010).

[53] M. K. Hamid, "The effect of some physical parameters of gold nanoparticles produced by laser ablation on antibacterial effect", Ph.D. thesis, Al-Nahrain University, (2014).

[54] M. Ratner and D. Ratner, "Nanotechnology: a gentle introduction to the next big idea", Prentice Hall, (2002).

[55] P. Harrison, "Quantum wells, wires and dots: theoretical and computational physics", John Wiley and Sons, New York , (2000).

[56] S. K. Kulkarni, "Nanotechnology : principles and practices", Capital Publishing Company, book. 3rd Edition, ch4,6,11, (2015).

[57] N. K. A. Donkor, "Structural and optoelectronic properties of copper, Zinc, cadmium lead chalcogenide nanocrystalline thin films deposited at the water-toluene interface", Ph.D thesis, Kwame Nkrumah University of Science and Technology, College of Science , Department of Chemistry, Kumasi,Ghana, (2013)

[58] V. Raghavan, "Materials Science and Engineering", Fifth edition, (2011).

[59] G. N. kumar, "Properties of nanomaterials", Nanostructured & Amorphous Materials, Inc., (2001).

[60] F. Mafune, J. Y. Kohno, Y. Takeda, T. Kondow and H. Sawabe,"Formation and Size control of silver nanoparticles by laser ablation in aqueous solution", J. Phys. Chem, 104(39), pp. 9111-9117, (2000).

[61] Y. Lu, M. Yu, M. Drechsler and M. Ballauff ,"Ag nanocomposite particles:preparation, characterization and application", Macromol. Symp, 254, pp. 97-102, (2007).

[62] R. W. Kelsall, I. W. Hamley, M. Geoghegan, "Nanoscale science and technology" John Wiley & Sons Ltd, England (2005).

[63] K. L. Kelly, E. Coronado, L. Zhao and G. C. Schatz, Journal of Physical Chemistry, 107(3), pp. 668-677, (2003).

[64] V. V. Mody, R. Siwale, A. Singh and H. R. Mody," Introduction to metallic nanoparticles", J Pharm Bioallied Sci, 2, pp. 282-289, (2010) .

[65] M. Hu, J. Chen, Z. Y. Li, L. Au, G. V. Hartland, X. Li, M. Marqueze and Y. Xia, "Gold nanostructures engineering their plasmonic properties for biomedical applications", Chem. Soc. Rev, Vol. 35, pp. 1084–1094, (2006).

[66] S. Mekapothula, "Gold nanoparticle–biomolecule conjugates synthesis, properties, cellular interactions and cytotoxicity studies", M.Sc, thesis, University of Missouri, (2008).

[67] M. K. K. Oo, Y. Yang and Y. Hu, "Gold nanoparticle-enhanced and size-dependent generation of reactive oxygen species from protoporphyrin IX", ACNANO, 6(3), pp. 1939–1947, (2012).

[68] M. Rai, A. Yadav and A. Gade, "Silver nanoparticles as a new generation of antimicrobials", Biotechnol Adv, 27: 76-83, (2009).

[69] J. S. Kim , E. Kuk , K. N. Yu, J. H. Kim, S. J. Park, H. J. Lee , S. H. Kim, Y. K. Park, Y. H. Park, C.Y. Hwang, Y. k. kim, Y. S. Lee, D. H. Jeong and M. H. Cho, Antimicrobial effects of silver nanoparticles. Nanomedicine, 3, pp. 95-101, (2007).

[70] K. W. Powers, M. Palazuelos, B. M. Moudgil and S. M. Roberts, "Characterization of the size, shape, and state of dispersion of nanoparticles for toxicological studies", Nanotoxicology, 1: pp. 42-51, (2007).

[71] L. D. Rampino and F. F. Nord, "Preparation of palladium and platinum synthetic high polymer catalysts and the relationship between particle size and rate of hydrogenation", J. Am. Chem. Soc, 63(10), pp. 2745-2749, (1941).

[72] K. K. Harish , N. Venkatesh, H. Bhowmik and A. Kuila, "Metallic nanoparticle: a review", Nagasamy venkatesh. biomed j sci & tech res, 4 (2), pp. 1-11, (2018).

[73] M. Shah, V. Badwaik and Y. Kherde, "Gold nanoparticles various methods of synthesis and antibacterial applications", Frontiers in Bioscience, 19, pp. 1320-1344, (2014).

[74] J. Turkevich, P. C. Stevenson and J. Hillier, "A study of the nucleation and growth processes in the synthesis of colloidal gold", Discuss. Faraday. Soc., 11, pp. 55-75, (1951).

[75] J. Kimling, M. Maier, B. Okenve, V. Kotaidis, H. Ballot and A. Plech, "Turkevich method for gold nanoparticle synthesis revisited", J Phys Chem B, 110 (32), pp.15700-15707, (2006).

[76] G. Frens, "Particle size and sol stability in metal colloids", Colloid & Polymer Science, 250 (7), pp. 736-741, (1972).

[77] G. Frens, "Controlled nucleation for the regulation of the particle size in monodisperse gold suspensions", Nature Physical Science, 241, pp. 20-22, (1973).

[78] B. K. Pong, H. I. Elim, J. X. Chong, W. Ji, B. L. Trout, and J.Y. Lee,"New insights on the nanoparticle growth mechanism in the citrate reduction of gold (III) Salt: Formation of the Au nanowire intermediate and Its Nonlinear Optical Properties", J. Phys. Chem. C, 111(17), pp.6281-6287, (2007).

[79] P. R. Santana, A. I. J. Abizanda, A. H. Creus and F. J. Moreno, "Synthesis and physical characterization of Ag nanoparticles and their interaction with Fe", Journal of Luminescence , 190, pp. 207-214, (2017).

[80] S. R. Makhsin, K. A. Razak, R. Noordin, N. Z. Dyana and T. S. Chun, "The effects of size and synthesis methods of gold nanoparticle-conjugated MαHIgG_4 for use in an immunochromatographic strip test to detect brugian filariasis", Nanotechnology. 23, pp. 49-57, (2012).

[81] S. Pratsinis, "Hot nanoparticles for cancer treatments", PHYS ORG, March (2014).

[82] G. A. Sotiriou, F. Starsich, A. Dasargyri, "Photothermal killing of cancer cells by the controlled plasmonic coupling of silica-coated AuFe_2O_3 nanoaggregates", Advanced Functional Materials, Vol. 24, No. 19, pp. 2818-2827, (2014).

[83] D. Kandpali, S. Kalele and S. K. Kulkarni, "Synthesis and characterization of silica–gold core-shell (SiO_2@Au) nanoparticles", Pramana -J. Phys., 69(2), pp. 277-283, (2007).

[84] L. Cherbas and L. Gong, "cell lines", Methods, 68(1), pp.74-81, (2014).

[85] R. I. Freshney, "Basic Principles of Cell Culture", Culture of Cells for Tissue Engineering, (2006).

[86] Aschner, M. Aschner and C. Sunol, "Cell Culture Techniques", Humana Press, New York, (2011).

[87] L. Wang, T. Jiang and D. Gusfield, "A more efficient Approximation scheme for tree alignment", SIAM Journal on Computing, 30 (1), pp. 283-299, (2000).

[88] Cell Culture Basics (handbook), ThermoFisher Scientific, (2016).

[89] A. V. Lee, S. Oesterreich and N. E. Davidson, "MCF-7 Cells-changing the course of breast cancer research and care for 45 Years", Journal of the National Cancer Institute. 107 (7), (2015).

[90] P. Balaram, "Electronic supplementary material for molecular biosystems rapid mass spectrometric determination of disulfide connectivity in peptides and proteins", The Royal Society of Chemistry, (2013).

[91] E. V. Gaffney. A cell line (HBL-I00) established from human breast milk. Cell Tissue Res, 227, pp. 563-568, (1982).

[92] M. Raja, A. G. Arasi, M. G. Rao and B. Anandhi, "Noble metal nanoparticles in cancer therapy: properties challenges and clinical applications", Int. J. Adv. Res. 5(9), pp. 127-135, (2017).

[93] S. A Loutfy, M. B. Mohamed, N. T. Abdel- Ghani, N. Al-Ansary, W. A. Abdulla, O. M. El-Borady, Y. Hussein and H. M. Eldin, "Metallic nanomaterials as drug carriers to decrease side effects of chemotherapy (In vitro: cytotoxicity study)", Journal of Nanopharmaceutics Drug Delivery, 1, pp.1-12, (2013).

[94] C. Buzea , I. Pacheco, K. Robbie , "Nanomaterials and nanoparticles: sources and toxicity", Biointerphases, 2, pp.17-71, (2007).

[95] M. E. Selim and A. A. Hendi , "Gold nanoparticles induce apoptosis in MCF-7 human breast cancer cells", Asian Pac J Cancer Prev, 13, pp.1617-20, (2012).

[96] E. Y. L. Hleb, Y. S. Kim, I. Belatsarkouski, A. M. Gillenwater, B. E. ONeill and D. O. Lapotko , "Intraoperative diagnostics and elimination of residual microtumours with plasmonic nanobubbles", Nat Nanotechnol, 11(6), (2016).

[97] R. Toy, "The Effect of Particle Size and Shape on the In Vivo", Journey of Nanoparticles", Ph. D Thesis Ph. D Thesis. Case Western Reserve University; Cleveland, OH, USA: (2014).

[98] R. Toy, P.M. Peiris, K. B. Ghaghada , E. Karathanasis , "Shaping cancer nanomedicine: The effect of particle shape on the in vivo journey of nanoparticles", Nanomedicine, 9, pp. 121-134, (2014).

[99] A. Verma and F. Stellacci, "Effect of surface properties on nanoparticle-cell interactions. Small", 6, pp. 12-21, (2010).

[100] J. S. García, R. P. Ortega, M. R. Cepeda, A. Vera, L. Leija and J. Estelrich, "Improved Thermal Ablation Efficacy Using Magnetic Nanoparticles: A Study in Tumor Phantoms. Prog. Electromagn", Res,128, pp. 229-248 (2012).

[101] S. Dutz and R. Hergt, "Magnetic particle hyperthermia-A promising tumour therapy", Nanotechnology, 25, pp. 452001, (2014).

[102] G. Busch and H. Schade, "Lectures on Solid State Physics", Pergaman Press, London, (1976).

[103] I. Abrahman and V. Padavettan, "Synthesis of silica nanoparticles by sol-gel size-dependent properties, surface modification, and applications in silica-polymer nanocomposites-a review", Journal of Nanomaterials, 2012, pp.1-15, (2012).

[104] A. Gole and C. J. Murphy, "Seed-mediated synthesis of gold nanorods: role of the size and nature of the seed", Journal of Materials Chemistry,16, pp. 3633-40, (2004).

[105] B. Abecassis, F.Testarda and T. Zemb, "Gold nanoparticle synthesis in worm-like catanionic micelles microstructure conservation and temperature induced recovery", The Royal Society of Chemistry, 5, pp. 974-978, (2009).

[106]V. Amendola and M. Meneghetti, "Size evaluation of gold nanoparticles by UV-VIS spectroscopy", J. Phys. Chem. C 113, pp. 4277-4285, (2009).

[107] A. D. Skoog, F. J. Holler and R. S. Crouch, "Principles of Instrumental Analysis" (6^{th} ed.). Belmont, CA: Thomson Brooks/Cole, pp. 169-173, (007).

[108] Y. A. Gandomi, D. S. Aaron, J. R. House, M. C. Daugherty, J. T. Clement, A. M. Pezeshki, T. Y. Ertugrul, D. P. Moseley, and M. M.

Mench,"Critical review-experimental diagnostics and material characterization techniques used on redox flow batteries", Journal of The Electrochemical Society, 165 (5), pp. A970-A1010, (2018).

[109] A. M. Funde, "Synthesis and study of hydrogenated nano crystalline silicon thin films grown by plasma CVD and hot wire CVD for solar cell applications", Ph.D. thesis, University of Pune, (2010).

[110] P. R. Griffiths and J. A. De Haseth, "Fourier transform infrared spectrometry", John Wiley & Sons, (2007).

[111] N. A. Bakr, "Studies on structural, optical and electrical properties of Hydrogenated nanocrystalline silicon (nc-Si:H) thin films grown by hot wire-CVD for photovoltaic applications," Ph.D thesis, University of Pune (2010).

[112] F. J. Giessibl, "Advances in atomic force microscopy", Reviews of Modern Physics, 75 (3), pp.949, (2003).

[113] A. Filonov, D. Y. Gavrilko and I. V.Yaminsky, "Scanning probe microscopy image processing software users's manual "FemtoScan"", Advanced Technologies Center, Moscow, (2007).

[114] T. Ando, N. Kodera, T. Uchihashi, A. Miyagi, R. Nakakita, H. Yamashita and K. Matada, "High-speed atomic force microscopy for capturing dynamic behavior of protein molecules at work", Journal of Surface Science and Nanotechnology, 3, pp. 384-392, (2005).

[115] M.Z. Baykara and U.D. Schwarz, "Atomic force microscopy: methods and Applications", Encyclopedia of spectroscopy and spectrometry, third edition, 1, pp. 70-75, (2017)

[116] J. Shiue and S. K. Hung, "A TEM phase plate loading system with loading monitoring and nano-positioning functions, Ultramicroscopy, 110 (9), pp.1238-1242, (2010).

[117] B. E. Guettler, "Soy-Polypropylene biocomposites for automotive applications", Master's thesis, University of Waterloo, (2009).

[118] W. Zhou and Z. L. Wang, "Scanning microscopy for nanotechnology: techniques and applications", Springer science & business media, (2007).

[119] B. J. Inkson, "Scanning electron microscopy (SEM) and transmission electron microscopy (TEM) for materials characterization. In Materials characterization using nondestructive evaluation (NDE) methods", Wood head Publishing, pp. 17-43, (2016).

[120] A. Paar, "(n.d.) Faster, more sensitive zeta-potential measurements with cmPALS and the litesizer™ 500", January 24 (2019).

[121] M. A. Farrukh (edit), "Atomic Absorption Spectrometry", InTech, Ch1, (2012).

[122] M.R AbdulMajeed, "Induction and characterization of SU.99 plasmacytoma cell line and its effect on mice immune response", Ph.D thesis, Nahrain University, (2000).

[123] R.I. Freshney, "Application of cell culture to toxicology", Cell Biol. Toxicol, 17, pp. 213-230, (2001).

[124] Z. Y. Sulaiman, "Plasmonic hot gold nanoparticles for treatment of cancer cell line", Ph.D thesis, University of Baghdad ,College of Science, Department of Physics, (2017).

الامتصاص$^{-1}$543cm و$^{-1}$ 426 cm^{-1} 484 cm^{-1} إلى حدوث توافق بين العناصر اللاعضوية (الفضة) والمركبات العضوية (حامض الكالك).

أظهرت نتائج القياسات التركيبية أن جسيمات الذهب النانوية لها توزيع حجم ضيق وشكل كروي مع معدل حجم nm(3-6). من جانب اخر لاحظنا بعد طلاء جسيمات الذهب النانوية بطبقة نانوية رقيقة من السيليكا، أن لهذه الجسيمات توزيع حجم ضيق مع زيادة طفيفة في حجم الجسيمات النانوية (9-18nm) إضافة الى الاحتفاظ بشكلها الكروي وزيادة استقرار الجسيمات من (25.02mV−) الى (25.92mV−). في نفس الوقت أظهرت نتائج القياسات التركيبية أن جسيمات الفضة النانوية المعادلة بواسطة هيدروكسيد الصوديوم ومحلول هيدروكسيد الأمونيوم لها شكل كروي مع معدل حجم nm(6-8) و nm(3-6) على التوالي. من جانب اخر لاحظنا بعد طلاء جسيمات الفضة النانوية المعادلة بواسطة هيدروكسيد الصوديوم ومحلول هيدروكسيد الأمونيوم بطبقة نانوية رقيقة من السيليكا، أن لهذه الجسيمات توزيع حجم ضيق مع زيادة طفيفة في حجم الجسيمات النانوية (10-19nm) و (12.9-16.7) على التوالي إضافة الى الاحتفاظ بشكلها الكروي وزيادة استقرار الجسيمات من (58.17mV−) و (15.68mV−) الى (62.86mV−) و (43.60mV−) على التوالي.

أظهرت نتائج قياسات فحص سمية رنين بلازمونات السطح من جسيمات الذهب والفضة النانوية الغير المطلية والمطلية بغشاء نانوي رقيق من مادة السيلكا أن لهذه الجسيمات القدرة على تدمير خلايا سرطان الثدي عند جميع التراكيز. بينما يُظهر رنين بلازمونات السطح من جسيمات الذهب والفضة النانوية تأثيرات مختلفة على خلايا الثدي الطبيعية.

لذلك فان افضل تركيز مثالي من جسيمات الذهب النانوية الغير المطلية والمطلية بغشاء نانوي رقيق من مادة السيلكا كان عند (50µg/ml) و (25µg/ml) على التوالي حيث حصلنا عند هذه التراكيز على افضل نسبة تدمير لخلايا سرطان الثدي وفي نفس الوقت اقل نسبة تدمير لخلايا الثدي الطبيعية. بينما افضل تركيز مثالي من جسيمات الفضة النانوية المعادلة بواسطة هيدروكسيد الصوديوم ومحلول هيدروكسيد الأمونيوم الغير المطلية والمطلية بغشاء نانوي رقيق من مادة السيلكا كان عند (50µg/ml) حيث حصلنا عند هذا التركيز على افضل نسبة تدمير لخلايا سرطان الثدي وفي نفس الوقت كان هناك زيادة في نمو خلايا الثدي الطبيعية عند هذا التركيز. وعليه نقدم في هذه الدراسة دليل قاطع على أن لرنين بلازمونات السطح من جسيمات الذهب والفضة النانوية تأثير سام على خلايا سرطان الثدي عند جميع التراكيز مقارنة بخلايا الثدي الطبيعية. لذلك هناك حاجة ماسة إلى مزيد من الدراسات لتوضيح الآلية الجزيئية الدقيقة المعنية بتثبيط نمو الخلايا وبالتالي السماح بتركيبة كيميائية من جسيمات الذهب والفضة النانوية لكي تستخدم كعوامل وقائية او العلاجية للسرطان.

الخـــــــلاصة

حصلنا في هذه الدراسة على رنين بلازمونات السطح بطاقة سطحية عالية من جسيمات الذهب والفضة النانوية الكروية المحضرة كيميائيا مع وبدون الطلاء بطبقة نانوية رقيقة من السيليكا لمعالجة الخطوط الخلوية (سرطان الثدي والخلايا الطبيعية للثدي).

حُضرت جسيمات الذهب النانوية الكروية كيميائياً بطريقة توركوفيج من حامض كلورواريك وسترات الصوديوم. وقد تم تحديد تأثير المتغيرات مثل درجة الحرارة وحجم الماء منزوع الأيونات وسرعة الخلط ومحتوى ثنائي اوكسيد السيليكا وحجم محلول الذهب النانوي وحجم الإيثانول على موقع رنين بلازمونات السطح وحجم الجسيمات وتوزيع الحجم وشكل جسيمات الذهب النانوية في مناطق الإزاحة الزرقاء و الحمراء. بينما حُضرت جسيمات الفضة النانوية الكروية كيميائياً بطريقة اختزال حامض الكالك من نترات الفضة وحامض الكالك، وقد تم تحديد تأثير المتغيرات مثل الزمن ووزن حامض الكالك ودرجة الحرارة ومحتوى ثنائي اوكسيد السيليكا وحجم محلول الفضة النانوي وحجم الإيثانول على موقع رنين بلازمونات السطح و حجم الجسيمات وتوزيع الحجم وشكل جسيمات الفضة النانوية في مناطق الإزاحة الزرقاء و الحمراء.

أظهرت نتائج القياسات البصرية أن قمة رنين بلازمونات السطح لجسيمات الذهب النانوية هي عند (515nm) وتزحف بعد الطلاء إلى (518nm). في نفس الوقت أظهرت نتائج القياسات البصرية أن قمة رنين بلازمونات السطح لجسيمات الفضة النانوية المعادلة بواسطة هيدروكسيد الصوديوم ومحلول هيدروكسيد الأمونيوم هي عند (396nm) و (398nm) وتزحف بعد الطلاء الى (405nm) و (415nm) على التوالي.

أظهرت نتائج قياسات طيف الاشعة تحت الحـــمراء قمم امتصاص قوية من جسيمات الذهب النانوية عند $3431\ cm^{-1}$ و$2341\ cm^{-1}$ و $1627cm^{-1}$ و $1506\ cm^{-1}$ و$1388\ cm^{-1}$ و$975\ cm^{-1}$ و$962\ cm^{-1}$ و $632\ cm^{-1}$ و $524cm^{-1}$ و $499\ cm^{-1}$ ، واظهرت ايضاً قمم امتصاص قوية عند $3431\ cm^{-1}$ و$2866\ cm^{-1}$ و$2802\ cm^{-1}$ و$2343\ cm^{-1}$ و$2320\ cm^{-1}$ و $1622\ cm^{-1}$ و $1616\ cm^{-1}$ و $1494\ cm^{-1}$ و$1489\ cm^{-1}$ و$1384\ cm^{-1}$ و$1379\ cm^{-1}$ و$1072\ cm^{-1}$ و $1062\ cm^{-1}$ و$966\ cm^{-1}$ و $655\ cm^{-1}$ و $636\ cm^{-1}$ و$543\ cm^{-1}$ و$484cm^{-1}$ و$426cm^{-1}$ من جسيمات الفضة النانوية المعادلة بواسطة هيدروكسيد الصوديوم ومحلول هيدروكسيد الأمونيوم، ولاحظنا ايضاً أن جسيمات الذهب والفضة النانوية بعد الطلاء لها نفس قمم الامتصاص مع إزاحة صغيرة لبعض قمم الامتصاص مما يدل على ان عملية الطلاء أدت إلى زيادة صغيرة في الحجم مع المحافظة على شكل الجسيمات ومنعها من التشوه. قمم الامتصاص $524cm^{-1}$ و $499cm^{-1}$ من جسيمات الذهب النانوية تشير إلى حدوث توافق بين العناصر اللاعضوية (الذهب) والمركبات العضوية (سترات الصوديوم)، بينما تشير قمم

جمهورية العراق
وزارة التعليم العالي والبحث العلمي
جامعة ديالى
كلية العلوم
قسم الفيزياء

رنين بلازمونات السطح من جسيمات الذهب والفضة النانوية لتطبيقات فيزياء الطب الحياتي

إطروحة مقدمة إلى

مجلس كلية العلوم- جامعة ديالى وهي جزء من متطلبات نيل درجة دكتوراه فلسفة في الفيزياء

من قبل

رسل كريم إسماعيل العكيدي

بكالوريوس علوم فيزياء ٢٠١٢
ماجستير علوم فيزياء الحالة الصلبة ٢٠١٥

إشراف

أ.د. تحسين حسين مبارك **أ.د. رعد محمد صالح الحداد**

١٤٤١هـ ٢٠١٩م